COEXISTENCE OF SURFACE DIFFUSION MECHANISMS: JUMP AND EXCHANGE FOR W ON W(100)

BY

TOMASZ OLEWICZ

DISSERTATION

Submitted in partial fulfillment of the requirements
for the degree of Doctor of Philosophy in Electrical and Computer Engineering
in the Graduate College of the
University of Illinois at Urbana-Champaign, 2015

Urbana, Illinois

Doctoral Committee:

Professor Joseph W. Lyding, Chair, Director of Research
Professor Pascal Bellon
Associate Professor John M. Dallesasse
Associate Professor Gang Logan Liu

ABSTRACT

The thermally-activated coexistence of two diffusion mechanisms, adatom jump and exchange, is a phenomenon that has important potential application in fabrication of quantum dot based devices. If one can initiate the occurrence of a particular diffusion mechanism by changing the temperature, then it is possible to control the moment when an adatom is incorporated into the surface layer. The buried adatom could then serve as a nucleation center for growth of a nanostructure.

This dissertation shows the first experimental evidence for the temperature-activated coexistence of two surface diffusion mechanisms, the adatom jump and adatom exchange, observed in a W on W(100) system. The adatom exchange was identified as the primary diffusion mechanism, and it is activated on a time scale of seconds at temperatures around 650 K. The occurrence of the secondary diffusion mechanism, adatom jump, was observed on a time scale of seconds at temperatures around 700 K. The experiments were conducted using a Field Ion Microscope (FIM) under Ultra-High Vacuum (UHV) conditions (~ 10^{-11} Torr). The activation energy for the exchange in a W on W(100) system was found to be 1.6 ± 0.24 eV. For the jump, the activation energy was estimated as ~2.1 eV. These values are in very good agreement with results from Density Functional Theory (DFT) calculations.

ACKNOWLEDGMENTS

The experimental part of the dissertation was supported by the Air Force Office of Scientific Research under grant number FA9550-09-1-248 and the Department of Materials Science and Engineering at the University of Illinois at Urbana-Champaign. The DFT calculations were done by Prof. Leszek Jurczyszyn from the Surface Theory Group at the University of Wroclaw via grant 1010/S/IFD. The computations were conducted at the Interdisciplinary Center for Mathematical and Computational Modeling of the University of Warsaw within Grant No. G44-10.

I would like to thank my adviser Prof. Gert Ehrlich for giving me the opportunity of conducting the research in his group. I am grateful for his support and guidance during my doctorate studies. I thank him for always finding time to discuss the research and other matters with me. I will never forget his precision and cautiousness in research, and the "donut hour" which was held every Friday at 11:00 AM. I would like to thank my second adviser Prof. Joseph W. Lyding for his guidance and support through the most difficult time of my doctorate, and for taking the role of my adviser after Prof. Ehrlich's passing. I also would like thank Prof. Pascal Bellon, Prof. John M. Dallesasse and Prof. Gang Logan Liu for taking the role of the members of my Doctoral Committee. I would like to thank Dr. hab. Grażyna Antczak, for introducing me to Prof. Gert Ehrlich, which initiated my journey to the doctorate degree at the University of Illinois at Urbana-Champaign. I am grateful for her help with the data interpretation and publishing. I give special thanks to Dr. Robert S. Chambers for teaching me the art of troubleshooting and for his significant help with maintaining and repairing the field ion microscope at the beginning of my endeavors. I also would like to thank Dr. Artur Trembułowicz for his help in the laboratory, especially between 9 PM and 6 AM. I would like to thank my dear friends Dr. Wacek Swięch, Zachary Estrada, Gloria See and Dr. Canan Dagdeviren for their support and advising during my time at UIUC.

I wish to acknowledge Physics and ECE Machine Shops for their technical support, especially Mr. Keith Kugel for his excellent glass works. I also would like to thank Mr. Steve Burdin and Mr. Ernie Sammann from the MRL at UIUC for their support with designing and repairing the electronic components of my apparatus. I am in debt to Prof. Steven J. Franke from the ECE Office of Student Affairs for his guidance and support during my transition to the ECE Department. I would like to acknowledge Mr. Jay Menacher from the MSE Department for his extraordinary support with administration affairs. I also would like to thank Ms. Janice L. Progen from Editorial Services in the ECE Department for proofreading my dissertation.

I would like to thank my parents, Urszula and Jerzy Olewicz, and my brother Marcin for their love and support at each step of my career. Finally, I wish to thank my wife Yen-Fang Cheng for her love and support in the good and the bad times, and for giving me the strength to overcome all the obstacles. Without that support completing my degree at UIUC would not be possible.

TABLE OF CONTENTS

PART I – DIFFUSION OF A SINGLE W ADATOM ON W(100)

1. INTRODUCTION

Surface diffusion plays a key role in various surface phenomena such as heterogeneous catalysis, surface reconstruction and crystal growth [1]. As the size of fabricated electronic devices decreases from micro- to nano-scale, the shape of grown structures and their arrangement on the substrate's surface play an important role in device properties. Thus, exhaustive understanding and better control over migration mechanisms of adatoms become much more desired than ever before. The coexistence of two diffusion mechanisms, adatom jump and adatom exchange, is a phenomenon that has an important potential application in nucleation and growth processes. If one controls the occurrence of particular diffusion mechanisms (e.g. jump and exchange) by changing the temperature, then the adatom could be moved to the desired area on the top of the surface (e.g. via electromigration jump [1]) and just by changing the temperature the adatom could be buried in the first layer of the surface. The buried adatom could serve as a nucleation center for growth of a nanostructure or as a part of a single atomic device, e.g. the channel in single-atom transistor devices [2].

Recently, W(100) surface has been used as a substrate for growing various nanostructures such as ferromagnetic Fe [3] nanoislands, potentially useful for spin electronics, or antiferromagnetic Cr [4] nanopyramids which are a good candidates for STM tips. Also, growth of Au nanoparticles on oxygen-covered W(100) surfaces has been reported recently [5]. It is potentially possible to achieve a non-random arrangement of grown nanostructures by taking advantage of the coexistence of adatom jump and exchange. However, the coexistence of the diffusion mechanism and the adatom exchange mechanism on any of bcc(100) surfaces has yet to be proven. Moreover, the morphology of finite-size W(100) is still a subject of intense debate.

In this dissertation, surface self-diffusion on W(100) is examined. A first experimental proof for the exchange mechanism and its coexistence with adatom jump on a W/W(100) system is delivered. An additional study is conducted for determining the morphology of a finite-sized W(100) surface. The experimental part of the work was conducted with a Field Ion Microscope (FIM) – a technique which allows imaging the surface in atomic scale. Obtained experimental results are compared with the output of the Density Functional Theory (DFT) calculations, which were conducted by collaborators at the Surface Theory Group from the University of Wroclaw and the Computational Materials Science Group at the University of Illinois at Urbana-Champaign.

The dissertation is divided into two major parts: Part I examines diffusion of a single W adatom on W(100) surface, and Part II discusses the influence of a second W adatom on the diffusion properties of W on W(100). Chapter 1 is an introduction to the conducted research on single adatom surface diffusion and the coexistence of surface diffusion mechanisms. A model of surface diffusion with basic equations used in our research is presented. Chapter 1 also discusses the most common diffusion mechanisms occurring for single adatom surface diffusion and describes the principles of field ion microscopy technique. The end of Chapter 1 presents the current state knowledge about the morphology of W(100) surface, the coexistence of surface diffusion mechanisms and the understanding of adatom exchange mechanism. Chapter 2 is a thorough description the equipment used in the experimental part of presented research. Chapter 3 describes measuring methods and procedures used for investigation of single adatom surface diffusion. Chapter 4 presents the completed work and discusses obtained results. Chapter 5 presents summary and conclusions for the Part I. Chapter 6 presents the current state of knowledge about the surface-mediated adatom interactions and their influence on surface diffusion. Chapter 7 describes the experimental procedures used for measurements of diffusing adatom pair. Chapter 8 presents obtained results and data analysis. Chapter 9 presents summary and conclusions of research described in Part II. Chapter 10 summarizes a whole dissertation and presents final conclusions.

1.1 Model of Surface Diffusion

The analysis of surface diffusion is based on a simple diffusion model, in which the adatom jumps between adjacent adsorption sites on an infinite surface. To move from one adsorption site to another, the adatom has to break the bonds with adjacent surface atoms. The energy required for breaking these bonds is represented by a potential barrier V_D (Fig. 1a). The total energy required for the adatom movement between adsorption sites is called the activation energy for diffusion, E_D. The activation energy varies for different diffusion mechanisms and diffusion systems. Its value can be determined from the measurements of the mean-square displacement $\langle(\Delta x)^2\rangle$.

Using the Einstein-Smlouchowski relation, the diffusivity D of a moving adatom at temperature T is determined by:

$$\langle(\Delta x)^2\rangle = 2mDt \tag{1}$$

where m is a dimensionality constant, m = 1, 2, 3 for one-, two-, and three-dimensional diffusion movement, respectively, and t is a time interval. A temperature dependence of the diffusivity can be expressed by the Arrhenius relation:

$$D = D_0 exp\left(-\frac{E_D}{k_B T}\right) \tag{2}$$

where T is the temperature, k_B is the Boltzmann constant, E_D is the activation energy for adatom diffusion and D_0 is a diffusion prefactor. By plotting the diffusivity as a function of temperature in a semi-logarithmic scale, from the slope of the linear fit one obtains the activation energy for the diffusion (Fig. 1b).

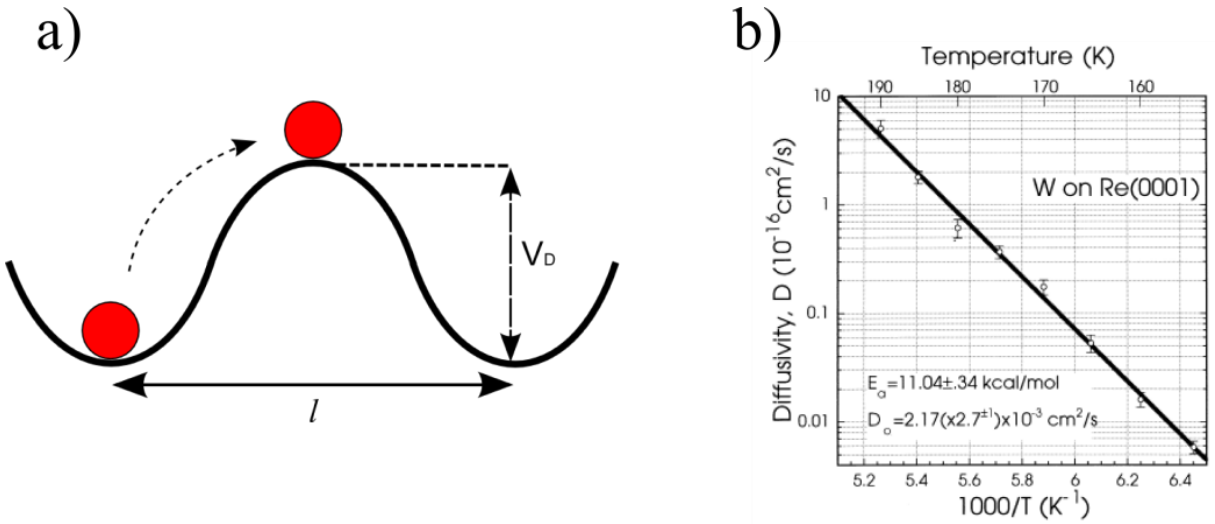

Fig. 1: (a) Model of adatom surface diffusion on an ideal surface. V_D is the potential barrier, equal to the energy required for breaking the bonds between the adatom and the surface atoms and *l* is the distance between the adsorption sites. (b) The Arrhenius plot of the diffusivity as a function of temperature in a semi-logarithmic scale. The activation energy is determined from the slope of the linear fit, and the diffusivity prefactor is equal to the intersection of the fit with the diffusivity axis [6][1].

1.2 Diffusion Mechanisms

There are various surface diffusion mechanisms. Each mechanism has different activation energy and each diffusion system can favor a different mechanism. The major factors that determine which diffusion mechanism will be imposed on the system are: the activation energy, the surface morphology, the chemical properties of the adatom and the surface, e.g. atomic mass and charge distribution [7, 8].

1.2.1 Adatom single jump

In this mechanism, an atadom migrates on the top of the surface between nearest-neighbor adsorption sites. Each jump is independent of the previous one, so the probability of visiting surrounding sites is

[1]Reprinted from *Surf. Sci.*, J. T. Goldstein and G. Ehrlich, "Atom and cluster diffusion on Re(0001)," vol. 443, pp. 105 - 115, 1999. Copyright 1999, with permission from Elsevier.

strictly related to the surface morphology and the kinetic energy of adatom. For diffusion on channeled planes, at low temperatures (e.g. W diffusion on W(211), below 300 K) the jump of adatom usually occurs inside the atomic channel [9]. In this case, the diffusion is considered as one-dimensional. Thus *m* in equation (1) is equal to one. At much higher temperatures, the adatom which diffuses on a channeled plane can jump across the channels. However, since the diffusion rates along and across the channels are asymmetrical, those movements must be considered separately, i.e. *m* in equation (1) is equal to one. On atomically flat surfaces with asymmetrically arranged adsorptions sites, e.g. W(110), the diffusion of the adatom is asymmetric [10]. Thus the diffusion along x and y directions should also be considered separately. For atomically flat surfaces with a fourfold symmetry, e.g. W(100), the jumps are equally probable for each of the four surrounding sites. In this case, the diffusion is considered as two-dimensional and $m = 2$.

1.2.2 The adatom exchange mechanism

When the adatom interacts strongly with the surface, it can replace one of its atoms [7]. This type of diffusion mechanism is called the exchange. In the exchange mechanism occurring on two-dimensional surfaces, (Fig. 2a) the adatom pushes one of the surface atoms to the top of the plane creating a dumbbell and a surface vacancy underneath it [11]. When the dumbbell breaks, the adatom is incorporated into the vacancy and the atom remaining on the top of the surface equilibrates into the nearest unoccupied adsorption site, from which it can diffuse further. The exchange mechanism can also occur on channeled surfaces (Fig. 2b) [12]. In that case, the adatom adsorbed into the atomic channel nudges one of the surface atoms located in the atomic row that separates the channels. When such created dumbbell breaks, the adatom incorporates into the row, whereas the atom of the row is pushed into the adjacent channel.

1.2.3 Long jumps

At sufficiently high temperatures, the adatom might have enough energy to make a direct jump into a second or even a third adsorption site away from the origin, without equilibrating on its way. This kind of

movement is called the long jump [7]. It has been shown theoretically [13] and experimentally [14] that this mechanism is more favorable for systems where the exchange of kinetic energy between the adatom and the surface is poor. In other words, the adatom will bounce on the top of the surface a few times, before it will be equilibrated in the adsorption site. The mechanism was experimentally proven by a comparison of the mean square displacement obtained from the experiments with the one obtained from the Monte Carlo simulations [15]. The presence of long jumps can also be detected with the Arrhenius plot [16]. At temperatures above 0.1 T_m (T_m – melting temperature), the diffusivity deviates from the linear fit of the Arrhenius obtained for low temperatures [16]. However, the main problem in detecting long jumps is a required number of statistics. To segregate long jumps from single jumps via analysis of the jump rate or by deviation from the Arrhenius fit, about 1000 observations of the adatom movement per each temperature must be collected [15].

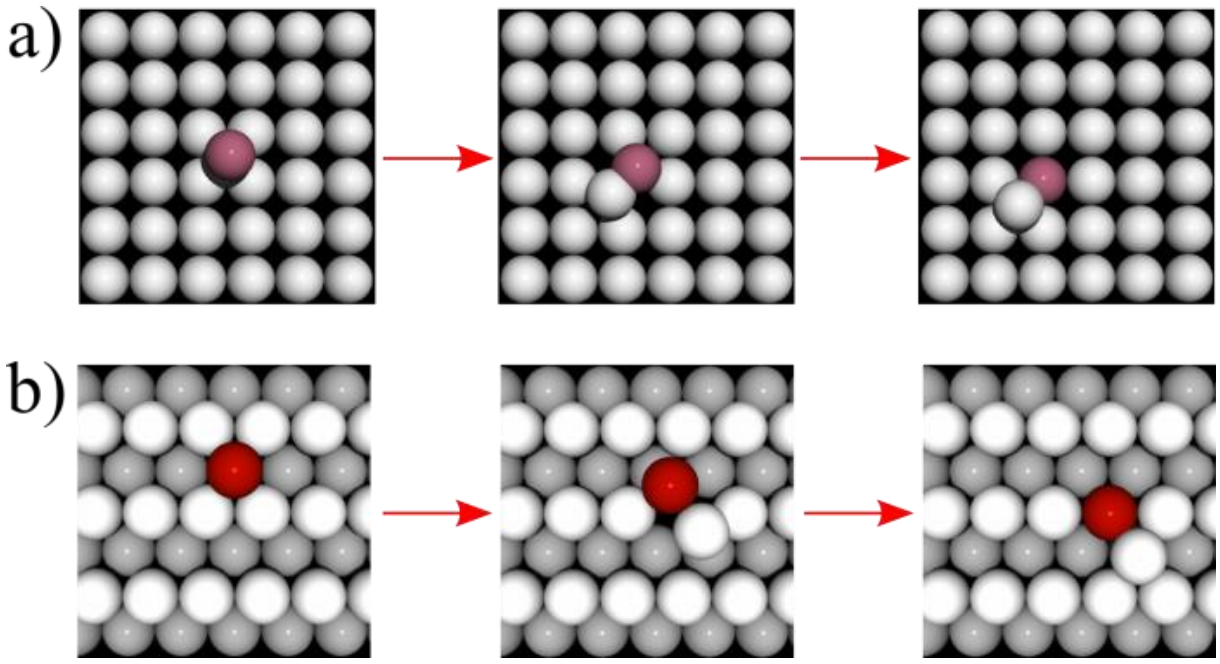

Fig. 2: (a) The exchange mechanism occurring on a two-dimensional plane. The nearest unoccupied adsorption site for the pushed surface atom is placed diagonally to the initial adsorption site. (b) The exchange occurring on a channeled plane. The nearest adsorption site for the pushed atom is placed in the adjacent channel.

1.2.4 Crowdion mechanism (multiple exchange)

The crowdion is a diffusion mechanism that in principle is very similar to a regular exchange. In crowdion, the adatom incorporates into the surface and congests the surface atoms (Fig. 3a,b). The caused stress propagates within the surface plane. As a result, one of the surface's atoms pops up to the top of the plane [7]. The crowdion mechanism is analogical to the long jump mechanism. Since the stress propagates rapidly beyond the nearest-neighbor atom, the adatom that is pushed to the top can be located a few atomic spacings from the point of adatom incorporation [17]. The crowdion mechanism has been postulated as a result of various DFT calculations [17, 18, 19]. However, it has never been proved experimentally.

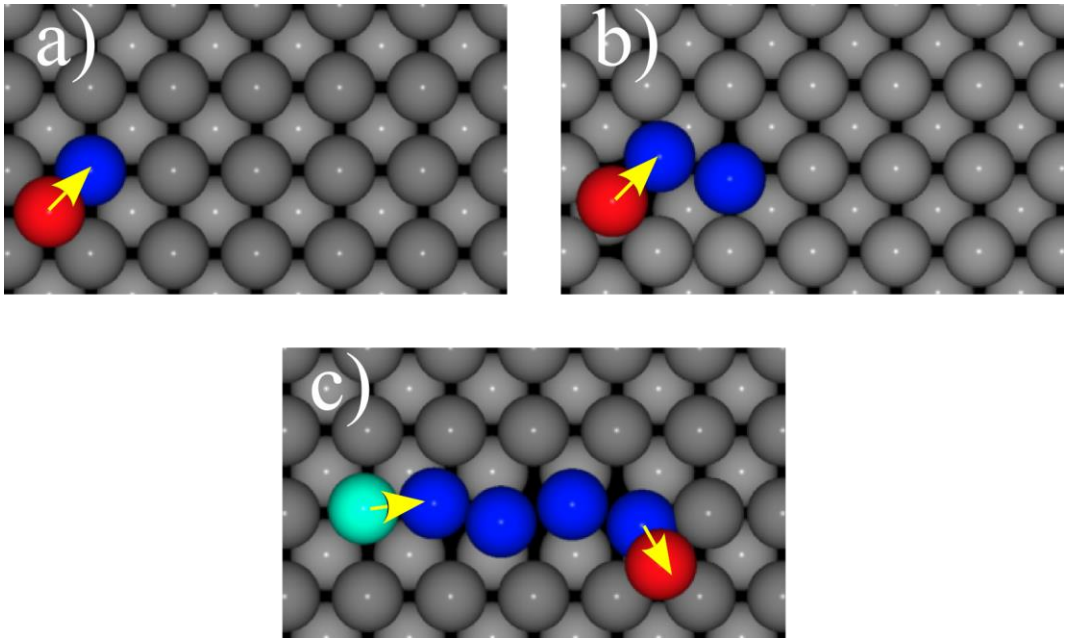

Fig. 3: The sequence of steps occurring during the adatom diffusion via the crowdion mechanism: (a) adatom incorporates into the surface, (b) suppresses the surface atoms, and (c) a buildup of the stress surface pushes the surface atom to the top.

1.3 Field Ion Microscope

Field Ion Microscope (FIM) is a technique which allows imaging the surface with atomic scale resolution. It is a very robust method. Unlike other surface sensitive techniques, the picture resolved in FIM cannot be affected by either the mechanical vibrations or the electronic noise. The sample can be made of almost any metal or semiconductor material, either mono or poly crystal [20]. FIM simultaneously resolves the picture of various crystal planes. It also allows controlling the number of surface atoms on a chosen crystal plane, which gives a huge advantage in the surface diffusion studies. The FIM is specifically chosen for studies of single adatom diffusion, because unlike the competitive techniques: Scanning Tunneling Microscopy (STM) or Atomic Force Microscopy (AFM), the measurements conducted with FIM do not affect the diffusion movement [7].

1.3.1 The idea of FIM technique

The sample used in FIM is a very sharp tip (~ 100 – 300 Å in radius) which is placed in a vacuum chamber in front of the screen. To resolve the surface's picture, an imaging gas (usually He or Ne) is introduced into the FIM chamber and a high voltage is applied between the tip and the screen, with positive polarity on the tip (Fig. 4a). The electric field polarizes the atoms of imaging gas creating dipoles. Since the field is not uniform and the dielectric constant of the imaging gas is higher than the vacuum, the dipoles of imaging gas are attracted toward the tip's surface with the force $\boldsymbol{F}$:

$$\boldsymbol{F}(r_0) = 2\pi\, \varepsilon_{gas} \frac{\varepsilon_{gas}-\varepsilon_0}{\varepsilon_{gas}+2\varepsilon_0} a^3 \nabla[\boldsymbol{E}^2(r_0)] \tag{3}$$

r_0 is the distance from the surface to the center of the dipole, ε_0 and ε_{gas} are the dielectric constants of the vacuum and the imaging gas respectively, a is the radius of imaging gas atom, and E is the applied electric field.

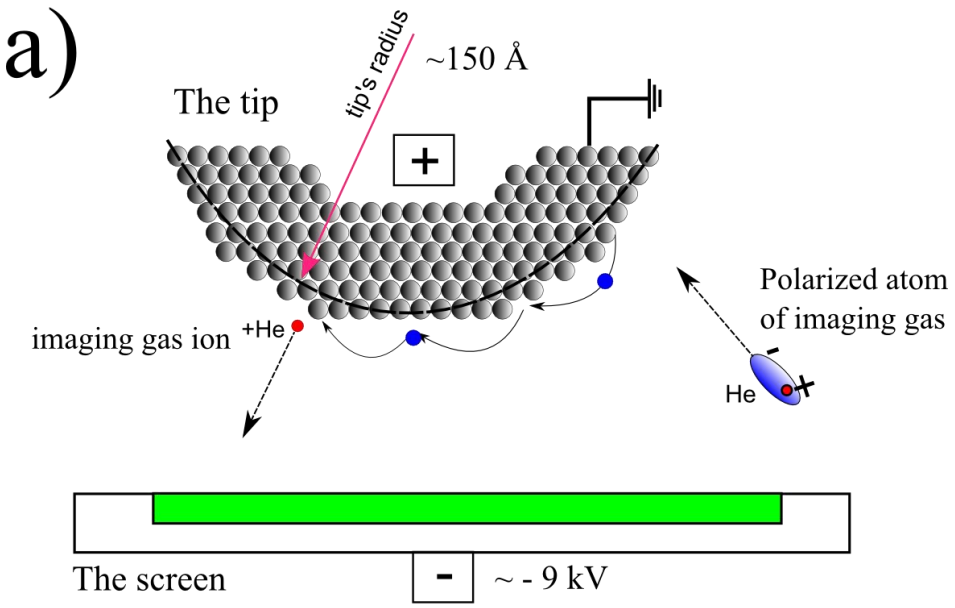

b)

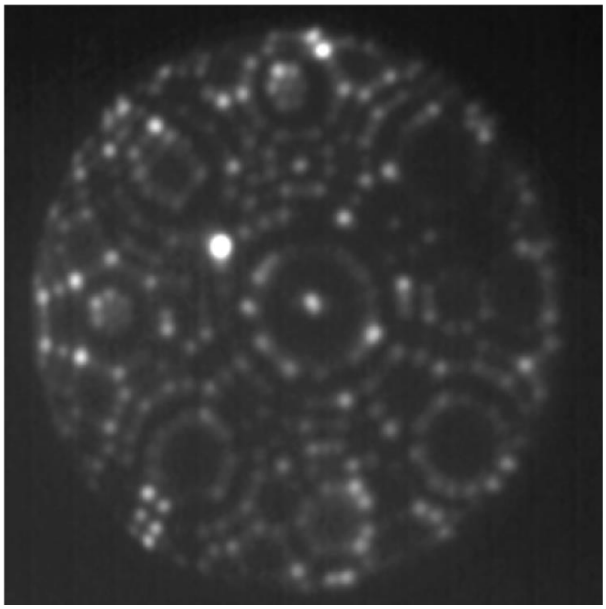

Fig. 4: (a) Schema of operation of field ion microscope, (b) FIM micrograph of W(100) surface with W adatom in the center of the plane. The surface was imaged with helium gas at 9.5 kV.

When atoms of the imaging gas reach the surface, they are ionized within ~ 4 Å above the sharpest areas of the surface [20], i.e. over the step edge atoms or adatoms. Afterward, the ions of the gas are repelled from the surface toward the screen, where they cause brightening (Fig. 4b). The spots observed on the screen correspond to the relative positions of the surfaces atoms. Usually the applied voltage for imaging is 3 – 10 kV and it depends on the tip radius, the imaged material, the imaging gas and the temperature of the tip. The imaging electric field is of the order of few V/Å. The field varies for different imaging gases e.g. for helium it is 4.4 V/Å and for neon it is 3.5 V/Å [20] .

1.3.2 Advantages and limitations of the FIM technique in surface diffusion studies

Atomic scale resolution makes FIM a suitable technique for investigating single atom surface diffusion. For a tip with a radius below 200 Å, which is cooled to 20 K and imaged with helium, the resolution is below 3 Å [21]. Thus, with FIM one can accurately determine the position of the adatom and the mean square displacement. Resolved with FIM the images of adsorbed adatoms can also provide information about the distribution of the surface's adsorption sites and the surface's morphology [22]. The shape of images of adatoms can also reveal information about the shape and the type of adsorption sites. Wang and Ehrlich [23] distinguished fcc from hcp-types of adsorption sites on fcc(111) by observing the orientation of the triangular shape of the imaged adatom. For the hcp sites, triangular imaging spots always point toward the [2-1-1] direction whereas for the fcc sites point away from the [2-1-1] direction [23].

FIM, as any other measuring technique, has its limitations. Since the electric field is the highest at surface protrusions, most of the imaging gas is ionized at the plane step edges, not at the surface interior (Fig. 5a,b). Except for adatoms and some atomically rough planes like bcc(311) (Fig. 5c), the surface's interior is practically impossible to resolve. The opportunity to slightly overcome those limitations appears when relatively small planes (~ 5 atoms in diameter) are imaged at voltages close to surface's evaporation field or when a mixture of imaging gases, with different ionization potentials is used (Fig. 5d). However, even then the result is far from impressive and much worse than the pictures resolved via a scanning tunneling

microscope. The alternative solution used for determining a surface's morphology involves using the adatoms as markers of adsorption sites. The map of adsorption sites for deposition of metal atoms onto a metal surface often corresponds to the arrangement of surface atoms [1]. However, one has to keep in mind that in the presence of the adatom, the surface atoms can also relax, which might corrupt the information [24]. With FIM it is not also possible to resolve the intermediate steps of some diffusion mechanisms, like the moment of adatom incorporation into the surface during the crowdion diffusion. Thus one relies only on the thorough analysis of the initial and final states. On the other hand, the adatom movement is undisturbed by any external factors, such the applied electric field.

FIM without an integrated mass spectrometer also has limited capability of distinguishing the imaged atoms. At first glance, all the spots observed on the screen look almost identical. The exceptions are some foreign adatoms and oxides attached to the surface, which have a different spot size than the native atoms [25]. However, the magnitude of the evaporation field might vary for different species, which can be used as criteria for distinguishing adatoms in FIM. One must keep in mind that both the spot size and the desorption field diverge from the center of a plane to the step edge. Thus, adatoms of two different materials, which have different evaporation fields, can be desorbed at the same voltage if one adatom is closer to the plane center and another is closer to the step edge.

1.4 Current Status

Since the time when the FIM technique was developed, much research has been conducted to investigate various diffusion mechanisms and the morphology of a W(100) surface. The experimental effort was additionally supported with DFT calculations. This chapter summarizes the key results of the experimental and theoretical work conducted on adatom diffusion mechanisms and the morphology of a W(100) surface.

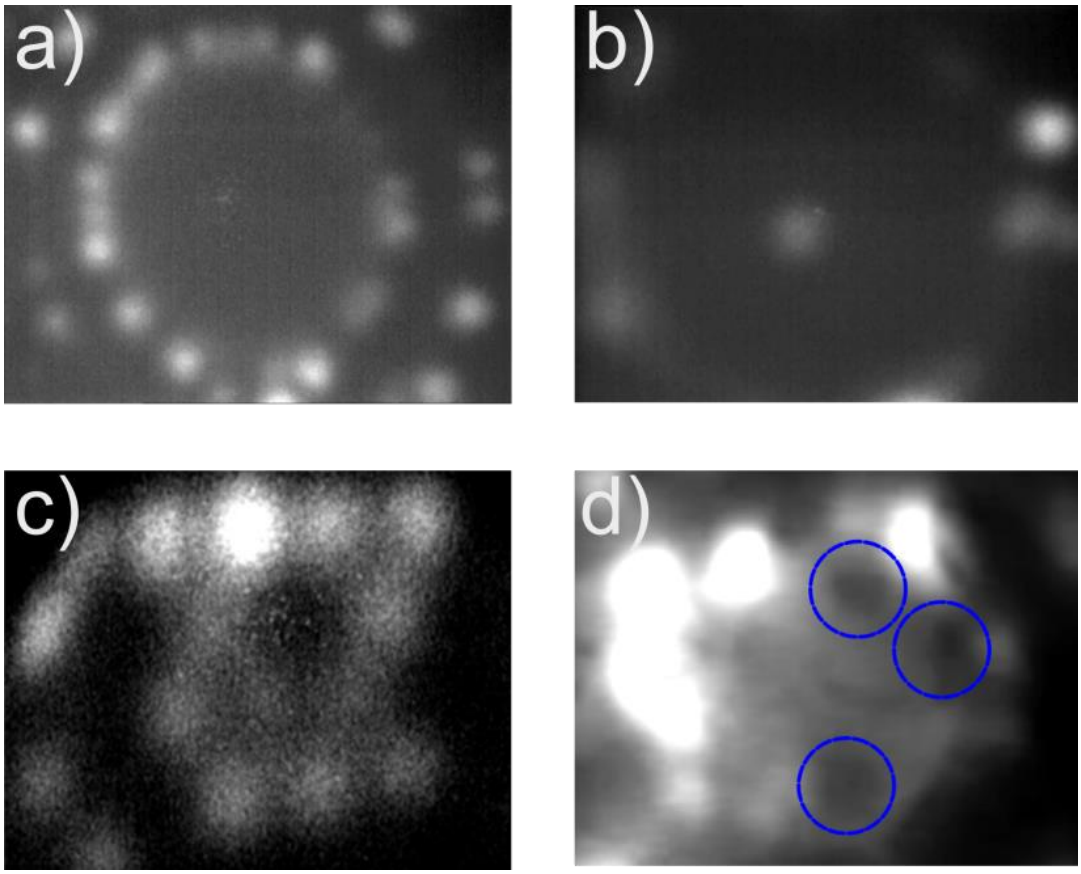

Fig. 5: (a) FIM micrograph of W(100) plane. The ionization occurs mostly at the surface's step edge. (b) FIM micrograph of magnified W(100) plane with W adatom in the center. (c) FIM micrograph of W(311) with interior atoms and a surface vacancy. (d) FIM micrograph of W(100) plane imaged in He-Ne mixture at near evaporation field. Blue circles show the surface mono vacancies.

1.4.1 The exchange mechanism

The idea of the exchange mechanism appeared in 1979 as a result of a work published by Bassett and Webber [26] who observed a two-dimensional movement of an adatom on a channeled surface. Initially they thought that the adatom diffuses through the gap in the atomic row created by thermal vibrations of the surface atoms. In 1980, Halicioglu et al. [27] and DeLorenzi et al. [13] conducted theoretical investigations of possible adatom diffusion mechanisms and they proposed the adatom exchange as an alternative to the jump mechanism. The major difficulty in delivering the experimental evidence for the exchange was demonstrating that the atom, which remains on the top of the plane after the diffusion, comes from the substrate and it is not the adatom which was previously deposited. Wrigley and Ehrlich [12] overcame this obstacle by using a very sensitive atom probe. They adsorbed a tungsten adatom on a Ir(110) surface and they heated the sample, allowing the adatom to diffuse. When they observed that the adatom moved to an adjacent channel, they desorbed it and investigated it with a mass spectrometer. They found that the desorbed adatom was Ir instead of W. Then they desorbed the first layer of the Ir(110) surface to find the W atom. The detected tungsten adatom completed a first experimental proof for the exchange mechanism. An alternative method of proving the exchange was delivered by Kellogg [25], who investigated the diffusion of Pt on Ni(110). He established that the field desorption of the Ni adatom deposited on the Ni(110) plane occurs at about 75% – 85% of the evaporation field of the whole plane, whereas the Pt adatom evaporates from the Ni(110) surface at the surface evaporation field, i.e. 35 V/nm. In addition, the spot observed on the FIM screen is much larger for the Pt adatom than for Ni. Therefore, Kellogg was able to detect the adatom exchange without using the atom probe.

In 1985 DeLorenzi and Jacucci [28] conducted a molecular dynamics simulations of the diffusion of the adatom on a model bcc(100) surface. They found that for diffusion via single jumps, the adatom moves between the nearest-neighbor adsorption sites, whereas in cases of the exchange, the adatom movement occurs between the nearest diagonal sites. Kellogg and Feibelman [22] took advantage of that result. They showed experimentally that a Pt adatom diffusing via exchange on an unreconstructed Pt(100) surface

creates a map of visited sites arranged as c(2x2) with respect to the map of the adsorption sites. If the diffusion occurred via jump, one would expect a (1x1) arrangement. The difference between the map sites visited by the adatom and the map of adsorption sites, they used as the criteria for distinguishing the exchange from the jump in two-dimensional self-diffusion movement. Even though the first simulations of the exchange were conducted on a bcc(100) surface, the experimental evidence for adatom exchange on any of the bcc(100) surfaces has yet to be delivered.

1.4.2 Coexistence of diffusion mechanisms

The coexistence of at least two diffusion mechanisms, adatom jump and exchange, is considered in most of the theoretical studies about single atom surface diffusion [7]. The mechanism with lower activation energy is taken as more favorable and more likely to be observed in the experiments. However, not much experimental work has been done to show directly the coexistence of exchange and jump mechanisms. Only few experimental studies conducted for diffusion on channeled planes [26, 29, 30] mention the occurrence of both adatom jump and exchange mechanisms. Basset and Webber [26] investigated self-diffusion on a channeled plane, Pt(110). They observed that a Pt adatom diffuses in two dimensions: along and across the channel. They suspected that in addition to the regular jumps, Pt adatom exchanges with one of the surface atoms placed in the atomic row. The calculated activation energies for the diffusion parallel and cross channel were 0.84 ± 0.1 eV and 0.78 ± 0.1 eV, respectively. Chen and Tsong [29] showed the coexistence of the exchange and the jump mechanisms on a channeled plane, for an Ir/ Ir(110) system. The obtained activation energies were 0.71 ± 0.02 eV for the exchange and 0.80 ± 0.04 eV for the jump. Prévot et al. [30] investigated mass diffusion of Pb on a channeled surface: Cu(110) with Rutherford Backscattering Spectroscopy (RBS). For the temperature range 500 – 800 K, they reported the coexistence of two diffusion mechanisms: in-channel jump and cross-channel exchange. The activation energy for diffusion of Pb was ~ 0.6 eV along and across the atomic channels. The energy difference between the jump and the exchange was calculated as 0.04 eV.

Since DeLorenzi and Jacucci [28] theoretically showed coexistence of jump and exchange mechanisms on a model bcc(100), various bcc(100) and fcc(100) surfaces were theoretically investigated. The coexistence of diffusion mechanisms on two-dimensional planes was theoretically shown for Ta, W, Mo, Fe, Cu, Ni, Pd, Pt, Rh, Ag and Au systems [7]. However, until now, no experimental evidence has been delivered for either bcc(100) or fcc(100).

1.4.3 W(100) surface

The mechanism of surface diffusion can be imposed by the arrangement of surface atoms. Diffusion properties like the activation energy and the diffusion pre-factor might be very different for reconstructed and non-reconstructed surfaces. Thus it is crucial to know the surface morphology as accurately as possible at every step of the diffusion process.

The morphology of the W(100) surface has been a subject of intense debate for over forty years. Yonehara and Schmidt [31] investigated the adsorption of H_2 on W(100) with LEED. For a clean W(100) surface, cooled to 78 K, they observed an extra (1/2, 1/2) peak in the LEED pattern. The peak, corresponding to a c(2x2) structure, disappeared at temperatures above 300 K. Yonehara and Schmidt were not sure if the observed effect was a result of the previously adsorbed H_2 or if it was related to the arrangement of the surface atoms. However, they suggested that below 300 K, the surface atoms of W(100) might be arranged as c(2x2) with a lateral shift of the atoms along the <010> directions. Felter, Barker and Estrup [32] carried out the investigation on reconstruction of a W(100) surface with LEED. In their research, much more attention was paid to the cleanness of the investigated surface. They observed that when a W(100) surface is slowly cooled below 300 K, the additional (1/2, 1/2) peaks appear gradually. They suggested a second order reversible phase transition of W(100) surface: from an arrangement (1x1) to c(2x2). In their model of W(100)-c(2x2), every second atom was protruding from the surface plane without any lateral shift (Fig. 6a). The model proposed by Felter et al. [32] we call the FBE. In the same year, Debe and King [33, 34] proposed an alternative model of W(100)-c(2x2) surface called the “zig-zag”, where every second

surface atom is laterally shifted along <110> directions (Fig. 6b) and there are no protruding atoms. Debe and King took a closer look into the intensity of LEED (n/2, n/2) beams. They noticed that (±n/2, ±n/2) and (±n/2, ∓n/2) beams have different absolute intensities, which would not occur if the morphology of W(100) surface corresponded to the FBE model [34]. Debe and King also suggested diminishing of the reconstruction at the surface's step edge [33]. Barker and Estrup [35] analyzed the intensity of the LEED spots as a function of the energy of primary electrons. From the LEED I-V analysis, they estimated the values of the lateral displacement of surface atoms as 0.15 – 0.30 Å. Altman and Estrup [36] used X-ray diffraction to determine the displacement of surface atoms in zig-zag W(100) surface. They reported the displacement equal to 0.24 Å. Spišák and Hafner [37] verified that result with the DFT calculations, by obtaining the shift 0.27 Å. Wengelnik et al. [38] utilized the STM to investigate the structure of the W(100) surface. For a clean surface, kept at 85 K, they resolved atomic rows which they related to the zig-zag model. They measured the distance between the rows, as 4.5 Å.

Even though the W(100) zig-zag model seems to be correct for large terraces, it has been undermined for small planes. Melmed et al. [39] investigated the structure of W(100) with FIM by field evaporation of a W(100) plane. For slow field evaporation conducted at 15 K, W(100) kept a (1x1) structure (Fig. 7a). However, they noticed that some of the surface atoms, which are adjacent to the step edge, evaporate easier than the step edge atoms. On the other hand, for field evaporation occurring at temperatures 430 – 460 K, the W(100) surface, containing ~ 19 atoms revealed squared c(2x2) structure (Fig. 7b), without any lateral displacement of the surface's atoms. Melmed et al. [39] interpreted that result as a preferable field evaporation of vertically protruding surface atoms and a proof for validity of the FBE model. Tsong and Sweeney [21] also investigated the W(100) surface with FIM. For W(100) plane, containing ~ 50 atoms, obtained via field evaporation of a W(100) oriented tip at 21 K, they observed a (1x1) structure. They questioned the zig-zag model and the existence of the c(2x2) reconstruction for small W(100) planes. In their analysis, they suggested that if surface atoms are laterally displaced, the shift must be less than 0.15 Å, which is below the resolution limit of the FIM. On the other hand, they did not explain the unusual

evaporation, leaving it as an open question. Nishikawa et al. [40] investigated the W(100) structure with FIM by the analysis of the atomic arrangement of adsorbed layers of Sn and Ga. After depositing the material on the W(100) surface, they slowly field evaporated it, while keeping the W tip at a temperature of 20 K. They noticed that the initially adsorbed layer of Sn has a (1x1) atomic arrangement and as the evaporation proceeds, it changes into c(2x2). For the Ga layer, they showed that the (1x1) structure remains unchanged during the entire field evaporation process. They interpreted the difference in atom arrangement for Sn and Ga layers as disprove of the FBE model. On the other hand, for both adsorbents, they did not observe any zig-zag structure. Based on these results they concluded that the W(100) plane with diameter ~ 50 Å, kept at 20 K, is not reconstructed at all, and observed the c(2x2) structure is related to the binding state of the adsorbed material, which changes as the evaporation proceeds.

Che et al. [41] investigated with DFT calculations the influence of the electric field on the arrangement of surface atom on W(100). Their results showed that in the presence of an electric field the W(100) plane with surface vacancies arranged as c(2x2) is more stable than a zig-zag. Thus, they concluded that the observed c(2x2) structure in FIM is a result of the applied electric field. However, their interpretation was flawed. In their calculations it was assumed that the vacancies in the c(2x2) surface already exist before the field is applied. That is not the case for a real experiment conducted with FIM, where the surface obtained from the field evaporation does not contain any vacancies. In addition, the electric field acts on all of the surface atoms, therefore should shift them uniformly. Also, the strength of the applied electric field is too small to change the zig-zag into the FBE arrangement during imaging. Tsong and Sweeney [21] calculated the force acting on W(100) surface during the FIM imaging as 10^{-9} N/atom. According to their interpretation, the force acting on each surface atom during the imaging process is too small to cause any significant vertical shift of the surface atoms.

Ernst et al. [42] investigated the phase transition of W(100) from (1x1) to c(2x2), using helium-atom-scattering. They found that the transition starts at 220 K, which is much lower than the minimum

temperatures considered in our diffusion experiments for W/W(100). However, the lack of exhaustive knowledge about the structure of small W(100) planes, and about its potential influence on diffusion mechanism demands a closer look into that issue.

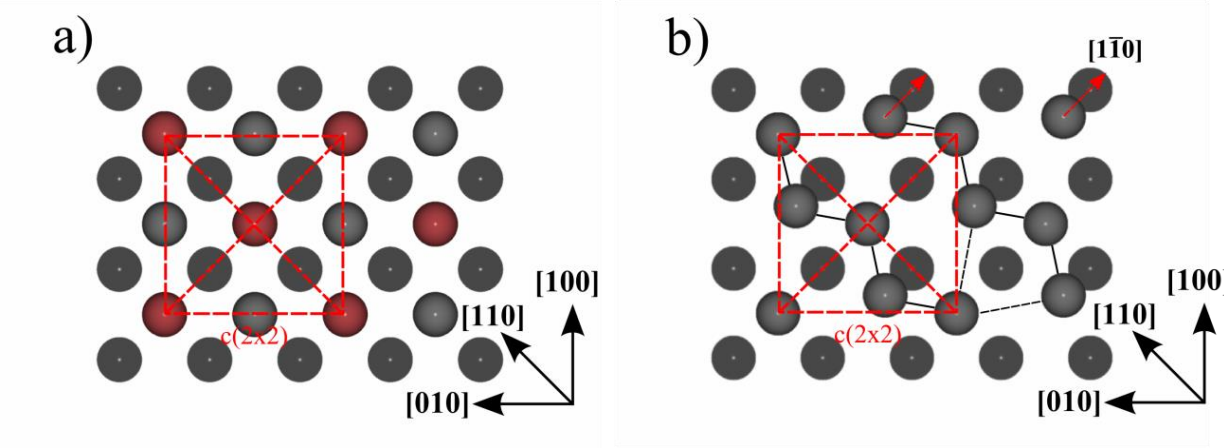

Fig. 6: (a) FBE model of W(100)-c(2x2) surface with protruding surface atoms; (b) the "zig-zag" model of c(2x2) reconstructed W(100) surface with surface atoms laterally displaced along [1-1 0] direction.

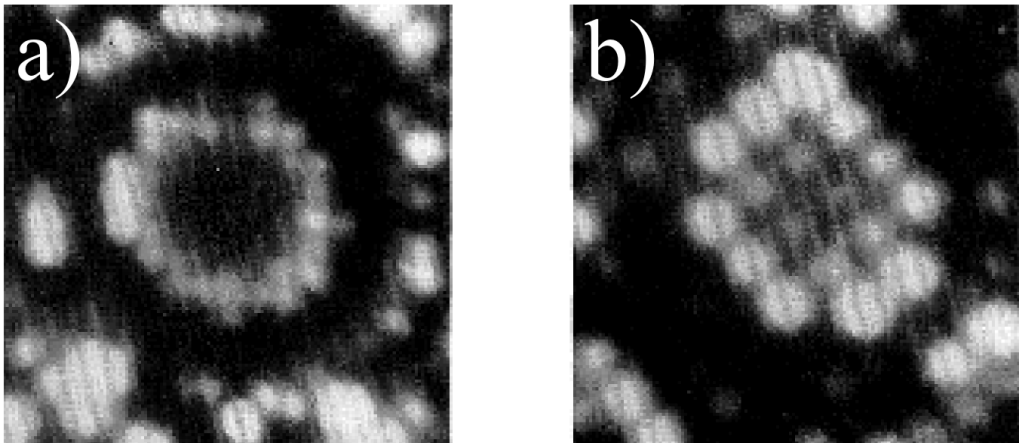

Fig. 7: (a) W(100) surface obtained from field evaporation at 15 K. The arrangement of surface atoms is (1x1). (b) W(100) surface obtained from field evaporation at 430 K. The arrangement of surface atoms is c(2x2).

1.4.4 Diffusion on a W(100) surface

Even though tungsten was the first and the most often investigated material in surface diffusion studies [7], not much work has been done about diffusion on the W(100) surface. Kellogg [43] investigated the diffusion of Ni adatoms and Ni dimers on a W(100) surface with FIM. He found that both the adatoms and the dimers diffuse via jump only. The measured activation energy for the diffusion of the Ni adatom was 1.01 ± 0.02 eV and the diffusion prefactor was assumed to be $2x10^{-3}$ cm^2/s. Kellogg [43] noticed that the diffusion of dimers at the time scale of seconds, starts at temperature about 50 K higher than diffusion of single atoms. In his measurements, Kellogg did not pay attention to the morphology of W(100) surface.

Spišák and Hafner [37] conducted DFT calculations on diffusion of Fe adatom on W(100) and W(110) surfaces. They found that on a non-reconstructed and a zig-zag reconstructed W(100), the Fe adatom diffuses more favorably via jump than exchange. The calculated values of the activation energies for the jump on zig-zag reconstructed surface along <011> directions were: 1.2 eV for the jump across the long bridge and 1.3 eV across the long short bridge. For non-reconstructed surfaces, the calculated energy for a jump was 1.6 eV and for the exchange it was 2.1 eV. For the adatom exchange on a zig-zag reconstructed surface, the activation energy was 2.3 eV. When Spišák and Hafner [37] allowed the surface to relax after depositing the adatom, they noticed that the zig-zag reconstruction around Fe adatom locally diminishes.
Recently, Chen and Ghoniem [19] used DFT calculations to investigate W adatom diffusion on free and strained W(100) surfaces. They reported the occurrence of three different diffusion mechanisms: crowdion, adatom exchange and adatom jump. For the diffusion on unstrained W(100) surface the obtained activation energies for the diffusion steps in crowdion were: 1.57 eV for the crowdion formation, 0.19 eV for crowdion migration, and 0.14 eV for crowdion to adatom transition. The activation energies for adatom exchange and adatom jump for the same surface were calculated as 1.84 eV and 2.57 eV, respectively. Until now it was the only work conducted for surface self-diffusion on W(100) surface.

2. EXPERIMENTAL SETUP AND SYSTEM PREPARATION PROCEDURES

Field Ion Microscopy (FIM) is a powerful technique which allows imaging the surface with atomic scale resolution [20]. The experiments on surface diffusion obey rigorous requirements for Ultra-High Vacuum (UHV) conditions and surface purity [7]. The base pressure in the FIM chamber must be as low as 10^{-11} Torr to not corrupt the measurements [7]. Also the amount of hydrogen must be at negligible level to not affect the diffusion measurements e.g. by reconstructing the surface [44]. The presence of hydrogen is a common issue for stainless steel systems and it is difficult to detect with standard Bayard-Alpert ionization gauges. To fulfill such strict requirements, a special kind of FIM was designed and built in Gert Ehrlich's Research Group, in the Materials Research Laboratory at the University of Illinois at Urbana-Champaign.

2.1 Description of the Microscope

The apparatus used in the experiments contains two chambers: the microscope chamber and the gas preparation chamber (Fig. 8). Both parts are made of Pyrex glass, which is almost impenetrable for residual gases other than helium [45]. In contrary to stainless steel systems, the glass-based apparatus contains reduced number of joints, which are potential sources of leaks. There are only three flanges, as a part of the bellow, which holds the sample. The pressure in both chambers is measured by standard Bayard-Alpert (B-A) ionization gauges sealed into the walls of system. The sensitivity limit for B-A ion gauges is 10^{-11} Torr, which is sufficient for the diffusion studies. The metal parts of the system and the Pyrex glass have different thermal expansion coefficients. Thus all the joints of the Pyrex with metal are mediated by a uranium glass.

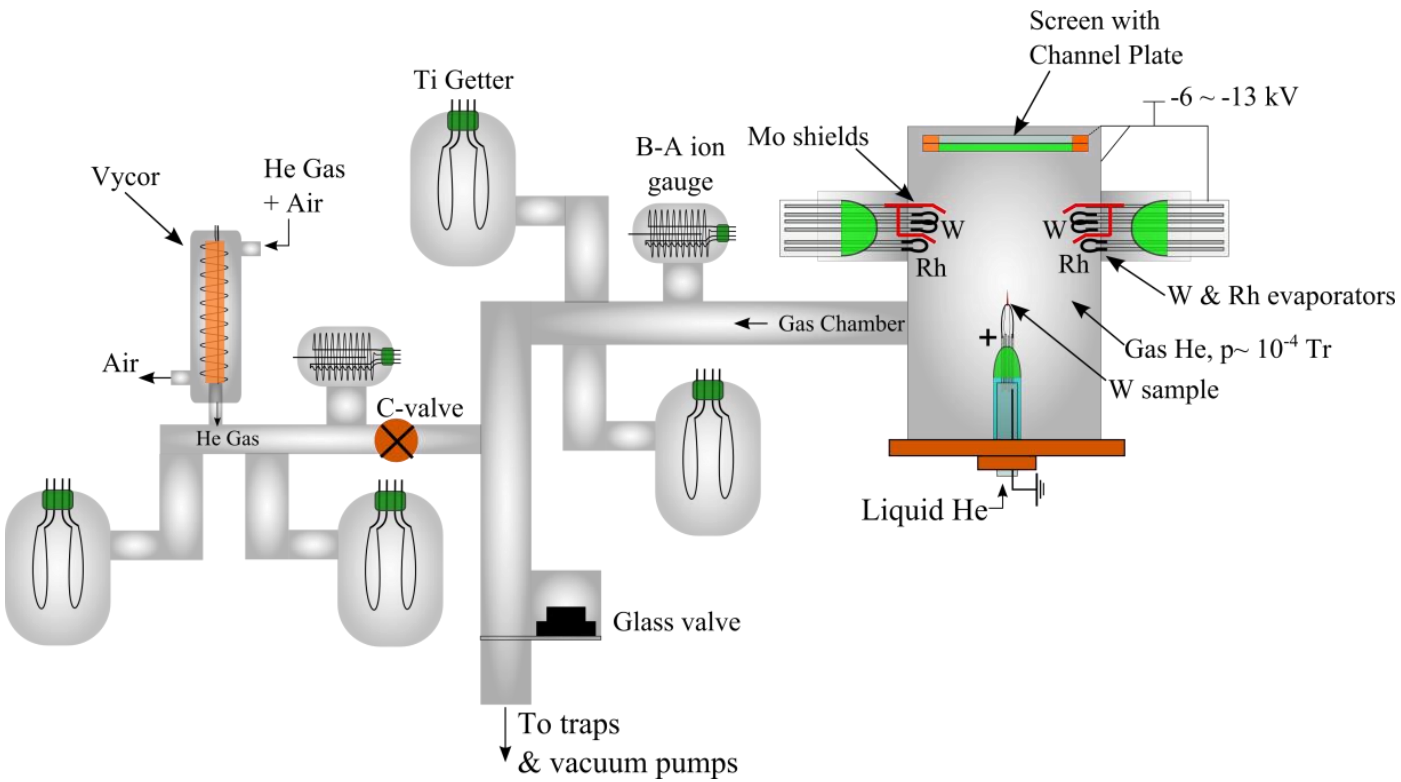

Fig. 8: Schematic of the apparatus used in the experiments. Gas and microscope chambers are separated by a closing valve. The chambers are mounted on the top of an asbestos table. The glass valve separates the system from the vacuum pumps, which are located below the table. The FIM chamber is coated with a Tin-Oxide layer to prevent collecting the electric charge during FIM imaging.

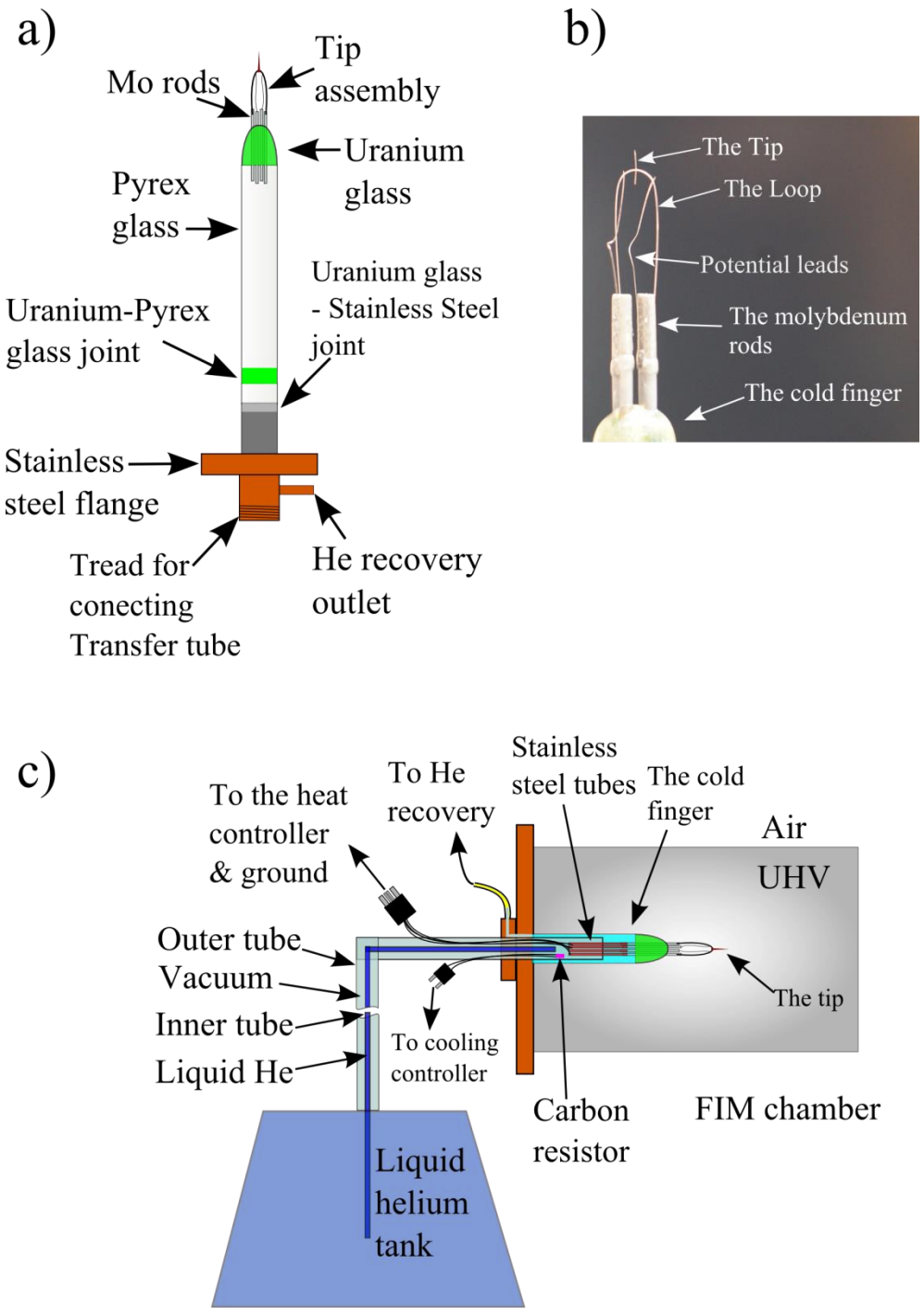

Fig. 9: (a) Schematic of a cooling and heating system. The transfer tube transports liquid helium from the tank to the cold finger and connects its pins to the temperature controller. (b) Picture of the cold finger with a tip assembly.

The imaging gas is introduced into the system by diffusing through the Vycor – a piece of quartz surrounded by the heater to accelerate the diffusion process. A DC current that is applied to the heater is set to 3.5 A when introducing helium. For introducing neon, the heating current is set to 4.5 A. In a standby condition, heating current is set to 2A to keep the Vycor clean.

The sample is mounted on a tungsten hairpin which is spot-welded to molybdenum rods melted into a glass-based assembly called the "cold finger". The cold finger **(**Fig. 9a,b) is a single-ended Pyrex tube with molybdenum rods in one end and a stainless steel flange at the other end. The melted-in molybdenum rods provide thermal and electrical contact between the sample kept in UHV chamber and the outside world. When the tip is cooled down, the rods on the air side of the system are cooled with liquid helium which is pumped through a transfer tube from a dewar. The transfer tube in addition to transporting the heat, serves also as a connector for the heat controller and as grounding for FIM imaging (Fig. 9c).

The tip is resistively heated by passing a DC current via Mo rods, through the loop. The resistance of the hairpin is measured by a pair of potential leads that are spot-welded on both sides of the tip (Fig. 9b). The resistance of the loop changes with its temperature. Thus to obtain desired temperature, one has to set corresponding resistance. The temperature controller modulates the current that is passed through the loop to reach and to keep constant desired resistance. As a result, the temperature of the loop is extremely stable and it can be calibrated with an accuracy of ± 1 K. The temperature controller was designed and built in Gert Ehrlich's research group by D. A. Reed [46]. A detailed description of the heat controller circuit and the controller calibration process is provided in Ph.D. thesis of Dr. S. Koh [47].

The evaporators (Fig. 8) which are used for adsorption of the material onto the tip are made in the same way as the cold finger. Rhodium and tungsten evaporators are made of 0.18 mm thick wires, which are spot-welded to the molybdenum rods that are melted into uranium glass. The evaporator is resistively heated by a direct current passing through the filament. The material is thermally desorbed from a hot

filament and adsorbed onto the sample. When the evaporator is at operation, a DC heating current is adjusted between 4.1 – 4.5 A. During the "stand by" condition the filaments are kept hot by passing the current of 2.5 – 3 A to prevent adsorption of the impurities on their surface. The evaporators are separated from each other by molybdenum shields to prevent cross adsorption from one filament to another. Behind the last evaporator, there is an additional Mo shield to prevent adsorption of the material onto the channel plate. The separation shields are additionally bent to direct the stream desorbed material toward the tip.

The picture of the tip's surface is resolved on a phosphorous screen placed at the front wall of the FIM chamber (Fig. 8). The projection is additionally intensified by a micro channel plate, which is assembled with the screen. A negative potential which accelerates ions during imaging in FIM is actually applied to a ring of the channel plate assembly that is facing the tip (front of the channel plate). During operation, the voltage applied across the channel plate is ~ 1.0 – 1.2 kV. To accelerate the secondary electrons emitted from the channel plate to the screen, an accelerating voltage of ~ 2.0 kV is applied to the screen. When the system is in a stand by condition, the channel plate and the screen are bombarded with electrons emitted from the evaporators. The bombardment is set, to clean both parts from the adsorbed impurities. During the stand by, the voltage across the channel plate is 0.5 kV while the voltage between the channel plate and the screen is 1.2 kV. When the system was previously opened in air, in addition to the standard cleaning of the channel plate with electrons, the FIM imaging is conducted. Due to their larger mass, helium ions that hit the surface of the channel plate clean it much more efficiently than the electrons.

The ultra-high vacuum conditions are achieved by using mercury diffusion pump supported by a rough pump (Fig. 10). The whole diffusion pump is made of glass. It is sealed into the glass tubes, which are connected to the gas chamber and to a metal hose of the mechanical pump. Before and behind the diffusion pump, the impurity traps are installed, which are cooled with liquid nitrogen. The role of both traps is to collect the back stream gases from diffusion and mechanical pumps. The trap between the microscope chamber and the diffusion pump additionally supports collecting the residual gases from the

FIM chamber. The traps must be kept cold at all times, except when they are baked out. To make sure that the dewars are filled with liquid nitrogen, special controllers have been built. In the controlling system there are two carbon resistors connected in series and separated from each other by ~ 15 cm (one resistor is placed on the top of the dewar, another is on the bottom). When the resistor is sunk in liquid nitrogen its resistance is much higher than when it is kept at room temperature. If the level of liquid nitrogen lowers below the bottom resistor, the current can pass through the circuit. Then the controller opens a solenoid valve between the liquid nitrogen tank and the trap, and the nitrogen is pumped into the dewar. The refilling continues until the upper resistor is sunk in the liquid nitrogen. For a properly insulated trap and calibrated controller, the refilling occurs every 4 – 5 hours.

The key elements of the vacuum system are the getters – micro-chambers with walls covered with titanium which is thermally desorbed from hot Ti filaments (Fig. 8). The getters (known also as a sublimation pumps) have dual functions: lowering the background pressure and purifying the imaging gas. During operation, a cloud of titanium vapor is emitted from a hot filament and spread onto the walls of the getters. The residual gases are pushed by titanium vapor toward the walls, where they are bonded. The titanium is also very effective in absorbing the hydrogen. Thus, when the imaging gas (helium) is introduced into the preparation chamber it is additionally purified from the hydrogen by the getters. During operation of the getter, a DC current is passing through the titanium filaments. The current is set to ~ 4 – 4.5 A, depending of the thickness and age of the filament. During the standby conditions, the filaments of the getters are kept hot by passing the current of 2.5 A, to prevent the adsorption of the impurities onto the filaments. The getters are at operation before and after introducing the imaging gas. To keep the walls of the microscope cool during the experiment, the getters are completely turned off right before starting the measurements. Without using the getters, the lowest base pressure achieved is ~ $3 \cdot 10^{-10}$ Torr. With the getters used right before introducing the imaging gas, the base pressure is as low as 10^{-11} Torr, which reaches the measuring limit of Bayard-Alpert ionization gauges.

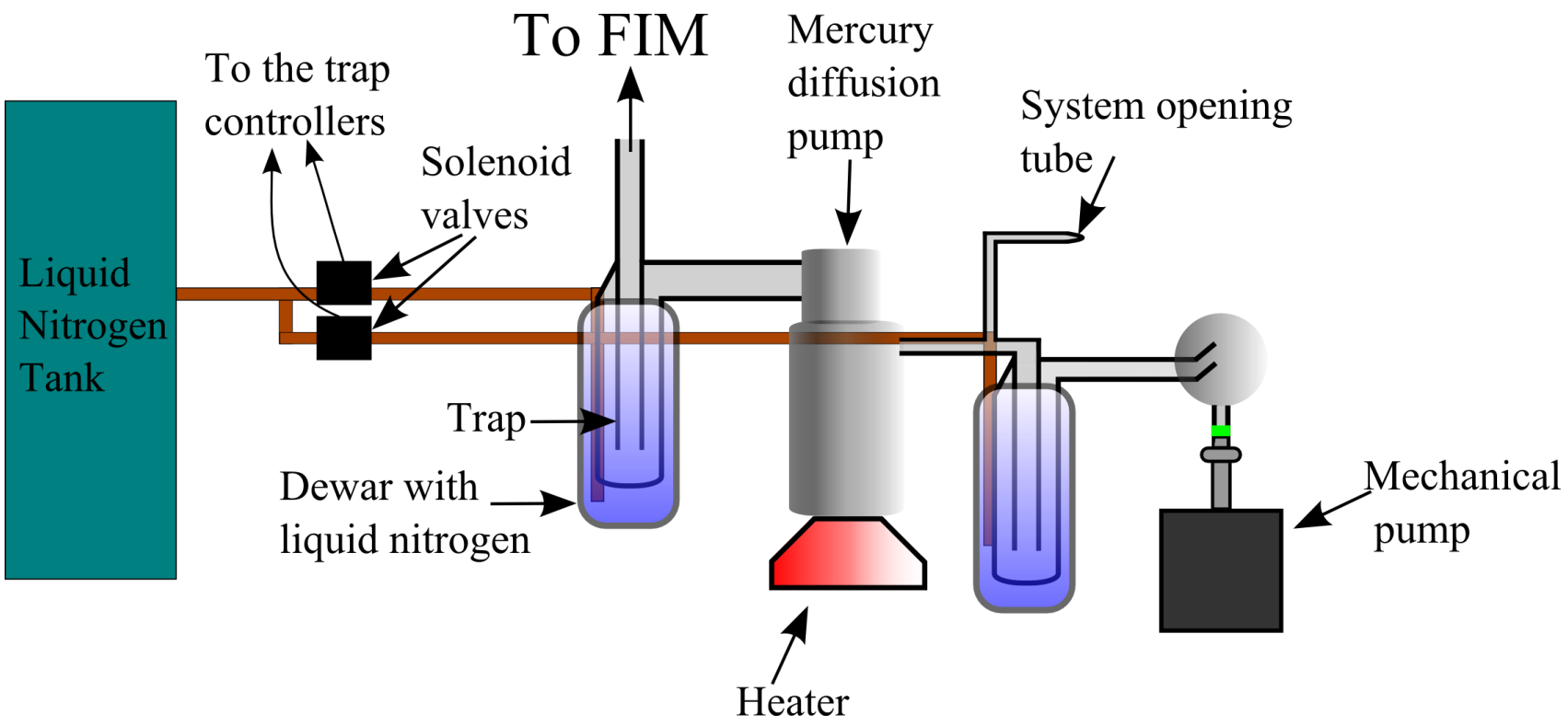

Fig. 10: Schematic of the pumping system. The pumping system is connected with chambers via a glass tube, 2.5 cm in diameter. The apparatus is vented by cracking the system opening tube in a presence of helium gas.

Since measured diffusivity is proportional to the time of heating the sample, a precise control over the heating interval is extremely important. Also after cooling the sample, one has to wait a set period of time before turning the electric field on. The measuring series requires about 60 – 140 repetitions of the following sequential steps: imaging, turning of the electric field, heating and cooling. To conduct the measurements without making a single mistake in any of the steps, a special controller was built in Gert Ehrlich Research Group, called the Sequencer (Fig. 11). The controller allows setting a time interval of each step of the cycle. The sequencer is connected to the heater and to the power supply of FIM, to turn them on and off at the proper time. The sequencer also counts and displays the number of cycles that have occurred. Each time after the controller is turned on, before starting the measurement series, the sequencer must be reset. Otherwise, it will keep the imaging field and the heating system turned off.

2.2 Data Collection and Processing

The image of the surface presented on the screen is recorded with a camera RCA TC1030/H25. The picture is transferred from the camera to the computer and to an external TV monitor via BNC cables. The current status of the sample is observed on both: computer and TV monitors. During the measurements, to provide instant information about adatom behavior, the current position of the adatom is marked on the screen of the monitor with an erasable marker. The schema of the setup for the data collection is presented in Fig. 12.

The data is recorded on the computer through a video card Kona LHi produced by AJA Video Systems ®. The program responsible for operating the video card and recording the pictures is called the Machina ™, and it was included in the software packet for the video card. The program allows recording the camera's picture in a form of a movie and also as a sequence of micrographs. In presented measurements the signal from the camera is recorded in a form of sequences of 20 pictures in a TIFF format. Each sequence is saved in a separate, properly named folder. Afterward the pictures are further processed with software called ImageJ, to enhance the contrast and to conduct the data analysis.

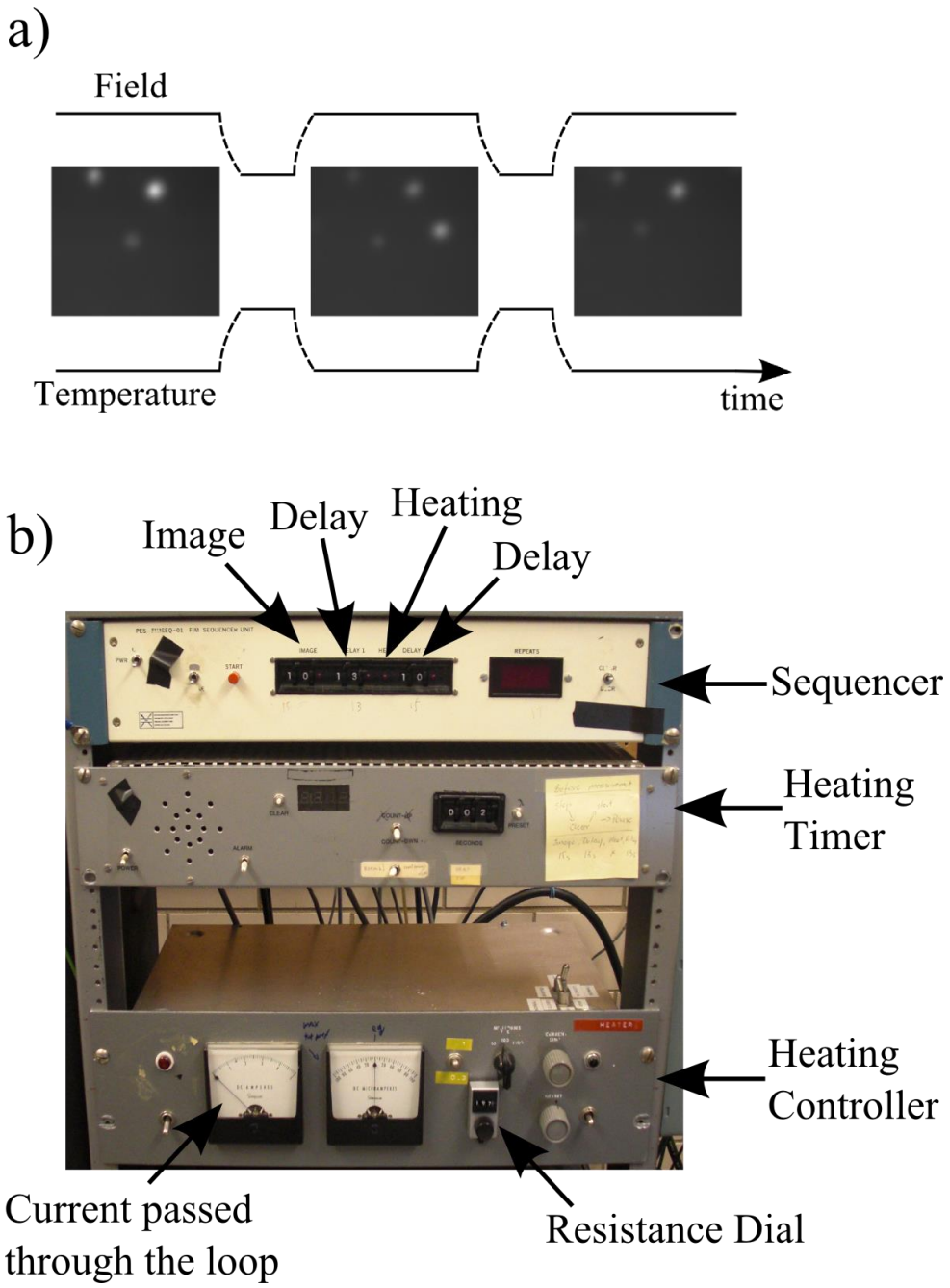

Fig. 11: (a) Measurement cycle: when the electric field is turned on the heating is turned off. When the field is turned off the heating is turned on. After a set period of time, the heating is turned off and the electric field is turned on again. (b) Photograph of the sequencer, the heating timer and the heat controller. The sequencer controls time intervals for imaging and heating. The delay between operations is set to 10 and 13 seconds to allow the sample to cool down and to make sure that the electric field is completely turned off.

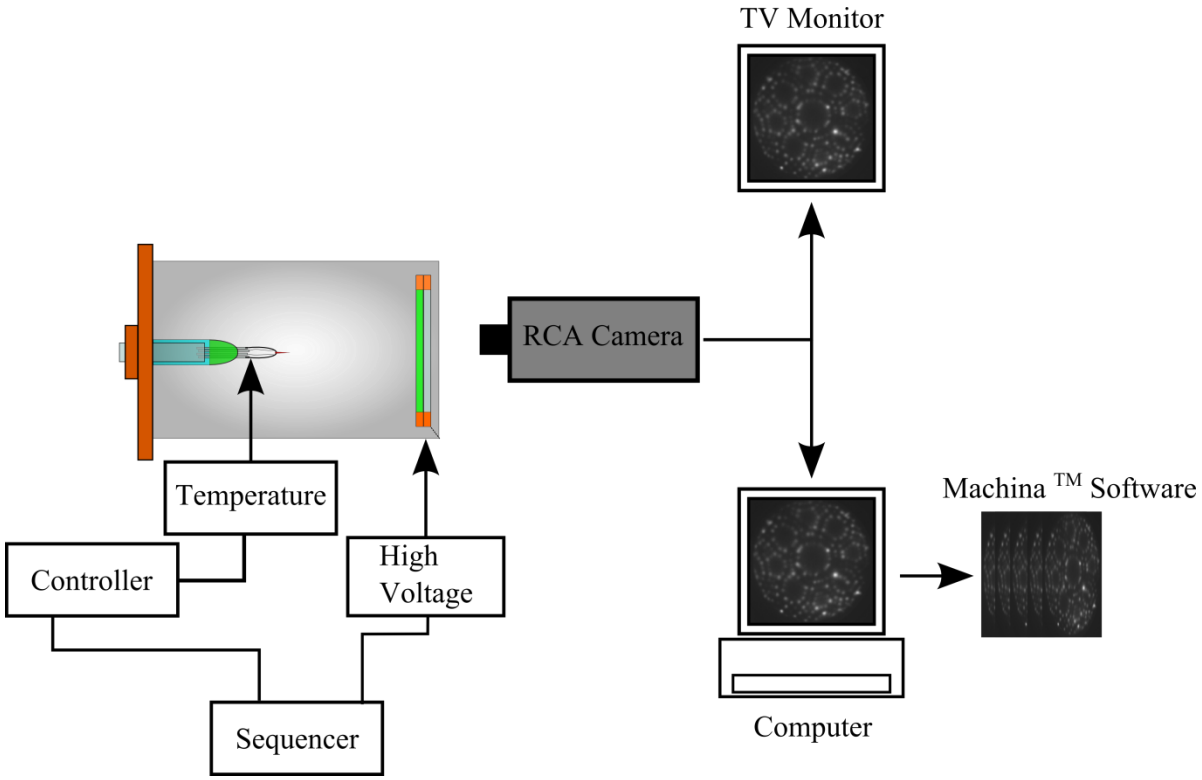

Fig.12: A schematic of the sequencer's control and the data collection. The sequencer interchangeably turns on and off the heating current and the imaging voltage. The picture of the screen is presented on the computer monitor and a TV monitor simultaneously. The picture is recorded on the computer in a form of a picture sequence.

2.3 Maintaining Ultra-High Vacuum Conditions

To maintain the base pressure of the system 10^{-11} Torr, the apparatus is baked every three weeks on a regular basis. If the system was vented, the bake-out must be done at least three times every two days. During the first stage of the bake-out procedure, the system is initially kept under the furnace at a temperature of 300 °C for 24 hours. At the same time, the trap between the FIM and the diffusion pump is baked as well, in an external furnace, at ~ 300 °C. During that process all filaments in the system and the Vycor are turned off. After 24 hours, the external furnace is turned off and the trap is cooled down to the room temperature. Then a dewar with liquid nitrogen is mounted around the trap. In the second stage of the bake-out, the temperature of the main furnace, heating the FIM is lowered to 150 °C. Then the evaporators, the getters, the ion gauges and the Vycor are turned on. To outgas the evaporator's shields, a high positive voltage ~ 1000 kV is applied to the shields. As a result, the electrons which are thermally emitted from the evaporators are bombarding the shields. In the meantime the cathodes of Bayard-Alpert ionization gauges are outgassing. The second stage of the bake-out takes about 5 hours. After the bake-out, when the system is cooled down to a room temperature, the channel plate is turned on to the standby conditions, for outgassing. To accelerate the outgassing process, additional FIM imaging is performed.

Each time after heavier imaging gas (e.g. neon) is introduced into the system, the vacuum conditions deteriorate. Introduction of the Ne requires increasing the temperature of the Vycor. Thus the atoms of the gases, which are smaller than the neon, are also introduced into the system. Some atoms and molecules of the impurities are absorbed by the Vycor during Ne introduction. After the temperature of the Vycor is decreased, the impurities are very slowly released into the system. Even though the B-A ionization gauge shows 10^{-11} Torr, the presence of impurities after introducing Ne is still noticeable with FIM, by flickering of the image. After using neon, the system can remain dirty for even three weeks. Thus introducing imaging gases other than He is not desirable. The cleaning of the Vycor can be slightly accelerated if one introduces helium while the Vycor is still hot. The impurities which are in the Vycor are relatively quickly removed, while the presence of helium gas prevents additional contamination of the Vycor.

The maintenance and the preparation of the system to the experiments requires a significant amount of time. Every major crack in the glass destroys all the evaporator filaments, the ion gauges and the tip assembly within a second. Most of the parts are handcrafted, and in cases of failure, they must be refabricated. Achieving and maintaining ultra-high vacuum conditions at a level of 10^{-11} Torr requires much work and one has to have enough luck to not open the system in the meantime. However the quality of the obtained results is extraordinary and pays for all the precautions.

2.4 Sample Preparation

The samples used in the experiments were tungsten tips about 150 – 200 Å in radius, obtained from a (100) oriented tungsten wire, with diameter of 0.127 mm, provided by FEI. There are two stages of the sample preparation: the electrochemical etching (outside the microscope) and the surface development (inside the FIM chamber). The maximum voltage that can be applied to the W(100) oriented tip before ripping it is ~ 14 – 15 kV. Thus, the tips are considered as "good", when their first imaging voltage right after etching is about 4 – 5 kV.

2.4.1 Electrochemical etching

In the electrochemical etching process, a tip wire and an external platinum loop are immersed in an ionic solution. When a DC voltage is applied between the wire and the loop, with a positive polarity to the wire, the ionic current etches it. The etching process can be controlled automatically or manually. Different materials are etched in different ionic solutions. For tungsten {100} oriented wire, two types of the ionic solutions were used: 2NaOH for automatic etching and NaOH for manual etching.

The method used for automatic etching is called the "Drop-off technique" [46]. The wire is sunk ~ 1 – 2 mm deep into the solution of 2NaOH and the voltage is applied (Fig. 13a). Due to the surface tension, the etching occurs more rapidly at the surface of the solution. As a result, the wire is thinner at the surface area. The created neck narrows as the etching progresses (Fig. 13b) and at some point it breaks leaving a

sharp tip (Fig. 13c). The etching process must be stopped as soon as "the head" of the wire falls off. For that purpose, a special device called "the tip etcher" was designed and built in Materials Research Laboratory at UIUC. The tip etcher turns off the circuit in the case of a dramatic drop of the ionic current. That situation occurs when the neck breaks (Fig. 13c). For fabricating FIM tips from W(100) oriented wire, the etching voltage is set to 9.9 V and the optimal initial etching current is ~ 2.2 mA. The initial current depends on the depth of sinking the wire. The tips are considered as "good candidates" to test in FIM, when the neck breaks at 0.05 mA – 0.07 mA. The first imaging voltage for the tips etched automatically is 4 – 5 kV.

If the tip is etched manually, the wire is sunk in the film of ionic solution NaOH, stretched on a platinum loop (Fig. 14a). The etching is controlled by a manual "trigger", which closes the circuit when it is pressed and immediately breaks it when it is released. Such a design gives very good control over the etching current. The voltage between the wire and the loop is controlled by a potentiometer. At first, the wire is narrowed by etching in the film (Figs. 14b1, 14b2). The applied etching voltage is decreased from 2 V to 1 V as the wire narrows, to slow down the etching process. When the voltage is decreased to ~ 600 mV, a thin film of the solution is replaced with a thick drop (Fig. 14b3). When the wire is sunk into the drop, the narrowing of the apex inside the drop is much slower than at the drop's surface. Thus one has better control over the etching process (Fig. 14b4). The tip is considered as sharp when the tip's apex is dimmed by the diffraction grating. Such sharpness can be achieved by careful narrowing the apex, or by adopting the drop-off method i.e. narrowing the neck of the wire until its head falls off. The manual etching is much more time consuming than the automatic etching. The sharpness of the wire strongly depends on one's judgment and control over the trigger. However, the tips etched manually are much sharper than tips etched automatically. Their first brightening voltage is ~ 3 – 4 kV. The manual etching can also be used to identify the flaws in the wire, which cause issues for automatic etching.

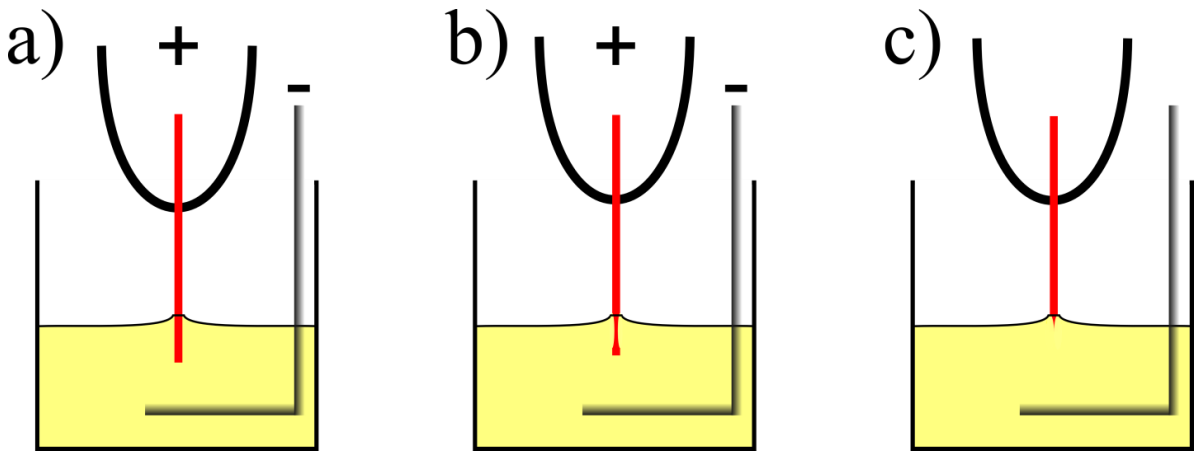

Fig. 13: Schematic sequence of tip etching via “drop-off method”. The wire is etched more rapidly at the surface of the electrochemical solution. After the neck breaks, the circuit is shut down.

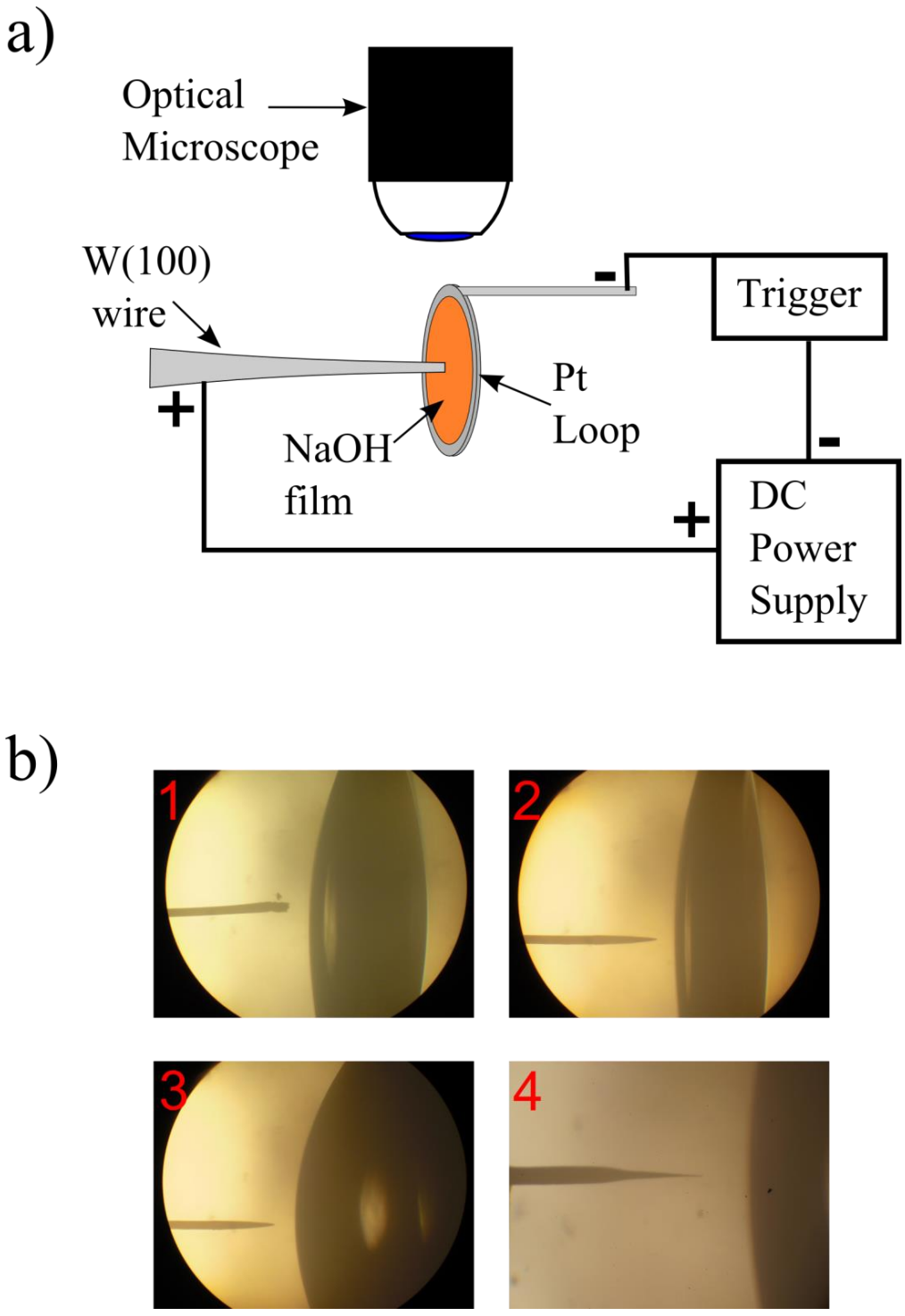

Fig. 14: (a) Schematic of the setup for the manual tip etching. (b) Sequence of the tip etching process: W wire etched in a NaOH film that is stretched on a Pt loop (1 – 2). The tip is being narrowed in a droplet of NaOH until the tip apex is dimmed by the diffraction grating (3 – 4).

2.4.2 Preparation of the sample in FIM chamber: Field evaporation and ion sputtering

After etching, the tip's surface is covered with oxygen, water and other contamination which must be removed. Also, the surface of the tip apex is very irregular. To clean the sample and to resolve the tip's crystal planes, further processing of the sample is required in the FIM chamber. The two major operations that are used for preparing the sample are: the field evaporation and the ion sputtering

Field evaporation

In the presence of a high electric field, the energy required for adatom desorption is lowered (Fig. 15). The field evaporation of the surface occurs when the electric field acting on the tip's surface is ~ 10 V/Å per atom [20, 48]. The most protruding areas of the tip's apex are evaporated first (Figs. 16a,b) [20]. As the desorption proceeds, most of the surface roughnesses and impurities are removed from the apex. Finally, a hemispherical shape of the tip apex is obtained (Fig. 16c). If there are no grain boundaries or other defects, the surface planes on the tip can be easily identified. In most cases the step edge atoms are desorbed first. By controlling the rate of the field desorption one can control the size of crystal planes. The selective evaporation of individual atoms, allows controlling the number of adatoms that are present on a crystal plane. Such control gives a tremendous advantage of FIM over other techniques used in diffusion studies.

Every time before starting the measurements few surface layers of the tip were field evaporated. The reason for that was to remove the dirt from the top of the surface and from underneath it. Also before the measurements, the tip was annealed and field evaporated in cycles, to remove the dirt from the shank of the tip.

Ion sputtering

If sufficient negative potential is applied to the tip, the electrons are emitted from its surface. If at that time the imaging gas is present, the electrons emitted from the tip hit the atoms of the gas ionizing it. The ions of the gas accelerate towards the tip striking its surface. The kinetic energy of the ions is proportional to

the applied voltage. As a result, the electron emission sources like atoms and molecules are knocked out from the tip's surface. The process of removing the material from the surface by the ion bombardment is called the sputtering [1]. In FIM, the sputtering process is mostly used for two purposes: cleaning the surface and re-sharping the tip. It is extremely useful method for restoring the sample, since it allows keeping the system at ultra-high vacuum conditions. However the effective sputtering must be conducted with gases, which atoms are larger than helium (e.g. Neon). Thus, even though the system was not opened, it still requires some cleaning after the sputtering process.

With developed recipes, the preparation of the sample takes about 1 – 2 days. If there is no accident, gently evaporated W(100) tip can be used for 2 – 3 weeks before next sputtering and for few months before next re-etching.

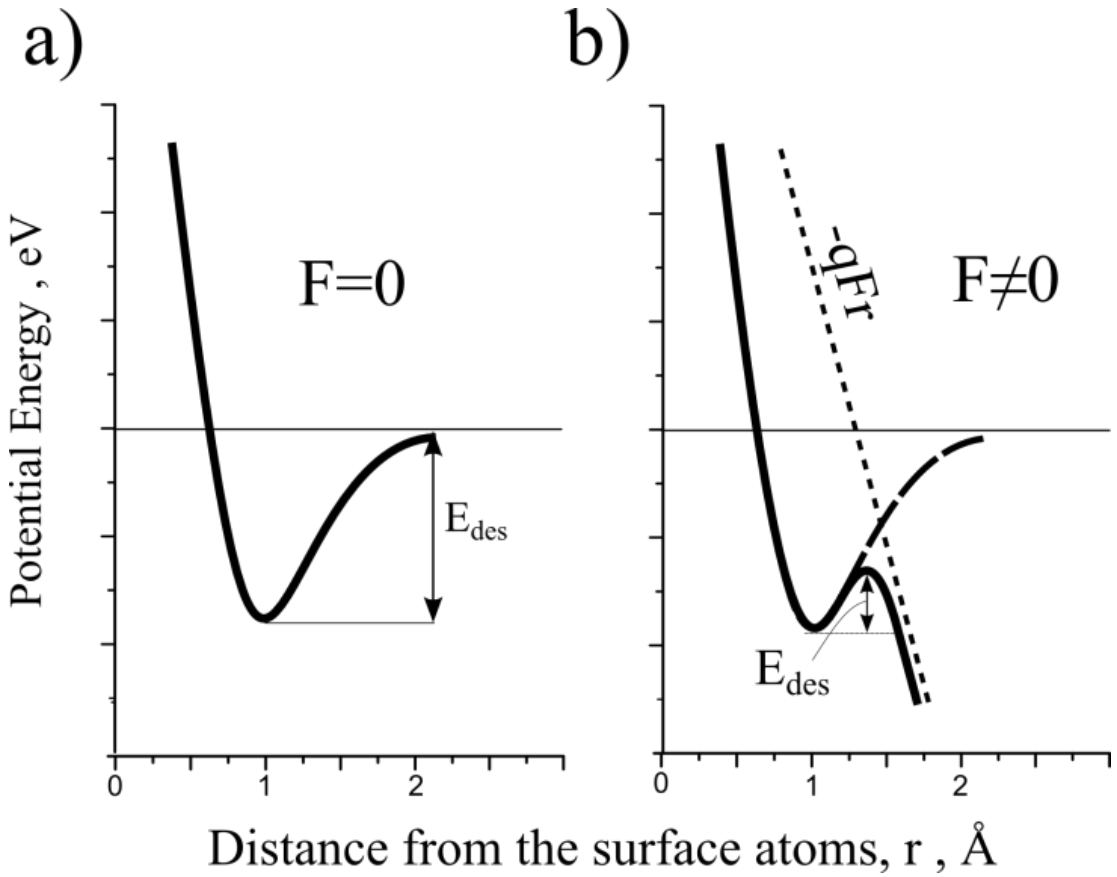

Fig. 15: Energy diagrams of the surface atom. E_{des} is the energy required for desorption of a surface atom. (a) If the electric field is turned off (F = 0), the shape of the potential energy corresponds to Lennard-Jones potential. (b) If a positive electric field is applied to the tip, E_{des} is lowered. Thus the potential barrier for the desorption can be overcome. The surface atom is desorbed in the form of a positive ion [49].

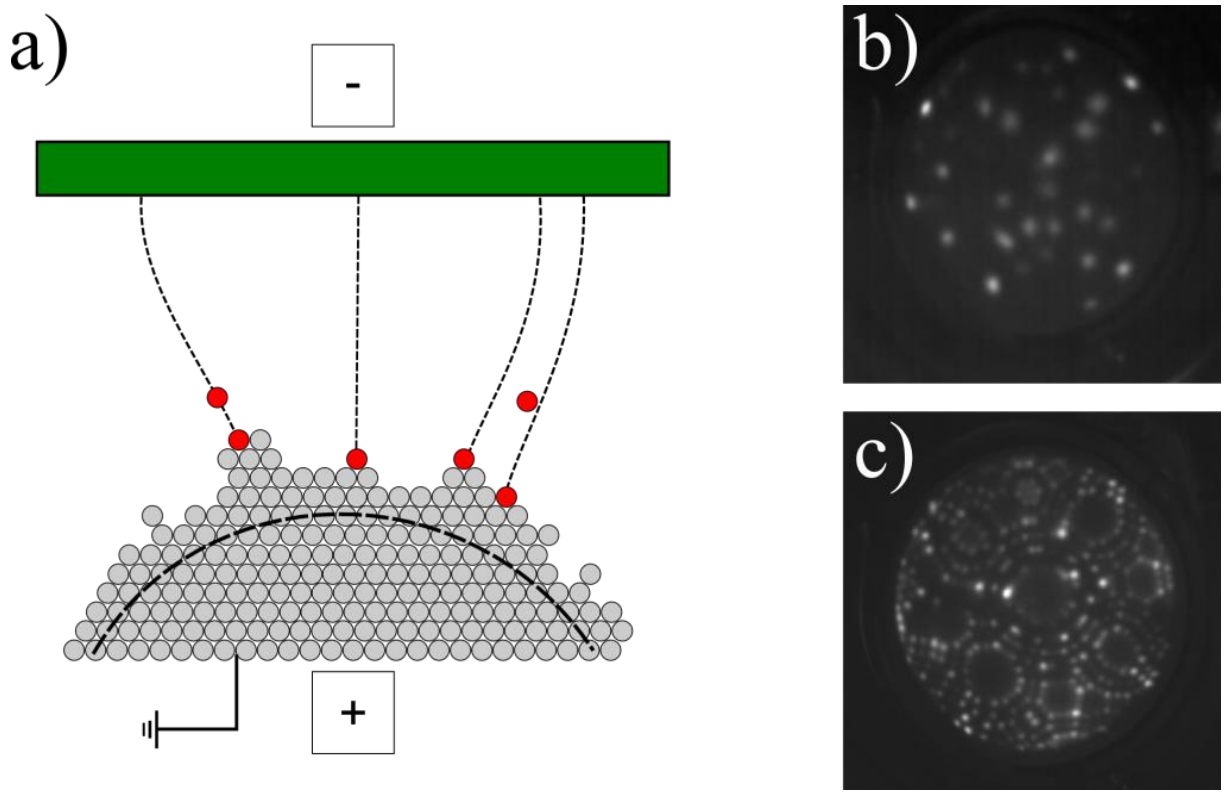

Fig. 16: (a) Schematic picture of field evaporation. The surface sharpnesses are desorbed first. (b) FIM micrograph of the surface of W(100) oriented tip right after etching. (c) FIM micrograph of W(100) oriented tip after field evaporations.

3. MEASUREMENT PROCEDURES

All the experiments are conducted in a presence of helium imaging gas, introduced into the FIM chamber. During imaging, the pressure of the gas is 10^{-4} Torr. Every time before starting the measurement session, the sample is cleaned by ~ 20 cycles of temperature flashing at ~ 500 K for 10 seconds, followed by field evaporation. The purpose of this procedure is to remove the impurities from the shank of the tip. Otherwise, the dirt can diffuse to the tip apex during the measurements and corrupt the results. Additionally, right before starting the experimental series, a few layers of the tip's surface are field evaporated to remove potential impurities from the sub-surface area and to obtain a well-defined W(100) plane. The field evaporation is conducted in the presence of helium gas in the FIM chamber, to observe the desorption process.

After cleaning the sample, tungsten and rhodium adatoms are deposited on the W(100) plane from W and Rh evaporators. During the adsorption process the surface is kept cold at 20 K and the electric field is turned off. The evaporators' deposition rates are set to adsorb on the W(100) plane only one adatom every four deposition attempts. All of the excessive adatoms that are accidentally deposited onto the W(100) plane are removed by a careful field evaporation. It has been found that the tungsten adatoms placed in the plane interior of a W(100), desorb at slightly higher voltage than the step edge atoms. Thus before the evaporation of the excess adatoms, the sample is heated first, to move the adatoms to the step edge. Since the field evaporation of additional adatoms can result in decreasing the size of the plane, it is important to keep the adsorption rate low.

W adatoms are also obtained by a gentle field evaporation of a whole W(100) plane. There is no physical difference between the adatom deposited from the evaporator and the adatom created from the field desorption of the surface [50]. Moreover, the method of obtaining the adatom from the surface is better for keeping the vacuum conditions, since the evaporators heat the walls of the chamber during operation [50].

3.1 Diffusion Experiments

After a tungsten adatom is deposited onto the W(100) surface, its position is resolved with FIM. The picture of the surface with the current position of the adatom is recorded with an RCA CCD camera and saved on the computer. Then the field is turned off and the sample is heated at an elevated temperature for a set period of time to allow the adatom to diffuse. Afterward, the sample is cooled down to 20 K and the electric field is applied again, to image a new position of the adatom (Fig. 17a). The cycle of imaging, heating, cooling, and imaging again is repeated ~ 70 – 140 times for temperature range 648 – 726 K. As a result an accurate map of visiting sites is resolved (Fig. 17b,c) and a proper statistic is collected for determining the values of the mean square displacement and the activation energy. For the analysis of single W adatom diffusion on W(100) surface, the total number of measuring cycles was ~ 1300.

During the measurements, great care must be taken to make sure that the diffusion of the adatom is not affected by any additional atoms crossing the W(100) plane. Over time, the imaging gas becomes contaminated with residual gas molecules. The presence of the impurities in the imaging gas can be detected during the imaging. If the imaging gas is clean, the picture of the surface has uniform intensity. If the gas is dirty, then the picture blinks. The reason for blinking is that the impure gas atoms have different ionization fields than the atoms of the imaging gas. The presence of the electric field can prevent some of the gas impurities from being adsorbed onto the surface. However, during the heating, when the electric field is turned off, the impurities can be adsorbed on the surface and diffuse across the tip. To make sure that such a situation does not occur, the whole tip is field evaporated and the imaging gas is changed after every two hours of uninterrupted measurements.

Since the diffusion process is investigated at temperatures 648 – 726 K, high index planes are decomposing over time. The diffusion of detached atoms across the tip is slowed down by the step edge barriers at the surface planes. However, if occasionally, some of the foreign adatoms climb up on top of

the W(100) plane, then the measurement is interrupted and the whole tip's surface is field evaporated. Then, a new adatom is adsorbed to a new W(100) plane and the measurement is resumed.

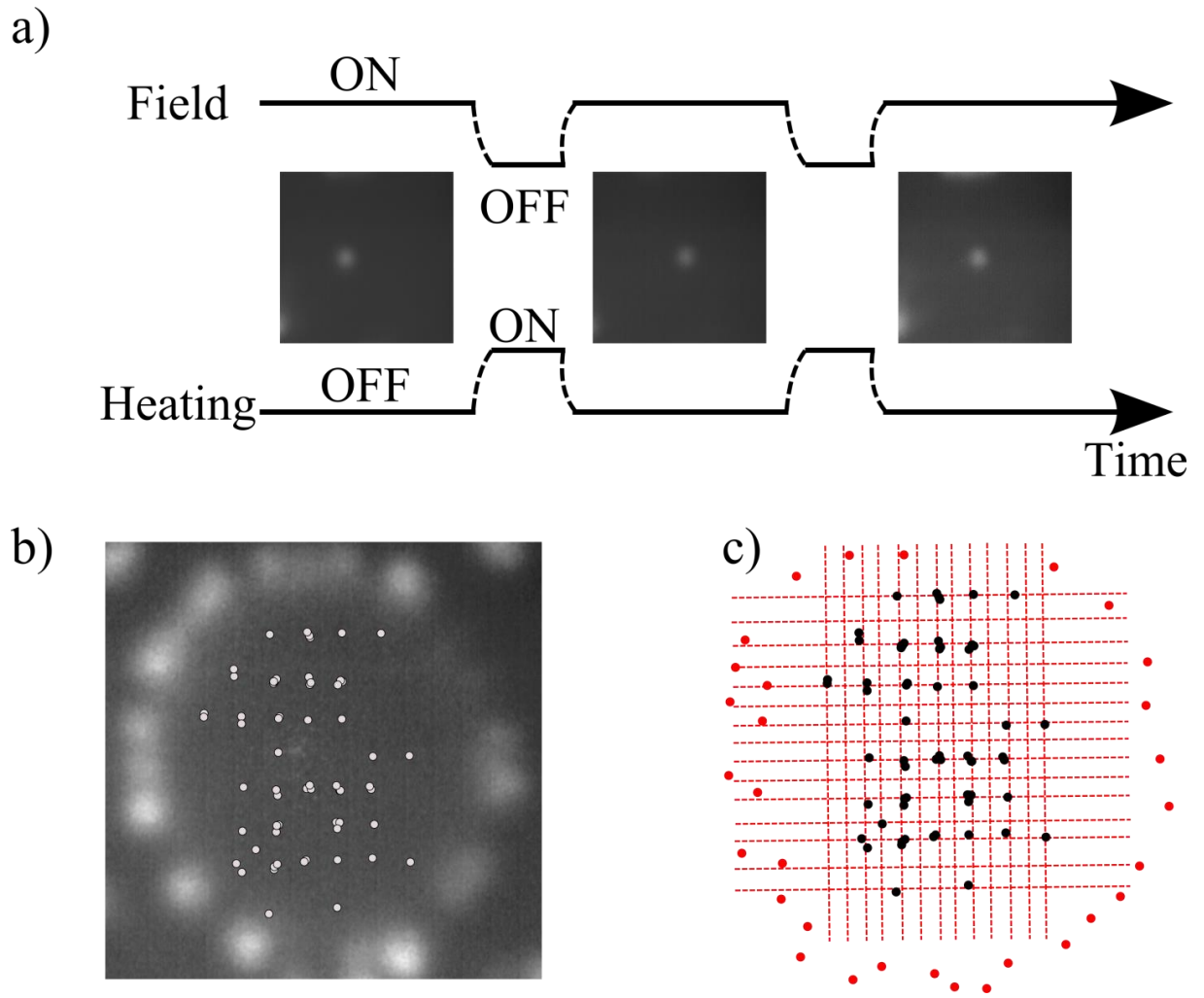

Fig. 17: (a) Measurement cycle – imaging, heating, imaging. (b) Magnified W(100) plane with marked positions visited by diffusing adatom. (c) Map of sites visited by the adatom (black dots) with a grid matched to the sites and with marked positions of the step edge adatoms (red dots).

3.1.1 Diffusion mechanism

The diffusion mechanism is found from the analysis of the map of sites visited by the adatom. When the map of sites is resolved, a grid is matched to the sites. Then, the orientation of the grid is determined by comparing it with the position of the surrounding planes (Fig. 18). For non-reconstructed bcc(100) surface, the orientation of the grid along <100> directions corresponds to a (1x1) arrangement of the adsorption sites. If the grid is oriented along <110>, then the arrangement of the adsorption sites is c(2x2). If the adatom diffuses via a jump or crowdion mechanism, the visited sites are arranged as (1x1), (Fig. 19a). If the adatom diffuses by the exchange, the arrangement of the sites is c(2x2), (Fig. 19b).

3.1.2 Mean square displacement, activation energy and diffusion prefactor

The picture resolved on the screen of FIM is a stereographic projection of a hemisphere. The distances between objects are magnified as they are projected away from the center of the screen [7]. Therefore a linear scale for the distances does not apply to FIM micrographs. To analyze the adatom movement, a new coordinate system is constructed based on the grid lines of the map of the visited sites. The numbers are assigned to the grid lines. The distances between points are recalculated to the units of a crystal lattice and to the metric units. A single displacement of the adatom is determined by subtracting the coordinates of its current position from the coordinates of the previous position. From the mean square value of the displacements $<(\Delta r)^2>$, the diffusion coefficient D is determined using the Einstein-Smoluchowski formula for two-dimensional diffusion:

$$\langle(\Delta r^2)\rangle = 4\,D\,\tau \tag{4}$$

τ is the time interval of heating the sample. The obtained values of diffusivities are plotted on a semi-logarithmic scale as a function of temperature. The activation energy E_D and the diffusion prefactor D_0 are determined from the Arrhenius relation:

$$D = D_0 \exp\left(-\frac{E_D}{k_b T}\right) \tag{5}$$

.

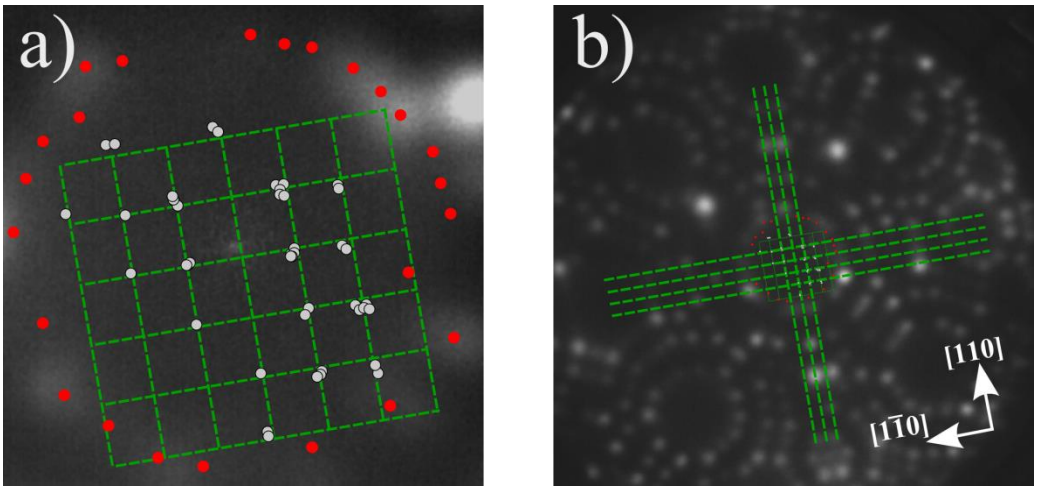

Fig. 18: (a) FIM micrograph of magnified W(100) plane with marked positions visited by an adatom diffusing at 682 K. (b) FIM micrograph of W(100) oriented tip taken at 10.3 kV, the grid is oriented along <110> direction.

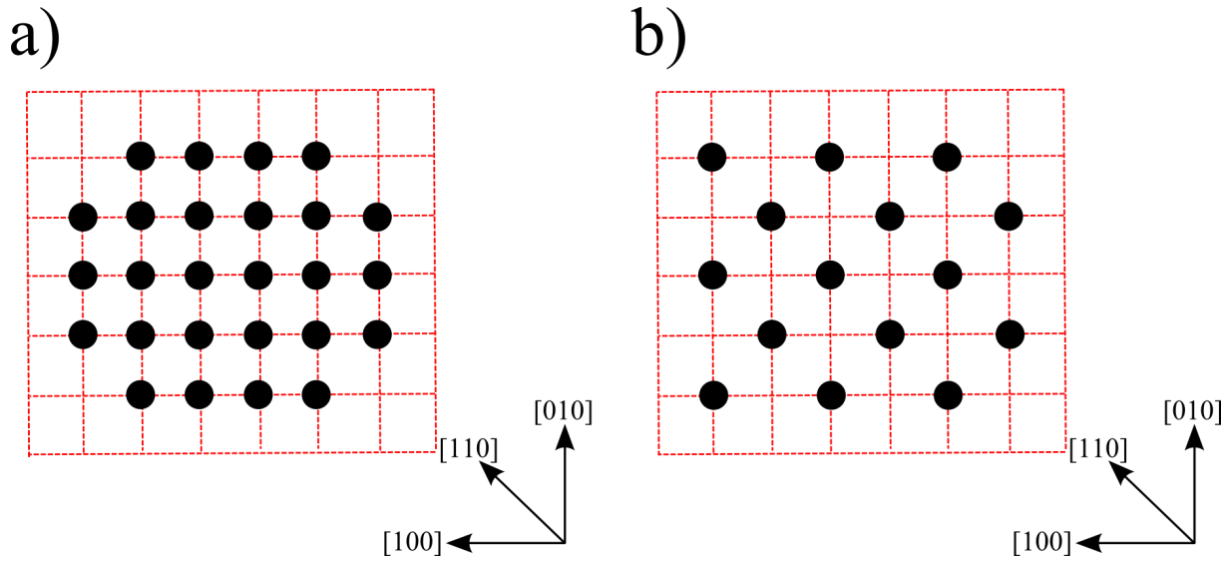

Fig. 19: (a) The map of sites visited by an adatom diffusing via the jump mechanism, corresponding as (1x1) to the arrangement of the adsorption sites on a bcc(100) surface. (b) The map of sites visited by an adatom diffusing via the exchange mechanism, corresponding as c(2x2) to the arrangement of the adsorption sites on a bcc(100) surface.

3.1.3 "Zero-time measurements" correction

The obtained values of the mean square displacements must be corrected for the adatom movement, during the heating and cooling process – before a desired temperature of the sample is reached. The correction is done by conducting so-called "zero-time measurements" (Fig. 20). In those measurements, the heating time interval is set to 0.01 s, so the sample is heated and immediately cooled down after reaching the desired temperature. The obtained "zero-time" mean square displacements $<(\Delta r)^2>_0$ are subtracted from the non-corrected results:

$$\langle(\Delta r)^2\rangle_{corr.} = \langle(\Delta r)^2\rangle - \langle(\Delta r)^2\rangle_o \tag{6}$$

The final result is a real value of the mean square displacement for investigated temperature. The zero-time correction is done for all temperatures.

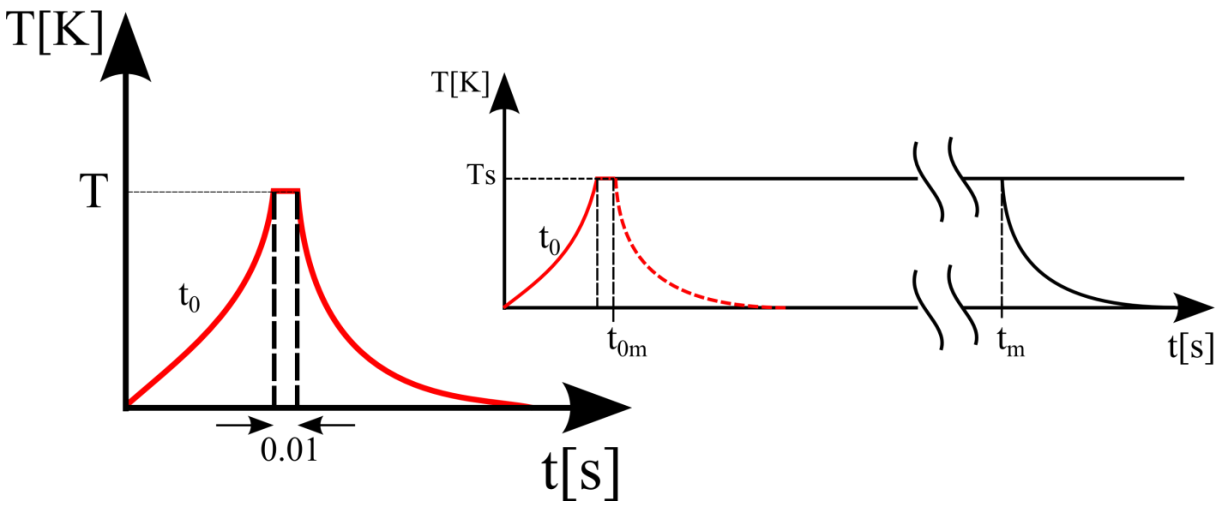

Fig. 20: The idea of the zero-time measurements. The heating time interval is set to 0.01 s, which is much less than the heating interval used for diffusion experiments i.e. 5 – 60 s.

3.1.4 Step edge barrier correction

An adatom diffusing on a finite surface occasionally encounters a step edge barrier, which affects measurements of the mean square displacement. For various surfaces, the step edge potential has a different magnitude and shape (Fig. 21a) [51, 7]. For a purely reflective step edge barrier, the corrected value of the mean square displacement $<(\Delta r)^2>_c$ is calculated from the formula derived by Ehrlich [52] :

$$\langle(\Delta r)^2\rangle_c = \langle(\Delta r)^2\rangle \left[1 - \frac{8}{3\pi R}\sqrt{\langle(\Delta r)^2\rangle/\pi}\right] \quad (7)$$

$<(\Delta r)^2>$ is a measured mean square displacement before the correction and R is a plane radius.

If the step edge barrier has an adjacent potential well (Fig. 21a), which is deep enough to trap the adatom, then the correction can be done on the level of the measurements. In that case, when the adatom incorporates into the trap the series is interrupted and the last cycle is rejected from the analysis. Then the trapped adatom is removed from the well by increasing the heating temperature. After moving the adatom from the near-trap zone, back to the center of the plane, the measurement is resumed as a new series. Thus diffusion of an adatom in the near step edge areas and the effect of the step edge barrier are removed from the analysis.

3.2 Single Atom Adsorption Experiments

To determine the surface diffusion mechanism by using the map of sites visited by the adatom, it is crucial to know the morphology of the surface on which the adatom migrates. It has been shown that a large W(100) surface reconstructs from c(2x2) into (1x1) at temperature ~ 300 K [34], which is much lower than the lowest temperature at which W adatom migration was observed. However, the knowledge about the morphology of a small W(100) plane observed in FIM is still not established. If there is any

reconstruction occurring during heating and cooling the sample, then the adatom movement and its final position observed in FIM, could possibly be affected.

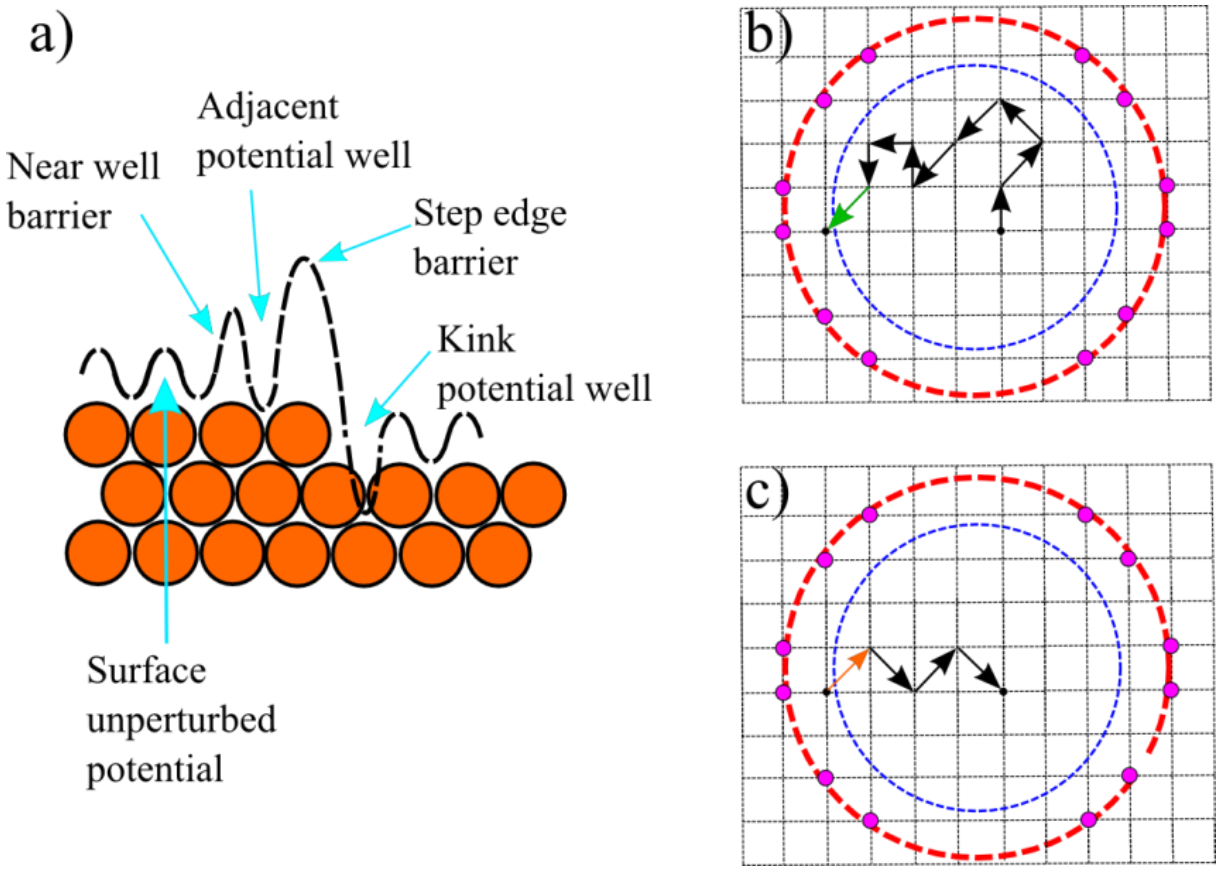

Fig. 21: (a) A schematic of the surface potential in the near step edge area. (b) Adatom diffuses on a finite plane (marked with red circle) at temperature T_m. Adatom enters to the near step edge area (blue circle), where it is captured. (c) After applying temperature $T > T_m$, the adatom is removed from the potential well and the series is resumed when the adatom returns to the surface interior.

The FIM cannot resolve the interior of atomically flat surfaces for which the diameter is larger than few atoms. To determine the morphology of W(100), the adsorption measurements were conducted. It is well known that the metal atoms deposited onto metal surfaces tend to adsorb into hollow sites, without any additional energy required for leaving the precursor site [1] (a transient diffusion phenomenon [7]). Thus from the map of adsorption sites one can determine the surface morphology.

The experimental procedure is as follows: a single adatom is adsorbed onto a W(100) plane and its position is recorded. Then the adatom is desorbed from the surface and a new adatom is adsorbed, to mark another adsorption site. The procedure is repeated until a sufficient map of adsorption sites is resolved. Afterward, a grid is matched to the adsorption sites and its orientation is compared with the position of the planes surrounding W(100). In presented experiments, W and Rh adatoms were used. The adsorption was performed on a cold surface (cooled with liquid helium). Since the diffusion of a W adatom on a W(100) surface occurs at temperatures above 300 K, to examine if any hysteresis effect occurs, the adsorption experiments were conducted for two types of W(100) surfaces: fresh – right after cleaning and preheated to 500 K.

3.3 Density Functional Theory Calculations

To improve the quality of conducted analysis, the obtained experimental results are compared with the results of Density Functional Theory (DFT) calculations which were done by Prof. Leszek Jurczyszyn from the Surface Theory Group in the Institute of Experimental Physics at the University of Wroclaw. The performed *ab initio* DFT calculations utilize Vienna Ab initio Simulation Package program (VASP) [53, 54, 55, 56]. The relaxed structure is obtained by using the conjugate gradient approach (CGA). The calculated lattice constant of the unit cell of the bulk is 3.175 Å. The size of the unit cell used in calculations is 4x4 and seven atomic layers thick, where the four topmost layers are allowed to relax and the three bottom layers are "frozen". The calculations determine the structure of a relaxed and a "frozen"

W(100) surfaces. The shape and the energetics of the adsorption sites are calculated with and without deposited W adatom.

The DFT calculations provide the values of the activation energy for adatom diffusion via the exchange and the jump. To simulate the path of the adatom exchange, the Nudged Elastic Band (NEB) method is used. The NEB is implemented into the VASP code [57]. The calculations for the adatom diffusion are performed on a zig-zag reconstructed and a non-reconstructed W(100) surfaces.

4. RESULTS AND DATA ANALYSIS

4.1 Morphology of W(100) Surface

To determine the map of adsorption sites on the W(100) surface, rhodium and tungsten adatoms were used as markers. After deposition onto the surface and marking their positions, the adatoms were field desorbed. The desorption voltage for the Rh adatom was ~ 9 – 10 kV, which is ~ 2 kV lower than the desorption voltage of the W adatoms. The arrangement of the adsorption sites matches the grid oriented along <100> directions for both Rh and W adatoms (Fig. 22). The orientation of the grid corresponds to a (1x1) arrangement of the adsorption sites, which suggests a non-reconstructed morphology of the W(100) surface. Preheating the surface before the adatom deposition did not change the result. The map of adsorption sites has a (1x1) arrangement for "fresh" and preheated surfaces. The FIM results undermine the FBE model of a W(100)- c(2x2) reconstructed surface with protruding surface atoms. The adsorption experiments did not reveal any lateral shift of the surface atoms, which would correspond to the "zig-zag" model. If there is any lateral displacement of the surface atoms, it must be smaller than the smallest distance possible to resolve with the FIM. That result agrees with the conclusion drawn by Tsong [21].

The DFT calculations that were conducted on a "frozen" (i.e. not allowed to relax) FBE reconstructed W(100) surface, showed the presence of shallow adsorption sites in the saddle points between protruding adatoms. If the bonding energy of the adsorption site in the saddle point is comparable with the binding energy at the hollow site, then the map of adsorption sites should be arranged as (1x1). However, DFT calculations showed a significantly shallower adsorption site at the saddle point, which would not prevent the adatom from transient diffusion into the hollow site. Also the modeled surface was extremely unstable. The FBE reconstruction disappeared immediately when it was allowed to relax, even without the presence of the adatom. In the experiments, the surface is kept at ~ 20 K. Thus the FBE model of W(100) can be rejected completely.

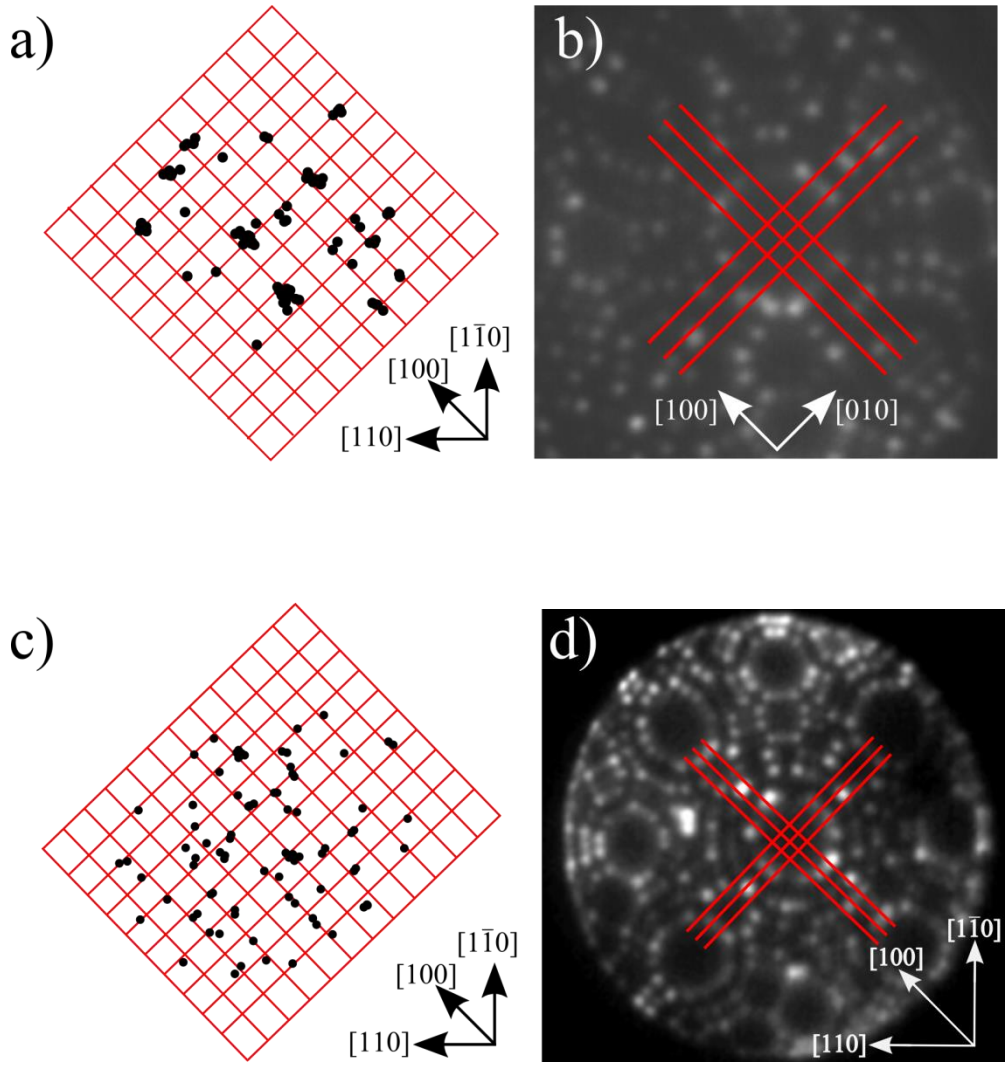

Fig. 22: (a) The map of adsorption sites obtained from re-deposition of W adatoms on a W(100) surface. (b) FIM micrograph of a <100> oriented tungsten tip with a W(100) plane in the center. The grid is matched to the adsorption sites and its orientation is compared with the position of adjacent planes. The orientation of the grid along <100> directions corresponds to a (1x1) arrangement of the sites. (c) Map of adsorption sites obtained from re-deposition of Rh adatom on the W(100) surface. (d) The orientation of the grid along <100> directions indicates (1x1) arrangement of the adsorption sites.

The DFT calculations showed that the most energetically favorable arrangement of a W(100) surface is the ziz-zag with the shift of surface atoms equal to 0.27 Å with respect to their positions in the square lattice. However, in the presence of the adatom, the surrounding surface atoms relax to a (1x1) structure. Thus, if there is any zig-zag reconstruction, it most likely has no effect on the adatom diffusion.

4.2 Diffusion Measurements for W on W(100)

The diffusion of a W adatom on a W(100) surface was initially observed in a time scale of seconds at temperature 633 K, when the sample was heated for 90 s. At those settings, the adatom diffusion rate was very low – less than 30% of heating cycles resulted with the adatom displacement. With such a low displacement rate, the vacuum conditions deteriorate, before a sufficient statistic is collected. The measurements used for the analysis of W adatom diffusion were conducted for adatom movement at temperatures 648 – 726 K and heating time intervals 60 – 5 s (shorter time intervals were used for higher temperatures). At those settings, the adatom was displaced after the heating cycle 50 % – 95 % of the time. Since the diameter of the W(100) planes used in the experiments was 40 – 50 Å, the heating cycles were adjusted to prevent the adatom from moving too rapidity across the plane. The average displacement of the adatom during one heating cycle was two adsorption sites.

4.2.1 Diffusion mechanism

The grid was matched to the map of the sites visited by diffusing W adatom. For the diffusion occurring at 648 – 663 K, the grid is oriented along <110> directions (Fig. 23), which corresponds to a c(2x2) arrangement. This can be a result of either the adatom diffusion by jump on a c(2x2)-FBE reconstructed W(100) surface, or by the diffusion via the exchange mechanism on a non-reconstructed W(100). The map of sites visited by the adatom was compared with the map of the adsorption sites obtained from the adatom deposition experiments (Fig. 24). The difference in the (1x1) arrangement of the adsorption sites and the c(2x2) arrangement of the sites visited by the adatom, indicates that the adatom diffuses via the exchange mechanism. The additional confirmation of the exchange mechanism was done by adsorbing an

adatom into the sites between the grid lines of a previously created c(2x2) map of visited sites. When a new adatom was deposited between the grid lines, it continued diffusion in the alternative c(2x2) grid. Thus, it was confirmed that the diffusion via the exchange mechanism is the only source of a c(2x2) arrangement. The result also shows the incorrectness of the FBE model of W(100).

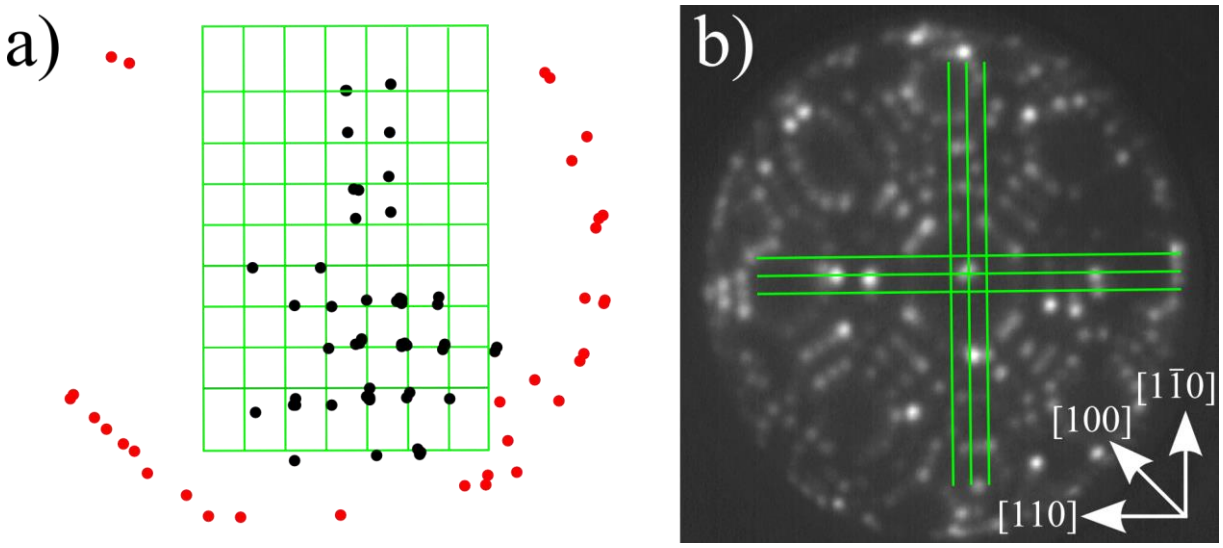

Fig. 23: (a) The map of sites visited by the adatom with the grid matched to the sites; black dots – positions of the adatom, red dots – positions of the step edge atoms. (b) FIM micrograph with the grid matched to the visited sites. The orientation of the grid is determined by comparing it with the positions of the crystal planes surrounding W(100).

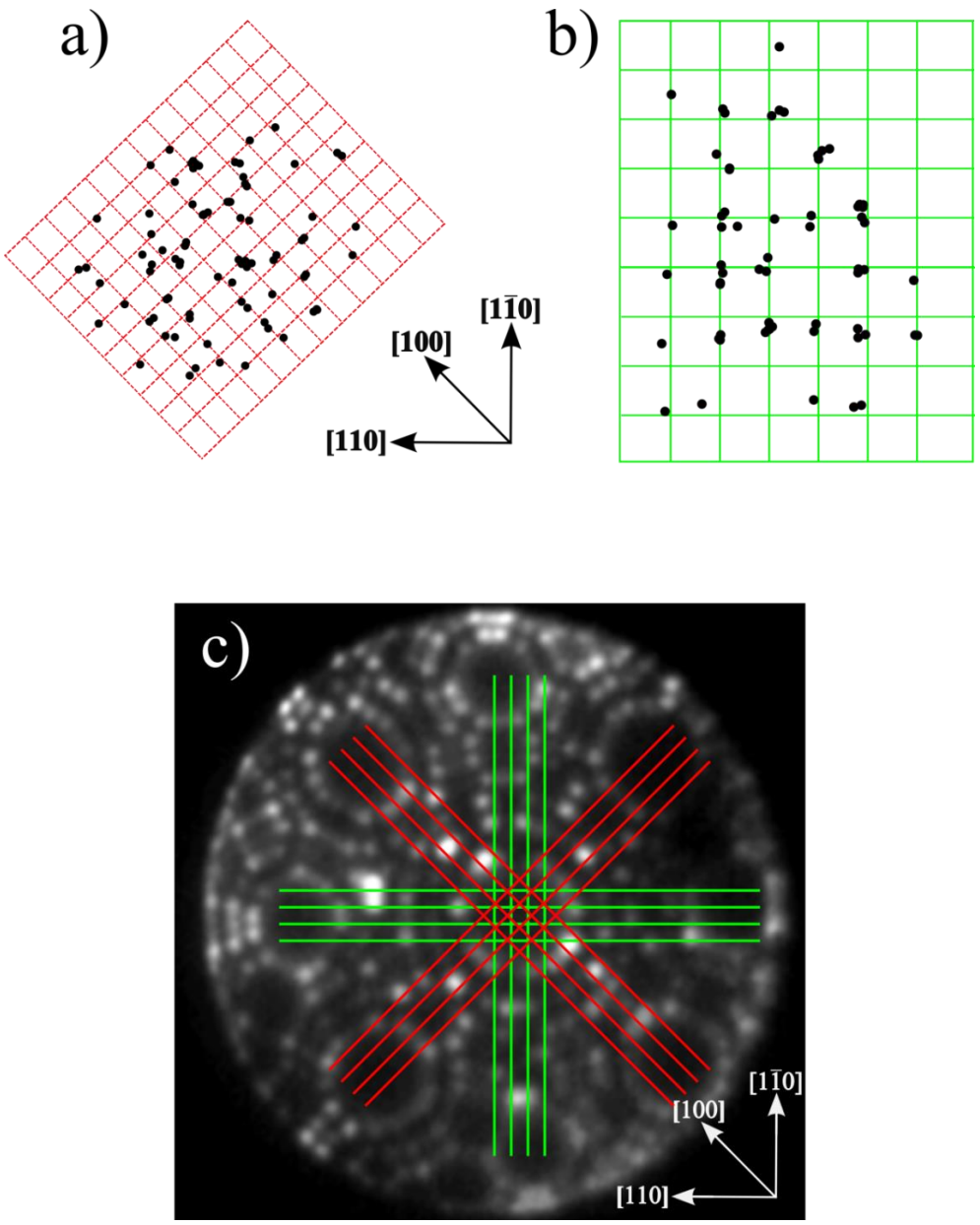

Fig. 24: (a) Marked positions of the adsorption sites for Rh adatoms deposited onto W(100). The grid that is matched to the sites corresponds to (1x1) arrangement. (b) Marked positions the sites visited by diffusing W adatom via the exchange mechanism at temperature 663 K. The grid matched to the sites corresponds to c(2x2) arrangement. (c) FIM micrograph taken at 10 kV. The grids of the adsorption (red) and the diffusion (green) experiments are matched to the position of neighbor planes, surrounding W(100).

During measurements of a W adatom diffusion on W(100), at temperature 677 K, after two cycles of heating the adatom moved to the site between a c(2x2) grid. The adatom continued to diffuse in the alternative c(2x2) grid (Fig. 25a). The change of the grid suggests that the adatom jumped. At higher temperatures, 688 – 720 K, the maps of the visited sites have a (1x1) arrangement, which corresponds to the adatom jump. A careful analysis of the adatoms' movements, showed that for most of the time, the adatom diffuses via exchange in a c(2x2) grid and it only occasionally jumps into an alternative c(2x2) grid (Fig. 25b).

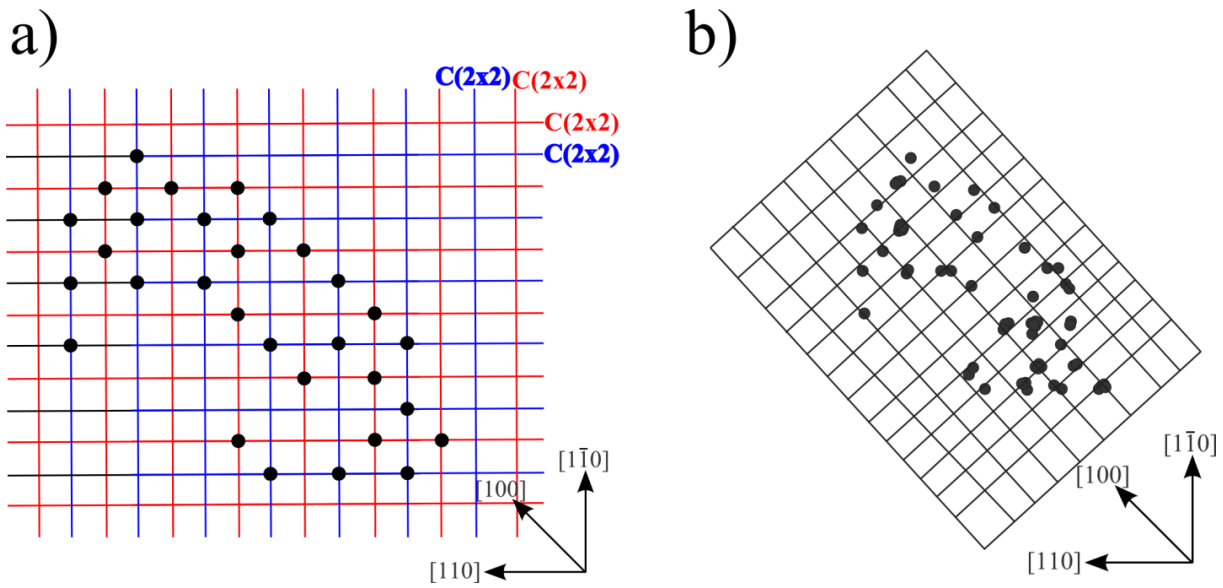

Fig. 25: (a) The map of sites visited by the adatom diffusing at temperature 720 K. The arrangement of the map is (1x1) with respect to the adsorption sites of a non-reconstructed W(100) surface. (b) The map of visited sites which is a combination of two c(2x2) maps. The adatom diffuses via the exchange mechanism in a c(2x2) grid. At some point the adatom jumps into the alternative c(2x2) grid where it continues the diffusion via the exchange. The combination of c(2x2) grids gives a (1x1) grid.

4.2.2 Activation energy and diffusion prefactor

To obtain the accurate value of the activation energy and the diffusion prefactor over 1300 observations of diffusing adatom were conducted. The obtained results for the mean square displacement were corrected with the zero-time measurements. In the calculations of the diffusion parameters, it was assumed that the adatom diffuses on a non-reconstructed W(100) surface. The obtained values of the diffusivity are plotted on the graph as a function of the temperature (Fig. 26a) in a semi-logarithmic scale. The activation energy for diffusion of a W adatom on a W(100) surface was obtained from the slope of the linear fit of the Arrhenius plot, its value is E_D = 1.60 ± 0.24 eV. The diffusion prefactor was calculated from the intercept of the fit with the vertical axis of the plot, its value is D_0 = 0.37 (x50.2$^{\pm1}$) x 10^{-4} cm^2/s. The experimental results were compared with the outcome of DTF calculations. The lowest calculated activation energy, 1.55 eV, was found for a W adatom diffusion on an unreconstructed W(100) via the exchange mechanism. The DFT result is in very good agreement with the experimental results.

The energetics of the adatom movement was also used to verify if W adatoms observed in FIM were diffusing on a zig-zag reconstructed or non-reconstructed W(100) surface. If the surface has a zig-zag reconstruction, then the diffusion would be asymmetric. Thus the analysis of adatom movement along [110] and [1-10] directions was conducted, to find any possible asymmetry in the adatom diffusion. The obtained from the FIM measurements diffusivities are plotted on a semi-logarithmic scale (Fig. 26b). The obtained activation energies for diffusion along [110] and [1-10] directions are: $E_{D[110]}$ = 1.60 ± 0.28 eV and $E_{D[1\text{-}10]}$ = 1.59 ± 0.24 eV, and the corresponding diffusion prefactors are: $D_{[110]}$ = 0.28 (x48.3$^{\pm1}$) x 10^{-4} cm^2/s and $D_{[1\text{-}10]}$ = 0.47 (x48$^{\pm1}$) x 10^{-4} cm^2/s. The negligible difference in the activation energy and in the diffusion prefactors drives the conclusion that if there is any zig-zag reconstruction, it has no effect to the diffusion of the adatom. The energetics of the adatom diffusion along [100] and [1-10] direction was also calculated with DFT. The activation energy for adatom diffusion via the exchange on a zig-zag reconstructed W(100) surface, was 2.05 eV along the [110] direction and 2.11 eV along the [1-10]

direction. Both results, FIM and DFT, confirm that the diffusion of the adatom occurs on a non-reconstructed W(100) surface via the exchange mechanism.

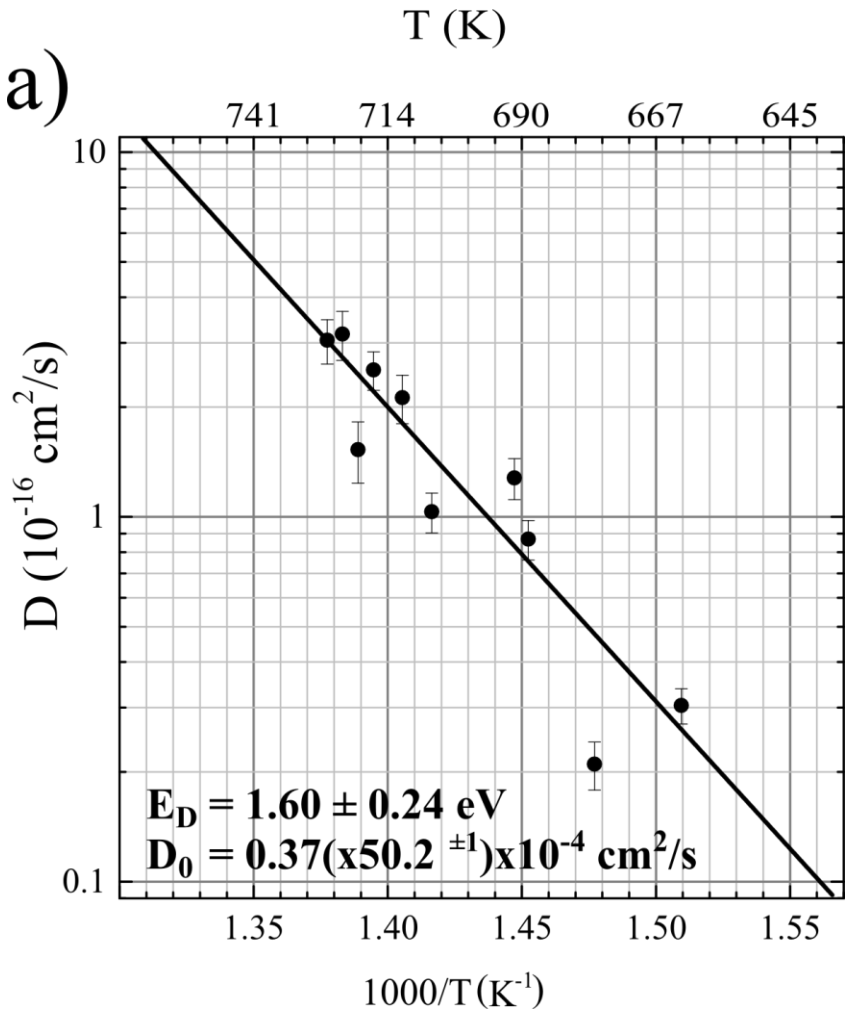

Fig. 26a: Arrhenius plot for W adatom diffusion on a W(100) surface with the assumption of a two-dimensional movement in the Einstein-Smoluchowski relation. The activation energy is calculated from the slope of a linear fit of the plot and the diffusion prefactor is obtained from the interception of the fit with the vertical axis.

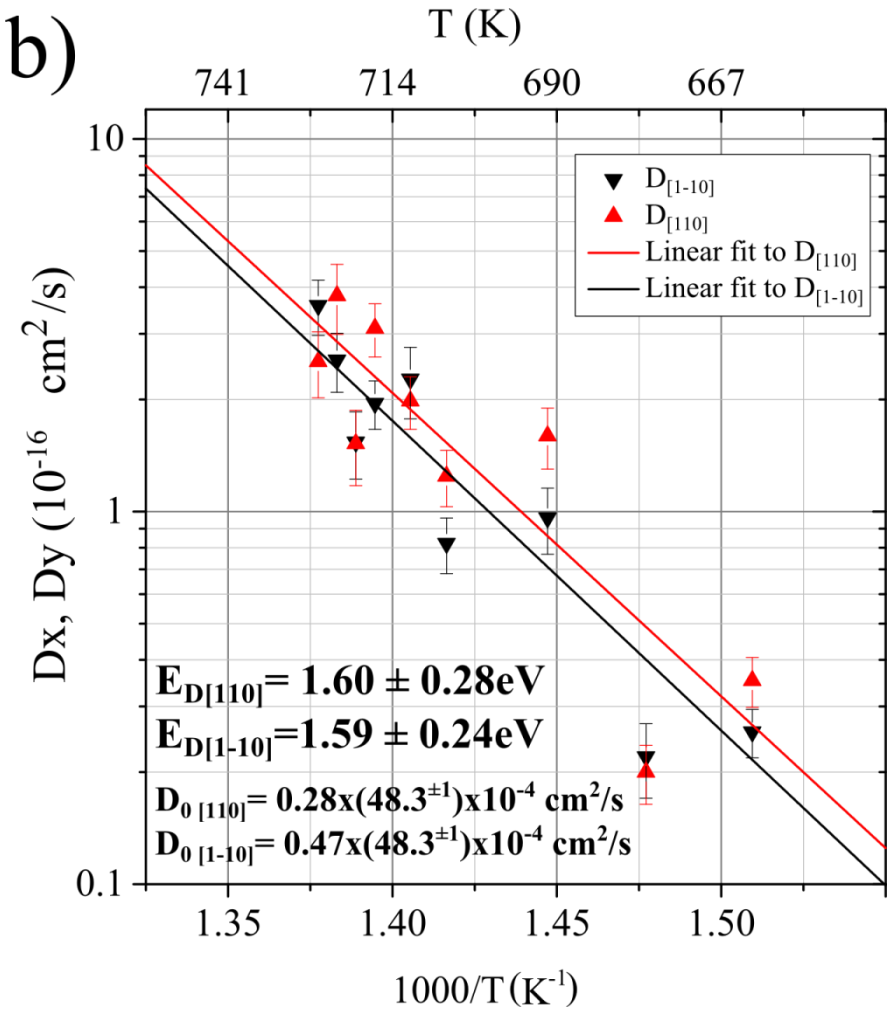

Fig. 26b: Arrhenius plot for W adatom diffusion on a W(100) surface with the assumption of a one-dimensional movement in Einstein-Smoluchowski relation along [110] and [1-10] directions. The value of the activation energies and the diffusion prefactors are almost the same for both analyses. There is no preferable direction for the surface diffusion. There is no effect of a zig-zag reconstruction on adatom movement.

At higher temperature, a diffusing W adatom creates the map of visited sites (1x1), by moving between two alternative c(2x2) grids. For most of time the adatom diffuses via the exchange mechanism in the c(2x2) grid. Even at high temperatures the jump between the grids very seldomly occurs. Thus, the collected statistic of adatom jumps is insufficient to determine the activation energy for the jump from the Arrhenius plot. However, the energy can be estimated by using the Arrhenius formula for the jump rate Γ:

$$\Gamma = \upsilon \cdot exp\left(\frac{E_D}{k_B T}\right) \tag{8}$$

ν is a frequency of lattice vibration, E_D is the activation energy for a jump, T is heating temperature and k_B is the Boltzmann constant. By assuming the frequency of lattice vibration $\nu = 10^{12}$ 1/s, the estimated value of the activation energy for the adatom jump is 2.1 eV. That result was again compared with the results of DFT calculations. The calculated activation for adatom jump on a non-reconstructed W(100) surface is 2.27 eV. A very good agreement of the experimental result with the outcome of DFT calculations confirms that the adatom diffuses via jump on a non-reconstructed surface.

The obtained results show explicitly the coexistence of two diffusion mechanisms: jump and exchange. It is the very first experimental evidence for the coexistence of diffusion mechanisms in one system for a two-dimensional diffusion.

4.2.3 Origin of the second diffusion mechanism

To establish if the presence of an additional diffusion mechanism is a temperature-triggered phenomenon, the jump rates were measured for temperature range 677 – 720 K. The rates were plotted on a semi-logarithmic scale as a function of a temperature (Fig. 27). A clear temperature dependence of the jump rate proves that the occurrence of a second diffusion mechanism – jumps, is a temperature-activated phenomenon.

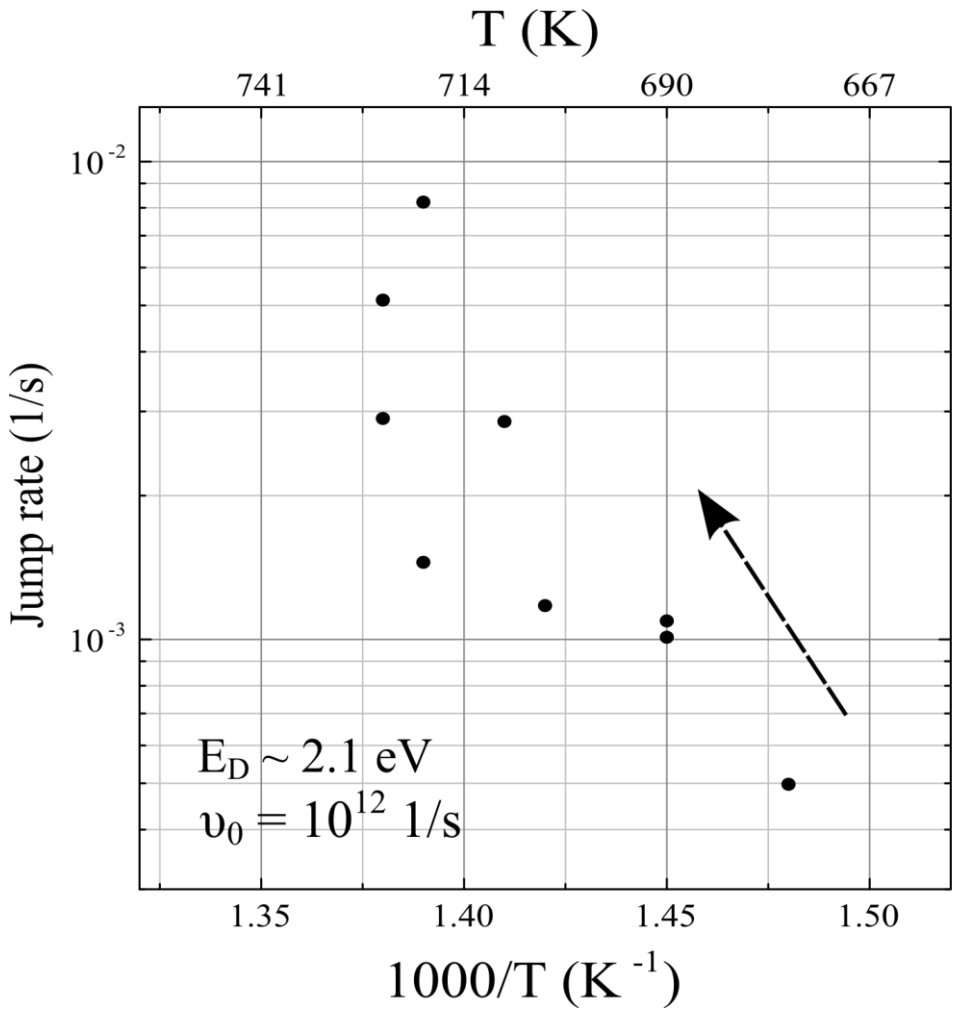

Fig. 27: The jump rate as function of the temperature for a diffusing W adatom on a W(100) surface. The rate is plotted on a logarithmic scale. The increase of the rate with the temperature confirms that the appearance of the jumps is a thermally-activated process.

4.2.4 Other diffusion mechanisms

The map of sites visited by the adatom which is arranged as (1x1) can also correspond to a crowdion mechanism. If there is no bias, the atom pushed by crowded surface atoms can land in any of the nearest neighbor adsorption sites. Thus the maps of the visited sites for diffusion via the crowdion and the jump mechanisms look exactly the same [19].

Chen and Ghoniem [19] calculated with DFT the activation energy for diffusion via crowdion of W adatom on W(100). They pointed a crowdion as a dominant diffusion mechanism for adatom self-diffusion on a W(100) surface. According to their results, when there is no stress applied to a W(100) surface the activation energy for formation of a crowdion is 1.57 eV and for the adatom exchange it is 1.84 eV. In that case the map of visited sites with a (1x1) arrangement should be observed at lower temperatures than the c(2x2) map. That situation did not occur in our experiments. The c(2x2) map of visited sites was observed first. The (1x1) arrangement occurred at higher temperatures.

The theoretical calculations done by Chen and Ghoniem [19] on the crowdion mechanism occurring for self-diffusion on W(100), do not agree with the experimental observations of our studies. Thus, the hypothesis of the crowdion mechanism as a source (1x1) map was rejected.

5. SUMMARY OF PART I

The migration of a W adatom on a W(100) surface was investigated with FIM. The movement of a W adatom is observed in a time scale of seconds, at temperatures above ~ 600 K. The dominant diffusion mechanism is the adatom exchange, which creates the map of visited sites arranged as c(2x2). At temperatures 688 – 720 K, the map of sites visited by the adatom changes from c(2x2) into (1x1), which is the effect of the presence of a second diffusion mechanism, identified as jumps. The measurements of the jump rates at various temperatures show that the occurrence of the second diffusion mechanism is a temperature-activated phenomenon. The experimental value of the activation energy for adatom diffusion with the exchange as a dominant diffusion mechanism is 1.60 ± 0.24 eV. The estimated value of the activation energy for the adatom jump is 2.1 eV. The results of DFT calculations conducted by the collaborators form the University of Wroclaw are in very good agreement with the experimental results. The calculated activation energy for W adatom diffusion on a non-reconstructed W(100) surface via the exchange is 1.55 eV and via the jump is 2.27 eV.

The map of adsorption sites obtained from deposition of Rh and W adatoms on a W(100) surface has a (1x1) arrangement. In the diffusion experiments, it was shown that a W adatom can be adsorbed into the sites between the c(2x2) grid lines and diffuse in the alternative c(2x2) grid. The experimental results undermine the validity of the FBE [32] model of a W(100) surface. The results of DFT calculations show that the FBE model of W(100) is very unstable and it disappears when the surface is allowed to relax. Thus, the FBE model of a W(100) surface is considered as invalid.

The adsorption experiments did not reveal any planar shift of the adsorption sites, which would be expected for the zig-zag model of reconstructed W(100). According to Tsong and Sweeney [21]: if there is any zig-zag reconstruction of a W(100) surface, for the plane which size is ~ 50 Å in diameter, the shift of the surface atoms might be too small to be observed in FIM. On the other hand, our DFT calculations

showed that in the presence of a W adatom, the adsorption sites of a zig-zag W(100) relax to the unreconstructed arrangement.

The influence of a possible zig-zag reconstruction on adatom diffusion was verified by analysis of the adatom movement along directions, which are parallel and perpendicular to the zig-zag chain, i.e. [110] and [1-10]. The obtained activation energies along [110] and [1-10] are 1.60 ± 0.28 eV and 1.59 ± 0.25 eV respectively. The lack of the asymmetry in the adatom movement shows that either W(100) is not reconstructed, or the zig-zag reconstruction has no effect on the diffusion of W on W(100). The asymmetric adatom diffusion on a zig-zag W(100) was also investigated with DFT. The calculated activation energies for the diffusion via exchange along [110] and [1-10] directions are 2.05 eV and 2.11 eV respectively, which is much larger than the experimental values. The best correlation between the experimental and the DFT results is obtained for adatom diffusing on a non-reconstructed W(100). Thus, we conclude that the diffusion of W adatom occurs on a non-reconstructed W(100) surface.

PART II – DIFFUSION OF TWO W ADATOMS ON A FINITE W(100) SURFACE

6. THE INFLUENCE OF A SECOND ADATOM ON DIFFUSION PROPERTIES

In potential applications of the coexistence for fabricating the electronic devices, multiple adatoms will be deposited onto the surface at the same time. Thus it is highly probable that two or more migrating adatoms will interact with each other. It has been shown theoretically and experimentally that the presence of additional adatom on the surface can change the diffusion mechanism and the diffusion parameters [7] i.e. the activation energy and the diffusion prefactor. Bassett and Parsley [58] showed that metal dimers of Re, Ir, Pt, and W adsorbed on (210), (321) and (110) tungsten surfaces have lower mobility than individual adatoms. Their later work on the same systems, [59] revealed that even when the adatoms do not create a dimer, their mobility is still lowered when both of adatoms are placed on the same finite surface. Bassett and Parsley [58] suggested that the effect of atomic interactions on adatom diffusion depends on the distance between the adatoms and the temperature of the surface. Therefore, even if the additional adatoms will not create a cluster, their presence on the surface can significantly affect the diffusion parameters and mechanisms.

The migration of a cluster involves breaking its bonds with the surface. A general expectation about a cluster's diffusion is that its mobility decreases as the size of the cluster increases [60]. Recently, Fu et al. [60] investigated surface self-diffusion of adatoms and clusters on W(111) surface. In contrary to what was expected, the mobility of a single W adatom was much lower than the mobility of small clusters. The activation energy that was found for W_2 dimer is ~ 1.6 eV, whereas the energy for migration of a single W is 1.9 eV. The activation energy oscillatory increased with increasing the number of atoms in the cluster. This result shows that the mutual interactions between adatoms play a crucial role in surface diffusion.

The interactions between adatoms can also cause formation of superstructures on the surface [61, 62], which can be used as an array of nucleation centers. Thus, the information about possible changes of the diffusion mechanism for interacting adatoms is extremely important for fabrication of arrays of devices.

6.1 Physical Influence of a Second Adatom on the Diffusion Process

The most basic way that one adatom can affect the movement of another is when it blocks the other atom from reaching a desirable surface site. In the case of diffusion occurring via jump, on a finite surface, the presence of additional adatoms decreases the number of available adsorption sites. When the probability of finding a single adatom on an empty plane in a position x after time t is $p_{1x}(t)$, in the case of two adatoms this probability changes into $p_{2x}(t)$:

$$p_{2x}(t) = p_{1x}(t) \cdot \left(1 - p_{1x}(t)\right) \tag{9}$$

where $p_{1x}(t)$ is the probability that adatom will reach site x, and $(1\text{-}p_{1x}(t))$ term is the probability that the site is unoccupied.

A similar situation occurs in the case of the exchange mechanism. The additional adatom can occupy the adsorption site which should be filled by the surface atom that is pushed to the top. The presence of an additional adatom not only requires "vacating" the site, but also overcoming the additional suppressing force created by the second adatom. As a result the diffusion via exchange in some directions might be less energetically favorable than in others (Fig. 28a,b).

For adatom jump, the width and the depth of the adsorption site depends on the distance between the surface atoms. In the presence of an adatom on the surface, the surface atoms can slightly shift from their equilibrium position [63]. Thus in a presence of additional adatom on a finite surface, some of available adsorption sites can be deformed, i.e. their shape and depth might be changed (Fig. 28c). If the relaxation

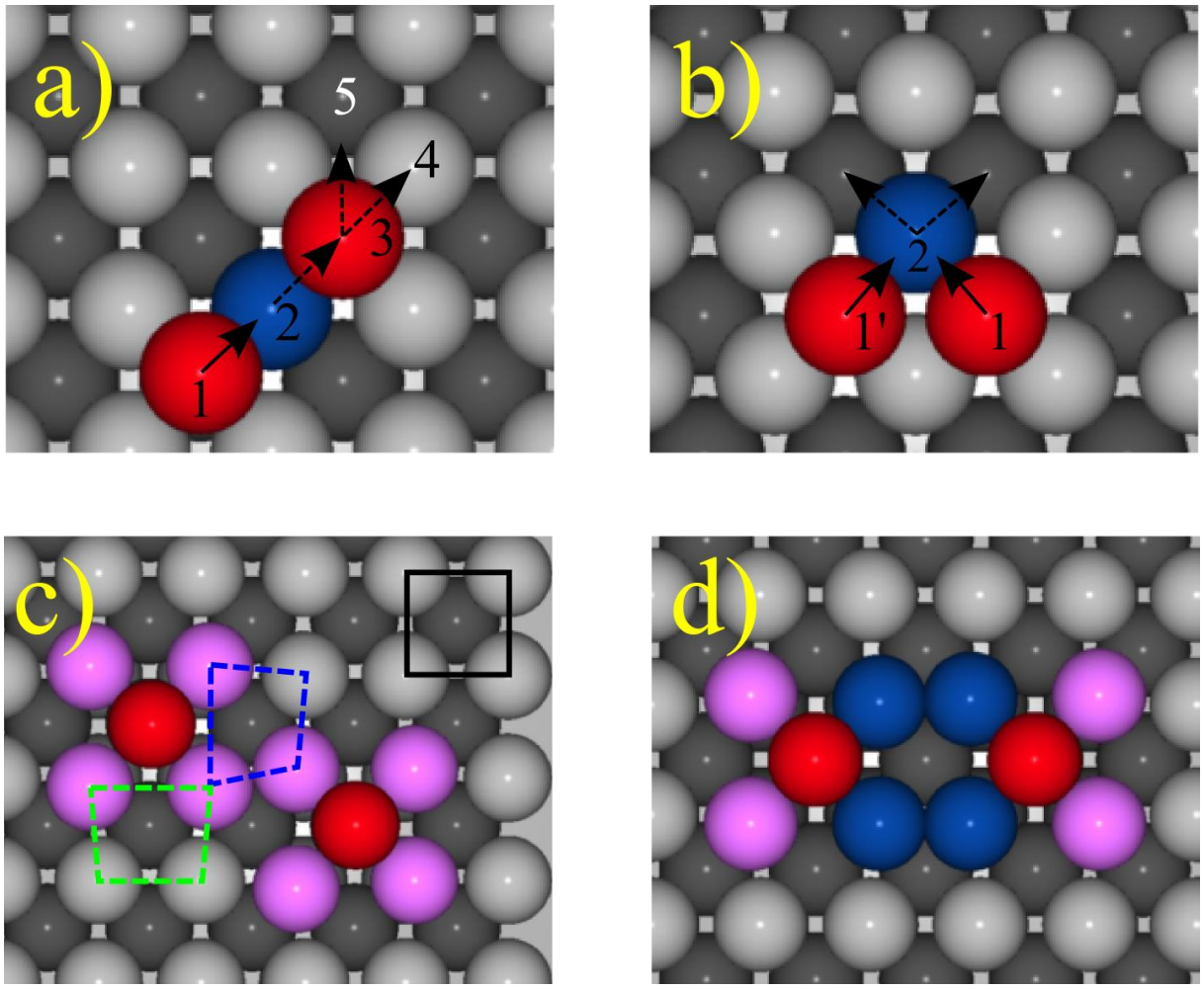

Fig. 28: (a) Adatom #1 (red) exchanges with a surface atom #2 (blue) which is blocked by adatom #3 (red). The adatom #3 (red) can yield the site by either exchanging with atom #4 (white) or by jumping into the site #5 (gray). If at lower temperature the exchange is a dominant mechanism, the jump will not be observed. (b) Surface atom (blue) is pushed simultaneously by two adatoms (red). (c) Relaxing surface atoms (pink) change the shape and the depth of adsorption sites. (d) Relaxed surface atoms (pink) can suppress each other (blue) blocking the exchange in some directions.

occurs, the distortion of surface atoms decreases with the distance from the adatom. Thus, the activation energy for a jump would depend on the distance between the adatoms and the direction of the jump. The shift of surface atoms due to the presence of an additional adatom also changes the strength of their bonds with their nearest neighbors [64]. The presence of an additional adatom can shift the surface atoms in the way that the direction of adatom exchange is biased (Fig. 28d).

6.2 Electronic Interactions

The electronic components play a crucial role in the interactions between the adatoms. The bond between the surface and the adatom can be weakened or strengthened due to the charge distribution on the adatom-surface interface. There are two major types of interactions [7]: direct and surface mediated. The electron clouds of two adatoms can overlap, even if the adatoms are separated from each other by a few lattice constants. If the bonding energy between adatoms is significantly larger than k_BT, then the adatom pair diffuses as a dimer for which new migration mechanisms must be considered [7]. If the interactions between adatoms are in the range of a few meV around k_BT, then the dimer is unstable and it breaks into two adatoms during the heating [65]. Then such adatom pair can migrate as two independent adatoms. However it does not mean that the diffusion properties like the activation energy and the diffusion prefactor correspond to the migration of non-interacting atoms. The strength of the direct bond decreases with the separation distance between adatoms d [66].

For separations beyond the nearest neighbor distance, surface mediated interactions play a more significant role than direct interactions [66]. There are electrostatic (dipole-dipole) and elastic fields interactions, which decay with interatomic separation distance d as $1/d^3$ [66]. For metal adatoms on a metal surface, the interactions are mostly due to Friedel oscillations of the surface electric charge [66]. The presence of an adatom on the surface perturbs the surface electric charge around it [63]. Due to a local variation of the surface charge density, the bond strength between the other adatom and the surface varies with the relative positions of the adatoms [63, 66]. The oscillations of the electric charge density around

the adatom decay as the distance between adatoms increases as: $-\frac{sin(q_F d)}{d^2}$, where q_F is an in-plane Fermi vector [67].

Tsong and Casanova [61, 65] related the oscillations with attractive and repulsive interactions between adatoms. They investigated the diffusion of Ir-Ir and Ir-W adatom pairs on a W(110) surface with FIM. They conducted over 700 observations of diffusion of an Ir-Ir adatom pair at 300 ± 5 K and about 900 measurements of a Ir-W pair at 300 ± 5 K and 330 ± 5 K. The life time of the Ir-Ir dimer was determined by calculating the number of observed dimer decompositions divided by the number of heating cycles multiplied by a heating time. The distribution of the adatoms' pair interactions was determined from the measurements of the frequency of the adatoms' appearances at various mutual distances. For two non-interacting adatoms, placed on a plane for which the diameter is ~ 50 Å, the distribution of distances has a Gaussian-like shape with a maximum at separation ~ 25 Å (Fig. 29a). However, the experiments conducted by Tsong and Casanova revealed that the distribution fluctuates with the separation distance (Fig. 29b), which suggested the presence of pair interactions between adatoms. The energy of the interactions as a function of a distance $E(r_i)$ was obtained from measurements of the probability $p_e(r_i)$ of finding two adatoms separated by distance r_i via relation:

$$\frac{p_e(r_i)}{p_0(r_i)} = C' e^{-E(r_i)/k_B T} \tag{10}$$

p_0 is a statistical weight which depends on the number of available adsorption sites in the strip Δr surrounding a circle area drawn with radius r_i, the C' is a constant. It was found that the pair interaction energy oscillates with the separation distance (Fig. 29c). Tsong and Casanova [65] assigned those oscillations to attractive and repulsive interactions between the adatoms. They also found that the oscillations decay as the separation distance between adatoms increases. The energy of adatom attraction in Ir-Ir pairs with adatoms at the nearest observed distance, 5 Å, was found to be ~ 55 meV. In the second nearest distance, ~ 7 Å, the adatoms repeal each other with the energy ~ 25 meV. At the separation

distance above 10 Å, the amplitudes of attractive and repulsive potentials decreased to ± 10 meV. Analogic behavior was found for W-Ir adatom pairs. Fink and Ehrlich [68], investigated with FIM a radial distribution of pair interactions between rhenium adatoms deposited on a W(110) surface. During 1000 observations, two Re adatoms diffusing on a plane with diameter ~ 64 Å, were observed only twice in a form of an equilibrated dimer Re_2. The radial of distribution of Rh adatoms was matched to a calculated distribution for non-interacting adatoms. It was found that the nearest neighbor interactions between Rh adatoms are repulsive and that the interactions oscillate as the distance between adatoms increases. On the other hand, it was found that Rh adatoms can create a stable Rh_3 cluster. The binding energy in Rh_3 was found to be ~ 0.25 eV and a life time of Rh_3 at 420 K was found to be 320 ± 90 s.

An alternative method to investigate the distance dependent adatom pair interactions was used by Watanabe and Ehrlich [63]. Their idea was to deposit two adatoms of two different materials to a finite surface, where one of the adatoms remained stable at its adsorption site and the other adatom was allowed to migrate. That procedure simplified the problem to single adatom diffusion around a frozen point defect. Therefore, the number of measurements required to obtain the distribution of distance dependent adatom pair interactions was significantly decreased in comparison to the method presented by Tsong and Casanova [65]. Additionally, since the immobile adatom was deposited in the center of the plane, the influence of the step edge barrier onto the results was considered only for the migrating adatom. The diffusion of adatom pairs was measured on a W(110) surface. Watanabe and Ehrlich [63] chose rhenium and tungsten as the "immobile" adatoms, and palladium was used as a migrating adatom. They conducted 1638 observations for diffusion of a Pd adatom around an adsorbed Re adatom at temperature 205 K and plotted a distribution of the pair interaction energies as a function of an interatomic distance (Fig. 30). They observed significantly large oscillations of interaction energies which would suggest that the Pd adatom should diffuse around Re within insolated narrow rings which was not observed. However, after a closer look into the map of the sites visited by the adatom they deduced that the adatom interactions are orientation-dependent. It was found that along <1-11> direction, Pd-Rh interactions are attractive, whereas

along <1-10> and <001> the interactions are repulsive. Also the lowest temperature of observed diffusion motion for Pd was changed in the presence of an Rh adatom. For a single Pd adatom the lowest diffusion temperature was ~205 K, whereas in the presence of Rh adatom within a nearest neighbor distance the migration was observed at 145 K. Watanabe and Ehrlich repeated the experiments using a W adatom instead of Rh. Again, the asymmetrical and oscillatory nature of interactions for Pd-W adatom pairs was observed. Measured energy of the nearest neighbor attractions for Pd-Rh was 36.8 meV and for Pd-W pair it was 50.4 meV.

The measurements with FIM were conducted on finite planes (~ 50 – 70 Å in diameter), where the maximum distance between adatoms 20 – 70 Å was limited by the plane's step edges for which the influence could not be completely neglected. These limitations were diminished for diffusion measurements conducted with an STM. Repp et al. [69] investigated the surface mediated long-range adatom interactions for self-diffusion on a Cu(111) surface. In their studies 0.003 ML of Cu adatoms was adsorbed onto the Cu(111) surface and allowed to diffuse at temperatures 9 – 21 K. To analyze the adatom pair interactions, Repp et al. [69] counted the number of adatom pairs at various distances d. From 3500 STM images they evaluated over 65 000 distances between adatom pairs and built a histogram of pair distance distribution, $g(d)$. To obtain the probability distribution and to evaluate the energy of the pair interactions $E(d)$ from the method provided by Tsong and Casanova [65], $g(d)$ was normalized by a factor $P(d)$ related to the size of scanned area:

$$P(d) = d[1 - d(4a - 4d + \pi d) / \pi a^2] \tag{11}$$

where a is scanning frame width. Thus the formula for pair interaction energy was defined as:

$$E(d) = -k_B T ln[g(d)/P(d)] \tag{12}$$

As a result, they observed long-range pair interactions, decaying oscillatory as $1/d^2$. The potential minima were resolved up to 71 Å of the interatomic separation. The amplitudes of attraction and repulsion potential were not symmetric, but the period of the oscillations was constant. Repp et al. [69] also calculated the pair potential energy using a method developed by Hyldgaard and Persson [70]. In that model the oscillations of the pair interaction energy are directly related to the oscillations of the surface Density Of State (DOS) which is caused by interference of the incoming and scattered surface electron wave from the adatom. The amplitude of the created standing wave decreases as the distance from the scattering source increases. Repp et al. [69] adopted Hyldgaard and Persson's [70] formula to calculate the interaction energy:

$$E(d) = -A(\delta_F, r)\left(\frac{4\varepsilon_F}{\pi^2}\right)\frac{sin(2q_F d+2\delta_F)}{(q_F d)^2}, \quad (13)$$

where ε_F is the Fermi energy level, q_F is a Fermi wave vector, δ_F is the Fermi level phase shift. The calculated potential minima were slightly shifted and their amplitudes were smaller in comparison to the measured energies, but the shape of oscillatory decaying interactions was preserved. The reason for discrepancy between experimental and calculated amplitudes in Repp's work was the scattering of the surface electrons into the bulk, which reduces the strength of the interactions. Rdepp et al. [69] did not include this effect into their calculations [7].

Stepanyuk et al. [67] used STM imaging combined with DFT calculations to investigate adatom pair interactions for Co on Cu(111). In their studies, a STM working in low bias regime was used to image oscillations of local density of states (Fig. 31a). The values of the pair interaction energies as a function of distance were in good agreement with DFT calculations and their interpretation for the oscillations was in agreement with the one provided by Repp et al. [69] (Fig. 31b).

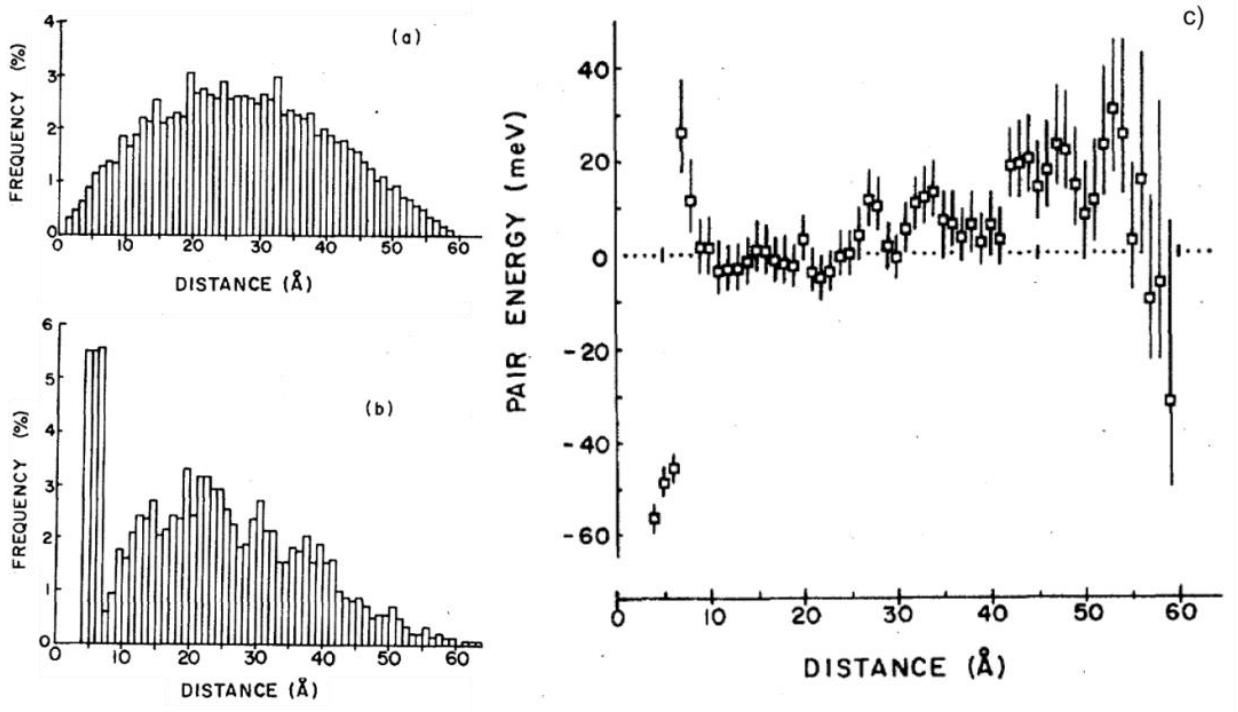

Fig. 29 [65][2]: (a) Calculated adatom pair distribution for two non-interacting adatoms diffusing on a W(110) plane with diameter 60 Å. The distribution has a Gaussian-like shape. (b) Pair distance distribution for Ir-Ir diffusing on W(110) at 330 K, obtained from 610 observations. Oscillations of the frequency are a function of a mutual distance between adatoms. (c) Pair interaction energy for Ir-Ir as a function of mutual adatom distance, calculated from equation (12).

[2]Reprinted figure from T. T. Tsong and R. Casanova, *Phys. Rev. B*, "Pair interaction of metal atoms on a metal surface," vol. 22, pp. 5590 - 5598, 1980, http://dx.doi.org/10.1103/PhysRevB.22.5590. Copyright 1980 by the American Physical Society. Figures 29a and 29b were adapted to clarify the labeling the axis.

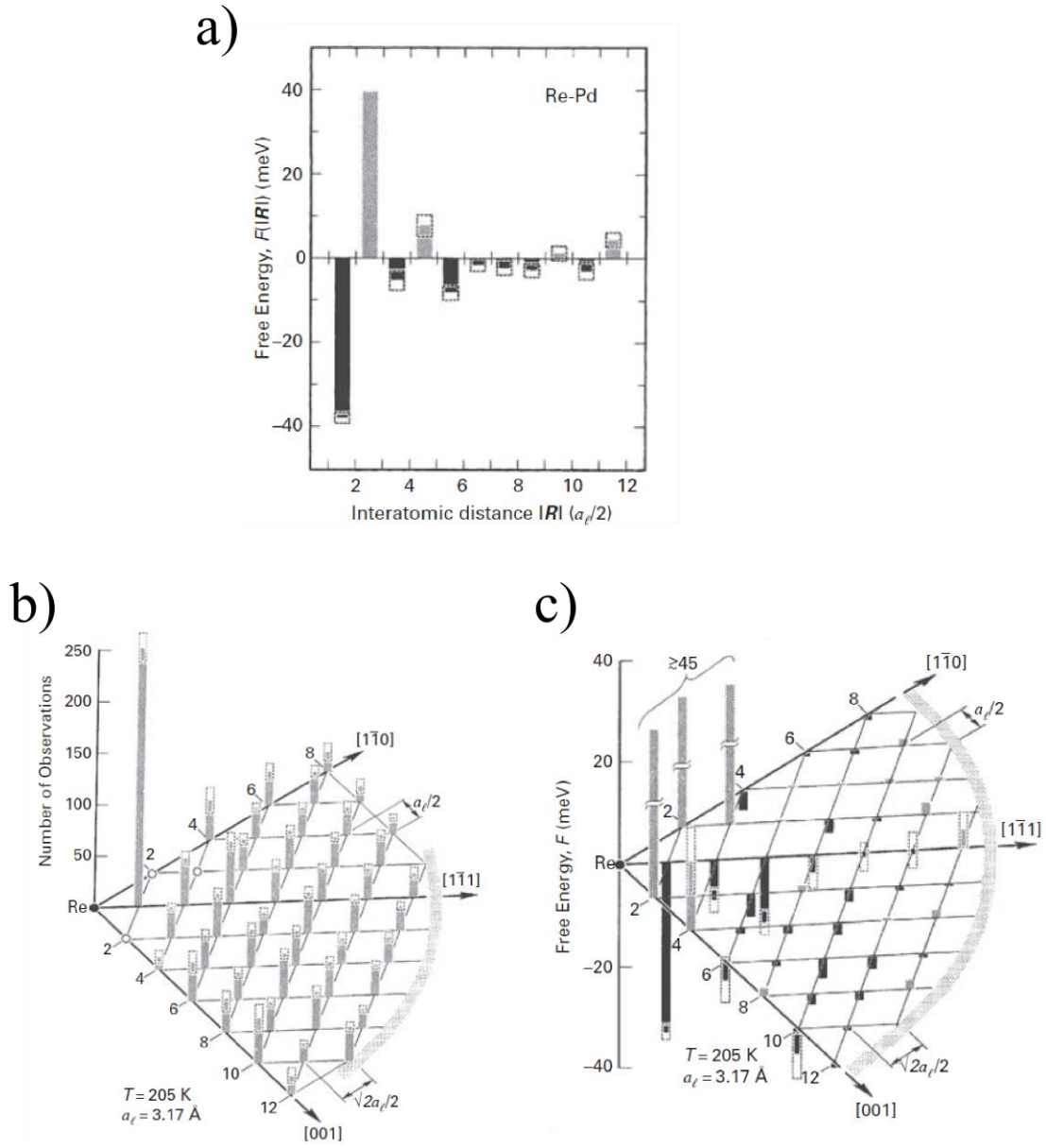

Fig. 30 [63][3]: (a) Distribution of pair interaction energy for Pd-Re adatoms as a function of their mutual distance |**R**|. (b) The map and the frequency of sites visited by a Pd adatom diffusing around a Re adatom placed in a center of a W(110) plane. (c) The interaction energy between Pd and Re adatoms assigned to adsorption sites on W(110).

[3]Reprinted figure from with permission from F. Watanabe and G. Ehrlich, "Direct observations of pair interactions on a metal: Heteropairs on W(110)," *J. Chem. Phys.*, vol. 95, pp. 6075 - 6087, 1991. Copyright 1991 AIP Publishing LLC.

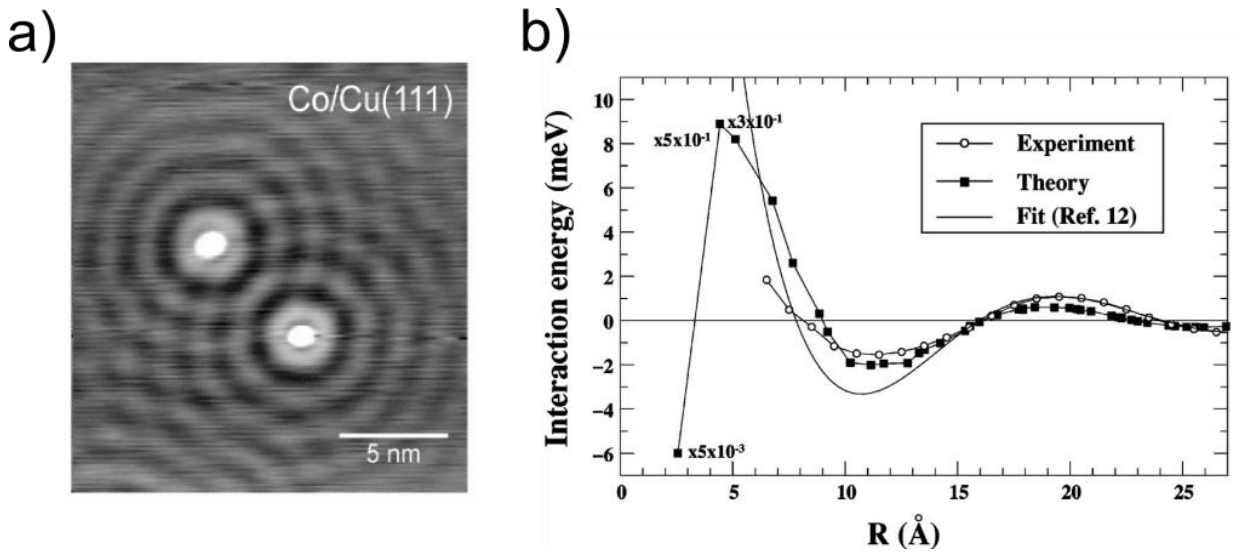

Fig. 31 [67][4]: (a) The oscillations of a local density of states imaged by STM with tunneling current I = 2 nA and bias voltage V = - 50 mV at temperature T = 6 K. (b) Calculated energies of the pair interactions for Co adatoms on Cu(111) surface obtained from experiment and from DFT calculations.

6.3 Possible Diffusion Mechanisms for Interacting Adatoms

Multiple adatoms deposited on a finite surface and interacting with each other can exhibit diffusion mechanisms that are common for tightly bonded clusters. The cluster diffusion occurs via translation and rotation movements [71, 72]. One of the most basic diffusion mechanisms is a collective gliding mechanism [73] (Fig. 32a,b) in which the cluster of atoms conducts a collective jump, moving its atoms in the same direction for the translation, and along the same angle for the rotation movement [71]. The collective gliding can also occur for dimers and trimers [50, 74, 72]. The alternative for the collective movement is diffusion of the cluster via sequential translations of its atoms: the sequential jump [74, 72],

[4]Reprinted figure with permission from V. S. Stepanyuk, A. N. Baranov, D. V. Tsivlin, W. Hergert, P. Bruno, N. Knorr, M. A. Schneider and K. Kern, "Quantum interference and long-range adsorbate-adsorbate interactions," *Phys. Rev. B*, vol. 68, pp. 205410 1 - 5, 2003, http://dx.doi.org/10.1103/PhysRevB.68.205410. Copyright 2003 by the American Physical Society.

the reptation [75] or the dimer sharing [76]. In the sequential jump a part of a cluster moves first and it is followed by the part that was left behind. In the case of dimers, one adatom jumps away and another follows it [74, 77] (Fig. 32c,d). A special case of the sequential mechanism is the reptation. In that case a part of a cluster also slides away and the other part follows it, but the movement of the cluster looks like a snake's glide (Fig. 32e) [75, 7]. Some of the sequential movements of a dimer can be classified as reptation (Fig. 32f). For the dimer sharing mechanism, the separated parts of a cluster are bridged by a dimer. In the case of small clusters (3 – 4 atoms), an atom breaks away from the cluster, leaving only one dimer connection, then the rest of the cluster sequentially follows it (Fig. 32g) [7]. The larger clusters can diffuse via evaporation and condensation mechanism. In that case an edge atom is detached from a cluster to diffuse freely on the surface as an adatom. Then the adatom reincorporates into the cluster again. As a result, the center of mass of a cluster shifts (Fig. 32h) [73]. For dimers evaporation and condensation means a complete dissociation of a dimer followed by its reunification in a new adsorption site.

Dimers and trimers can also diffuse via exchange [72]. Similarly to the exchange of single adatom, the process occurs when there are strong interactions between the cluster atoms and the surface. The process can occur collectively (Fig. 33a) or via sequential exchanges of individual cluster's atoms (Fig. 33b). In sequential exchange of dimers and trimers, it is possible that one cluster's atom exchanges whereas the other atoms remain on the top of the surface [72].

Diffusion mechanisms which are common for closed-packed clusters can also occur for diffusing adatom pairs which are separated beyond the nearest neighbor distance, but still interacting with each other. Knowledge about those mechanisms helps understanding the behavior of diffusing adatom pair.

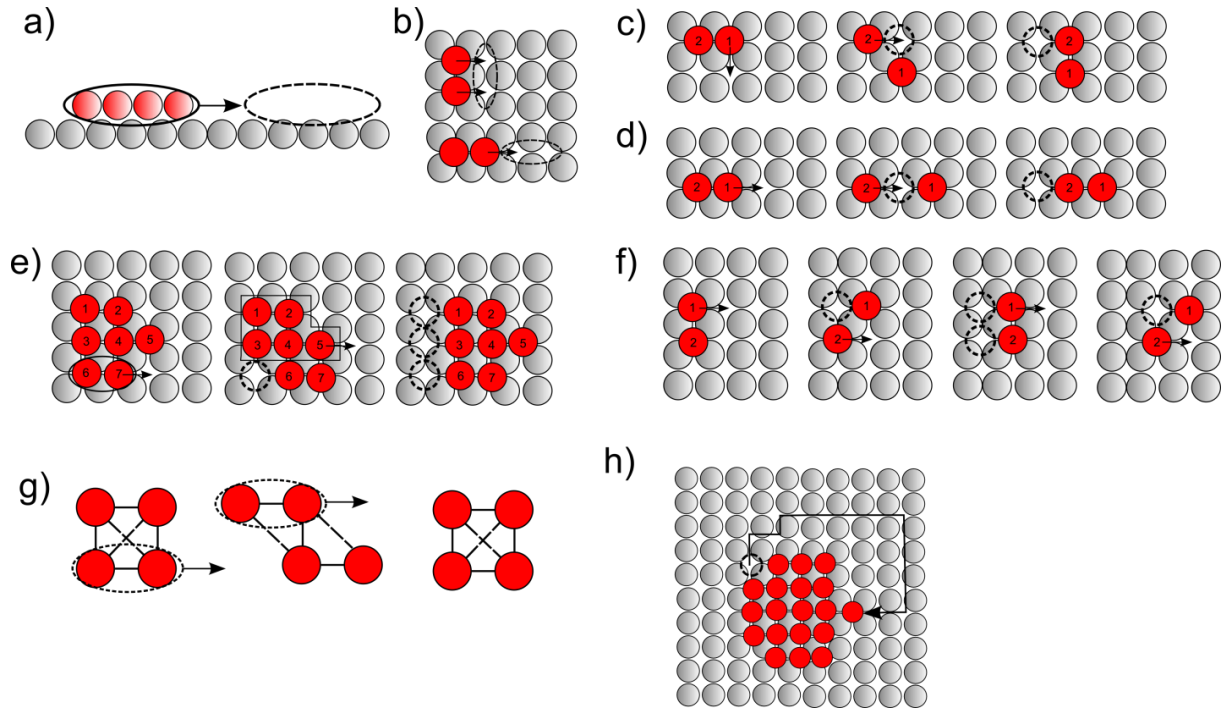

Fig. 32: Collective gliding mechanism: (a) of cluster, (b) of dimer. Sequential jump of a dimer: (c) rotation, (d) translation. Reptation mechanism: (e) of a cluster, (f) of a dimer. (g) Dimer sharing mechanism. (h) Evaporation and condensation mechanism.

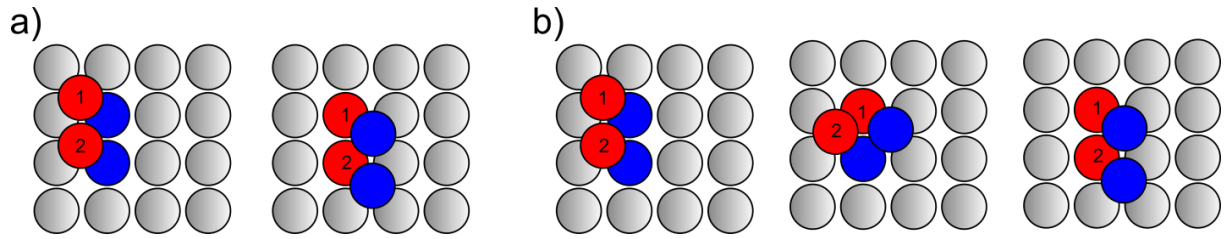

Fig. 33: (a) Collective exchange of a dimer. (b) Sequential exchange of a dimer.

7. MEASUREMENT PROCEDURE FOR DIFFUSION OF ADATOM PAIR

The procedure for measurements of two-adatom diffusion is analogous to the measurements of single adatom diffusion. The adatom pair is obtained by either the adatom deposition from the evaporator or by the field evaporation of a W(100) surface. In the adatom deposition method, the evaporator is calibrated to deposit at least one but not more than three adatoms onto a W(100) plane during one deposition attempt. Obtaining the adatom pair by slow field evaporation of a W(100) plane (Fig. 34a – d) is usually much easier than obtaining a single adatom with the same method. The adatom dimer is the last atomic structure that remains during a slow field desorption before the W(100) starts decreasing (Fig. 34d). After the adatom pair is created, the adatom movement is measured in the same way as the diffusion of a single adatom. The sample is heated at temperatures 613 K, 647 K and 695 K for time intervals 60 s, 60 s and 20 s, respectively. The positions of the adatoms are marked after each heating cycle. After the map of sites visited by adatoms is obtained, the grid is matched to the sites to determine the diffusion mechanism. The collected information about displacements of the adatoms is used to determine the activation energy for adatom diffusion in a presence of another adatom.

The total number of measuring cycles collected for the analysis is 99. It is not enough to calculate the energy of pair interactions. However, the collected statistic allows one to estimate the activation energy for adatom diffusion in the presence of a second adatom. By comparing that energy with the activation energy obtained from the measurements of single adatom diffusion, one can tell if the adatoms interact.

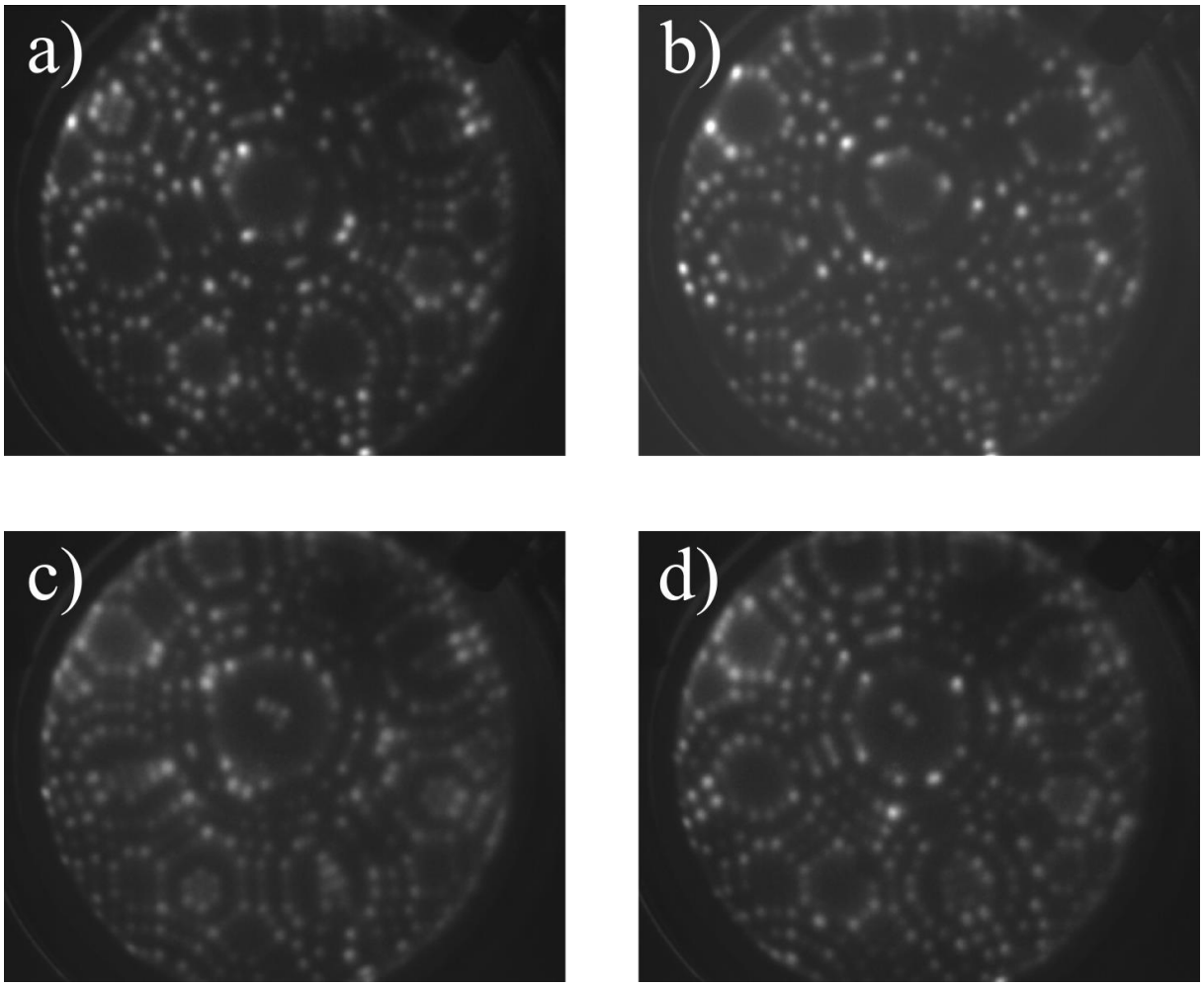

Fig. 34: (a) – (d) Obtaining the adatom pair from the field evaporation of a W(100) oriented tip. A gentle desorption of the surface allows obtaining two adatoms aligned along <110> directions, separated from each other by $\sqrt{2}$ of the lattice constant. The average diameter of the plane is ~50 Å.

8. RESULTS AND DATA ANALYSIS

The diffusion of two adatoms was observed in a time scale of seconds, at temperatures slightly lower than the diffusion of a single adatom, i.e. 617 K. For most of the time, the adatom pair did not diffuse as a dimer, but rather as two separated adatoms. Only occasionally, the adatoms moved collectively in the same direction, i.e. parallel and perpendicular to the axis of the adatom pair (Fig. 35). The smallest separation distance observed between adatoms is equal to the distance between the nearest diagonal sites (Fig. 36a). The most frequent separation, at which the adatoms were observed, was equal to two lattice constants of a non-reconstructed W(100) (Fig. 36b). The collected statistics are insufficient for determining the shape of the pair interaction energy distribution from the distance distribution. However, the information about the most popular distance between the adatoms is useful for the calculations of the pair interaction energy with the DFT method. One can calculate the energy of adatom migration from the most popular configuration to the arrangement with further and closer separation.

8.1 Diffusion Mechanism

The grid that was matched to the sites visited by the adatoms is oriented along <110> directions, which corresponds to a c(2x2) lattice (Fig. 37). Based on the criteria for identifying the diffusion mechanism, it has been concluded that both W adatoms diffuse via the exchange mechanism. For all three temperatures 617 K, 647 K and 695 K, a dominant diffusion mechanism is the adatom exchange. The jump was observed only once, at temperature 695 K. The adatom pair moved collectively into an alternative c(2x2) grid. Afterward, the pair broke and the adatoms diffused separately via the exchange.

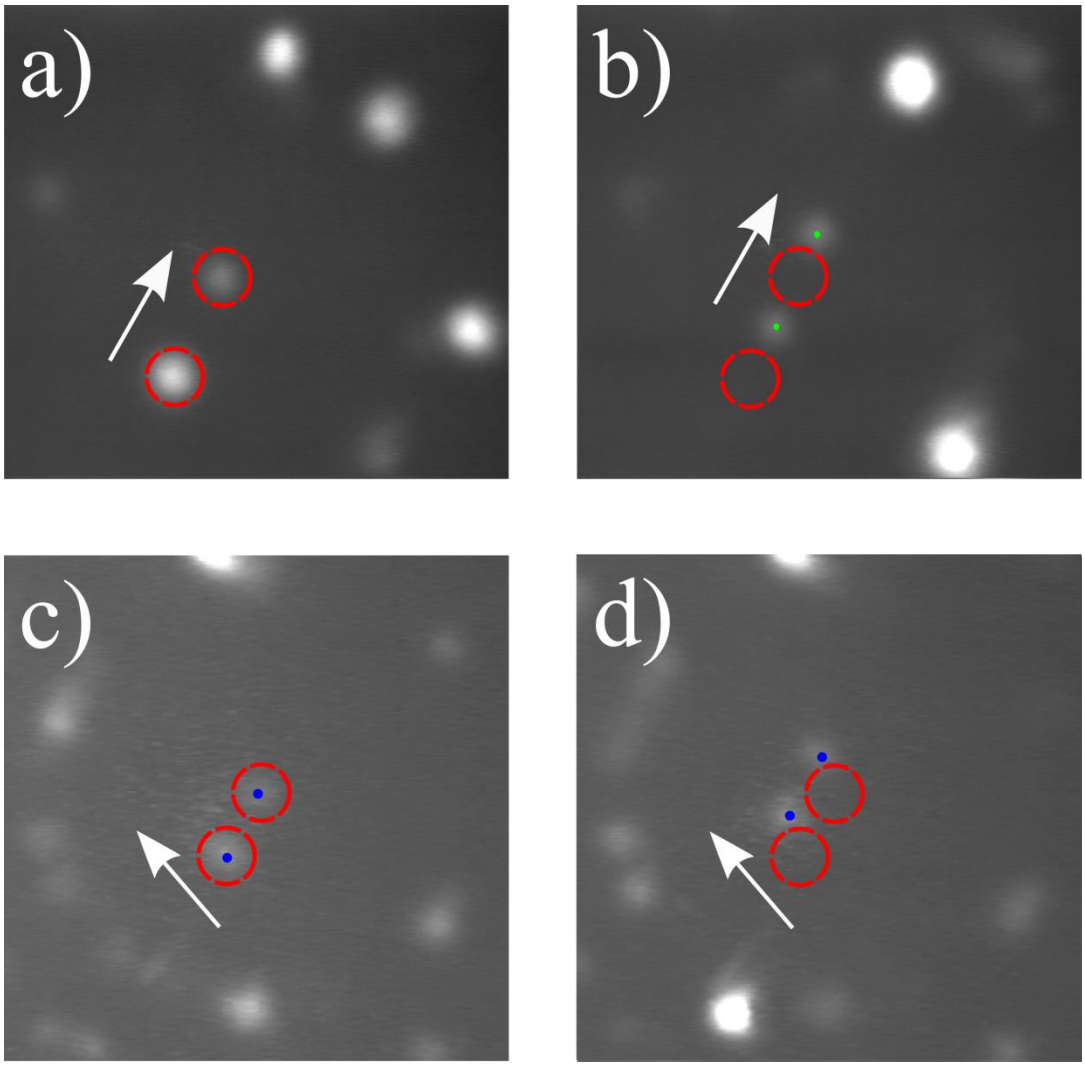

Fig. 35: The movement of the adatom pair: (a) – (b) the adatom pair moves along the pair's axis, (c) – (d) the adatom pair moves perpendicular to the pair's axis. The displacement could occur due to either the sequential or the collective exchange.

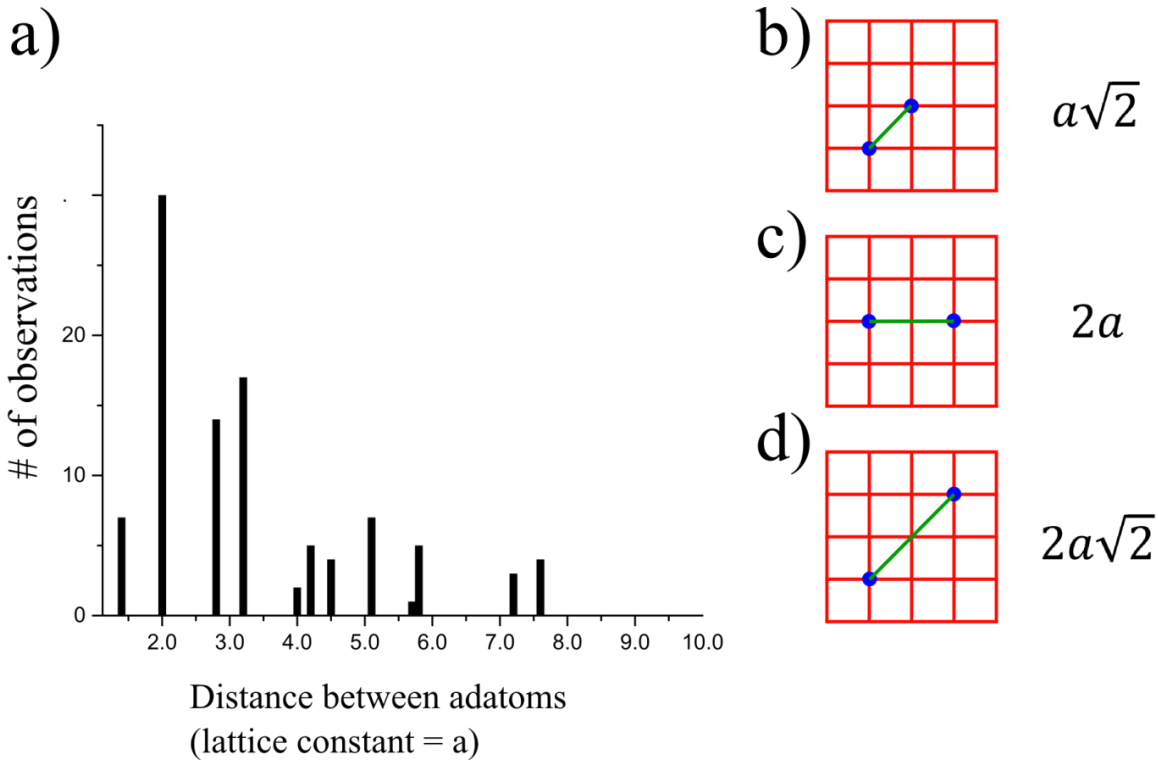

Fig. 36: (a) Distribution of the distances between the adatoms of the pair. (b) – (d) commonly observed configurations of the adatom pair on the surface, *a* is equal to a lattice constant of non-reconstructed W(100). The most popular configuration of the pair is (c).

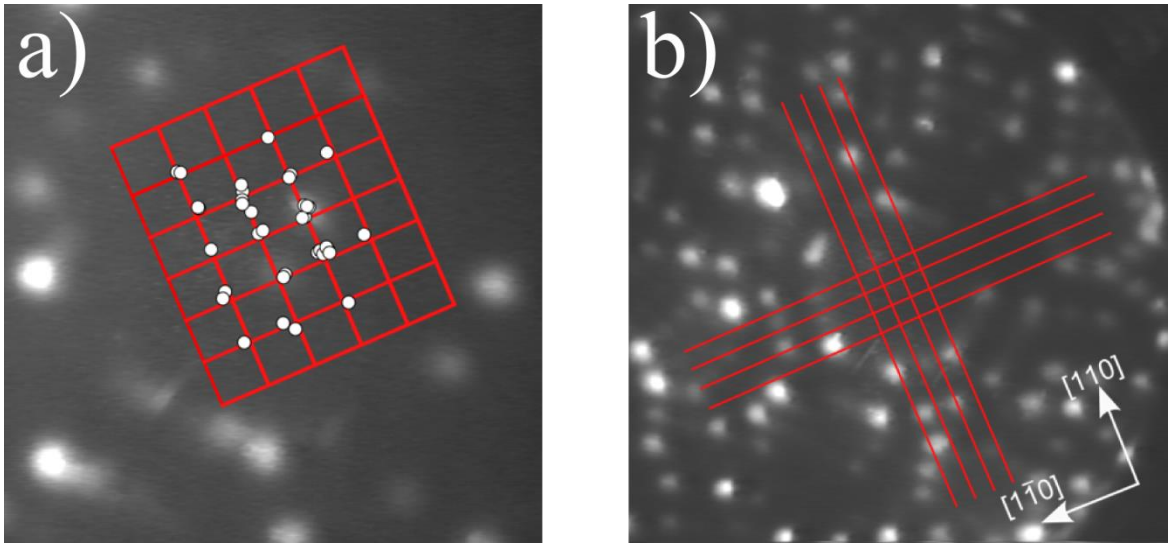

Fig. 37: (a) FIM micrograph of a magnified W(100) plane with marked positions visited by diffusing adatom pair and matched grid. (b) FIM micrograph with a grid matched to the visited sites. The orientation of the grid is along <110> directions, which corresponds to a c(2x2) arrangement for the visited sites.

8.2 Activation Energy for Adatom Diffusion

Initially, it is assumed that two adatoms do not interact. If the adatoms do not interact, then the activation energy per adatom should be equal to the activation energy measured for a single adatom. The obtained value of the energy per adatom is compared to the value of the activation energy obtained from measurements of single adatom diffusion.

Two W adatoms are chemically indistinguishable and tracking the path of a particular adatom might be a very difficult task to accomplish flawlessly. Therefore, one has to be extremely careful in the interpretation of the adatoms' movements. The activation energy for the diffusion per adatom was obtained using two methods: the analysis of the mean square displacement and the analysis of the migration rate. The values of the energies are compared to each other for checking the calculation methods.

8.2.1 Analysis of the mean square displacement: Red and Blue adatoms

Even though the adatoms are chemically identical, their spot sizes imaged observed in FIM can be different due to their position on the surface plane. Therefore, sometimes it is possible to distinguish two atoms from each other – mark one adatom as "Red" and the other as "Blue" (Fig. 38).

In this part of the analysis, one adatom was marked as Red and another as Blue. The diffusivity of each adatom at temperatures 613 K, 647 K and 695 K was calculated analogically to single adatom diffusion, by using the Einstein-Smoluchowski relation:

$$\langle \Delta r^2 \rangle = 4D\tau \tag{14}$$

The values of the diffusivities were plugged directly into the Arrhenius relation:

$$E_D = -k_B T ln\left(\frac{D}{D_0}\right) \tag{15}$$

It was assumed that the lattice vibration frequency is 10^{12} 1/s and the displacement length l is equal to a distance between nearest diagonal adsorption sites on a non-reconstructed W(100) surface. Additionally, the entropy part of D_0 was assumed to be equal one. Thus the diffusion prefactor was estimated from the formula:

$$D_0 = v \cdot l^2 = 2 \cdot 10^{-4}\, cm^2/s \tag{16}$$

The activation energy for the diffusion per adatom is obtained by averaging the calculated energies for all measured temperatures. Its value is 1.85 ± 0.35 eV. For comparison, exactly the same diffusion prefactor and the same calculation method was used to estimate the activation energy for diffusion of a single adatom on W(100). The obtained value is 1.701 ± 0.003 eV. The ~0.15 eV difference in the values of the energies suggests a possible interaction between the adatoms.

In the presented method, the tagging of the adatoms depends only on the size of observed spots. Even if the adatoms are migrating very slowly and are far from each other, the analysis is still based on very subjective judgment. Thus, the obtained result is verified with an alternative method: the analysis of the migration rate.

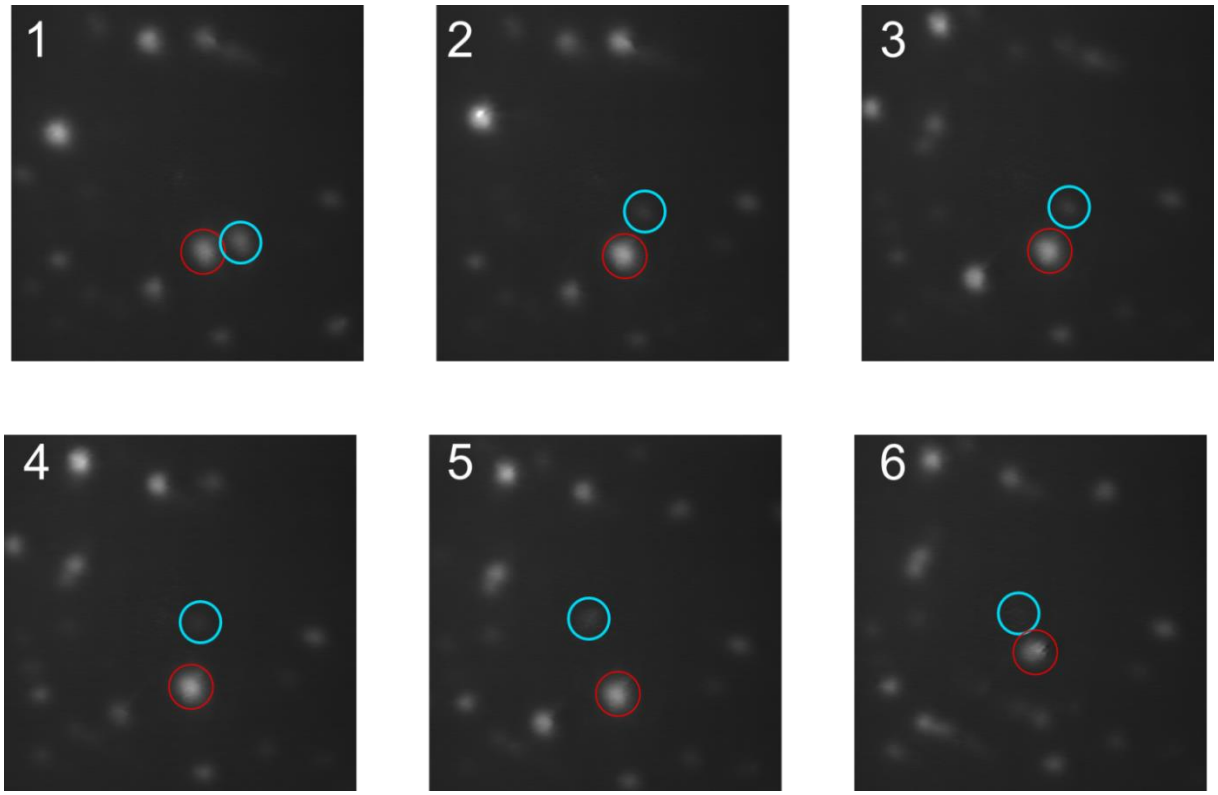

Fig. 38: A set of micrographs with two W adatoms diffusing on a W(100) plane. The adatoms are distinguished from each other by the size of the observed spot.

8.2.2 Analysis of the migration rate

In the experiment, the temperature and the heating time were adjusted in the way that each diffusing adatom usually do not make more than one exchange per heating cycle. The displacement rate Γ of an adatom is measured by calculating the total number of adatom displacements and dividing it by the number of heating cycles and the time of heating in a single cycle:

$$\Gamma = \frac{\#\ displacements}{\#cycles \cdot time\ of\ a\ cycle} \tag{17}$$

In the analysis it was initially assumed that two adatoms do not interact with each other. Thus the total number of displacements counting migration of both adatoms was divided by two. The number of displacements per adatom was used to calculate the jump rate per adatom. The activation energy for diffusion per adatom E_D was estimated directly from the Arrhenius formula:

$$E_D = -k_B T ln\left(\frac{\Gamma}{v_0}\right) \tag{18}$$

It was assumed that the lattice vibration frequency is 10^{12} 1/s.

The calculated activation energy for the diffusion of a W adatom on a W(100) plane in the presence of a second adatom is 1.80 ± 0.15 eV. Using the same method the activation energy for adatom diffusing alone on the surface is 1.49 ± 0.03 eV. If the adatoms are diffusing independently, the calculated activation energies should be the same for both situations: with and without the presence of additional adatom. The difference between obtained energies shows that the adatoms interact.

9. SUMMARY OF PART II

The diffusion of a W adatom pair was investigated to examine how the presence of an additional adatom affects the diffusion properties of a W/W(100) system. It was observed that two W adatoms diffuse separately for most of the time, not as a dimer. In the presence of a second adatom, the obtained activation energy for the diffusion via exchange is ~ 1.8 eV, which is about 0.2 eV higher than the activation energy for the diffusion of a single adatom, 1.6 eV. The difference between the activation energies suggests that the adatoms interact. However, the presence of an additional W adatom on the W(100) plane does not change the dominant diffusion mechanism – the adatom exchange.

The adatom diffusion via jump was observed only once during 99 heating cycles. At temperature 695 K, both adatoms of the pair moved into the alternative c(2x2) grid, and then they continued diffusion separately via the exchange for 36 heating cycles. The collected statistic of jumps is insufficient to estimate the activation energy for the jump mechanism. Still, the movement into the alternative c(2x2) shows that both diffusion mechanisms, jump and exchange, can occur.

10. SUMMARY AND CONCLUSIONS

In the dissertation, the coexistence of two surface diffusion mechanisms, jump and exchange, in one system was investigated for W adatom migrating on a W(100) surface. The goal of the research was to deliver the first experimental proof for temperature-activated coexistence of diffusion mechanisms. The key steps of the proof involved: (a) determining the morphology of the W(100) surface; (b) identifying the surface diffusion mechanisms; (c) verifying that the occurrence of the additional diffusion mechanism is a temperature-triggered phenomenon. The additional studies were conducted to examine how the presence of an additional W adatom on a finite plane affects the diffusion properties of W on W(100). The experimental results were supported with the results of density functional theory calculations.

The results of the adsorption and the diffusion experiments, supported with the DFT calculations, showed that a W(100) plane with the diameter ~ 50 Å is not reconstructed. This result directly confirms the conclusion of Nishikawa et al. [40] who suggest that the FBE model supported by Melmed et al. [39] is invalid.

The observed exchange mechanism for the diffusion of W adatom on a W(100) surface is the first experimental evidence for the occurrence of the exchange on a bcc(100) surface. For a temperature range 648 – 726 K, the adatom exchange is a dominant diffusion mechanism for W on W(100). At temperature 677 K, a second diffusion mechanism was observed – the adatom jumps. The adatom jump for W on W(100) was investigated for temperature range 677 – 726 K. It was observed that the jump rate increases with the higher temperatures. Thus, we conclude that the occurrence of the second diffusion mechanism is a temperature-controlled phenomenon. This result is the first direct experimental proof for the temperature-controlled coexistence of two diffusion mechanisms in one system.

The experimental values of the activation energies for diffusion of single W adatoms on W(100) surface are in a very good agreement with the results of DFT calculations. The activation energy for the diffusion by the exchange as a dominant mechanism is 1.60 ± 0.24 eV, where the calculated value is 1.55 eV. The experimental value of activation energy for the jump is ~ 2.1 eV and the value obtained by DFT calculations is 2.27 eV.

The additional experiments showed that the W adatom pair diffuses on a W(100) surface in form of two separated adatoms not as a dimer. The observed adatoms diffuse predominantly via exchange. The measured activation energy for the diffusion per adatom is ~ 1.8 eV, which is about 0.2 eV larger than the energy obtained for the diffusion of a single adatom. This result suggests a possible interaction between the adatoms. Nevertheless, the presence of an additional W adatom does not change the primary diffusion mechanism for W/W(100), which is the adatom exchange.

REFERENCES

[1] K. Oura, V. G. Lifshits, A. A. Saranin, A. V. Zotov and M. Katayama, *Surface Science: An Introduction*, Berlin Heidelberg: Springer, 2003.

[2] M. Fuechsle, J. A. Miwa, S. Mahapatra, H. Ryu, S. Lee, O. Warschkow, L. C. Hollenberg, G. Klimeck and M. Y. Simmons, "A single-atom transistor," *Nat. Nanotechnol.,* vol. 7, pp. 242 - 246, 2012.

[3] W. Wulfhekel, F. Zavaliche, R. Hertel, S. Bodea, G. Steierl, G. Liu and J. Kirschner, "Growth and magnetism of Fe nanostructures on W(001)," *Phys. Rev. B,* vol. 68, pp. 144416 1 - 9, 2003.

[4] R. A. Bennett, J. S. Mulley, H. A. Etman, A. Sparkes, T. Eralp, G. Held, S. A. Cavill and S. S. Dhesi, "Chromium nanostructures formed by dewetting of heteroepitaxial films on W(100)," *Phys Rev. B,* vol. 86, pp. 045454 1 - 10, 2012.

[5] E. Y. Afanas'eva, "Adsorption of gold on oxidized tungsten," *Technical Physics,* vol. 58, pp. 793 - 798, 2013.

[6] J. T. Goldstein and G. Ehrlich, "Atom and cluster diffusion on Re(0001)," *Surf. Sci.,* vol. 443, pp. 105 - 115, 1999.

[7] G. Antczak and G. Ehrlich, *Surface Diffusion*, Cambridge: Cambridge University Press, 2010.

[8] L. J. Lauhon and W. Ho, "Direct observation of the quantum tunneling of single hydrogen atoms with a scanning tunneling microscope," *Phys. Rev. Lett.,* vol. 85, pp. 4566 - 4569, 2000.

[9] G. Ehrlich and F. G. Hudda, "Atomic view of surface self-diffusion: Tungsten on tungsten," *J. Chem. Phys.,* vol. 44, pp. 1039 - 1049, 1966.

[10] S. -M. Oh and G. Ehrlich, "Non-nearest-neighbor jumps in 2D diffusion: Pd on W(110)," *Phys. Rev. Lett.,* vol. 88, pp. 236102 1 - 4, 2002.

[11] T. T. Tsong and C. -L. Chen, "Atomic replacement and vacancy formation on iridium surfaces," *Nature,* vol. 355, pp. 328 - 331, 1992.

[12] J. D. Wrigley and G. Ehrlich, "Surface diffusion by an atomic exchange mechanism," *Phys. Rev. Lett.,* vol. 1980, pp. 661 - 663, 1980.

[13] G. DeLorenzi, G. Jacucci and V. Pontikis, "Diffusion of adatoms and vacancies on otherwise perfect surfaces: A molecular dynamics study," *Surf. Sci.,* vol. 1982, pp. 391 - 413, 1982.

[14] D. C. Senft and G. Ehrlich, "Long jumps in surface diffusion: One-dimensional migration of isolated adatoms," *Phys. Rev. Lett.,* vol. 74, pp. 294 - 297, 1995.

[15] G. Antczak and G. Ehlrich, "Long jump rates in surface diffusion: W on W(110)," *Phys. Rev. Lett.,* vol. 92, pp. 166105 1 - 4, 2004.

[16] G. Antczak and G. Ehrlich, "Long jumps in diffusion of iridium on W(110)," *Phys. Rev. B,* vol. 71, pp. 115422 1 - 9, 2005.

[17] W. Xiao, P. A. Greaney and D. C. Chrzan, "Pt adatom on strained Pt(001)," *Phys. Rev. B,* vol. 70, pp. 033402 1 - 4, 2004.

[18] J. E. Black and Z. J. Tian, "Complicated exchange-mediated diffusion mechanisms in and on a Cu(100) substrate at high temperatures," *Phys. Rev. Lett.,* vol. 71, pp. 2445 - 2448, 1993.

[19] Z. Chen and N. Ghoniem, "Biaxial strain effects on adatom surface diffusion on tungsten from first principles," *Phys. Rev. B,* vol. 88, pp. 035415 1 - 12, 2013.

[20] E. W. Müller and T. T. Tsong, *Filed Ion Microscopy*, New York: American Elsevier Publishing Company, Inc., 1969.
[21] T. T. Tsong and J. Sweeney, "Direct observation of the atomic structure of W{100} surfaces," *Solid State Commun.,* vol. 30, pp. 767 - 771, 1979.
[22] G. L. Kellogg and P. J. Feibelman, "Surface self-diffusion on Pt(001) by an atomic exchange mechanism," *Phys. Rev. Lett.,* vol. 64, pp. 3143 - 3416, 1990.
[23] S. C. Wang and G. Ehrlich, "Determination of atomic binding sites on fcc(111) plane," *Surf. Sci.,* vol. 246, pp. 37 - 42, 1991.
[24] J. Houze, S. Kim, S. -G. Kim, S. -J. Park and R. M. German, "The effect of Fe atoms on the adsorption of W atom on W(100) surface," *J. Appl. Phys.,* vol. 103, pp. 106103 1 - 3, 2008.
[25] G. L. Kellogg, "Direct observations of adatom-surface-atom replacement: Pt on Ni(110)," *Phys. Rev. Lett.,* vol. 67, pp. 216 - 219, 1991.
[26] D. W. P. R. Basset, "Diffusion of single adatoms of platinum, iridium and gold on platinum surfaces," *Surf. Sci.,* vol. 70, pp. 520 - 531, 1978.
[27] T. Halicioglu, "An atomistic calculation of two-dimensional diffusion of Pt adatom on Pt(110) surface," *Surf. Sci.,* vol. 79, pp. L346 - L348, 1979.
[28] G. DeLorenzi and G. Jacucci, "The migration of point defects on bcc surfaces using a metallic pair potential," *Surf. Sci.,* vol. 164, pp. 526 - 542, 1985.
[29] C. -L. Chen and T. T. Tsong, "Self-diffusion on the reconstructed and nonreconstructed Ir(110) surfaces," *Phys. Rev. Lett.,* vol. 66, pp. 1610 - 1613, 1991.
[30] G. Prévot, C. Cohen, J. Moulin and D. Schmaus, "Surface diffusion of Pb on Cu(110) at low coverage," *Surf. Sci.,* vol. 421, pp. 364 - 376, 1999.
[31] K. Yonehara and L. D. Schmidt, "A LEED study of structures produced by H2 on (100)W," *Surf. Sci.,* vol. 25, pp. 238 - 260, 1971.
[32] T. E. Felter, R. A. Barker and P. J. Estrup, "Phase transition on Mo(100) and W(100)," *Phys. Rev. Lett.,* vol. 38, pp. 1138 - 1141, 1977.
[33] M. K. Debe and D. A. King, "Space-group determination of the low-temperature W{001}(2√×2√)R45° surface structure by low-energy-electron diffraction," *Phys. Rev. Lett.,* vol. 39, pp. 708 - 711, 1977.
[34] M. K. Debe and D. A. King, "New evidence for a clean thermally induced c(2×2) surface structure on W(100)," *J. Phys. C: Solid State Phys.,* vol. 10, pp. L303 - L308, 1977.
[35] R. A. Barker and P. J. Estrup, "Structural models of the reconstructed W{001} surface," *Solid State Commun.,* vol. 25, pp. 375 - 379, 1978.
[36] M. S. Altman and P. J. Estrup, "Multilayer reconstruction of the W(001) surface," *Phys. Rev. B,* vol. 38, pp. 5211 - 5214, 1988.
[37] D. Spišák and J. Hafner, "Diffusion of Fe atoms on W surfaces and Fe/W films and along surface steps," *Phys. Rev. B,* vol. 70, pp. 195426 1 - 13, 2004.
[38] H. Wengelnik, D. Badt and H. Neddermeyer, "Scanning tunneling microscopy on W(100) at 80 K and room temperature," *Surf. Sci.,* Vols. 307 - 309, pp. 619 - 624, 1994.
[39] A. J. Melmed, B. T. Tung, W. R. Graham and G. D. W. Smith, "Evidence for reconstructed {001} tungsten obtained by field-ion microscopy," *Phys. Rev. Lett.,* vol. 43, pp. 1521 - 1524, 1979.

[40] O. Nishikawa, M. Wada and M. Konishi, "FIM observations of W, Ga and Sn structures on W and Mo {001}," *Surf. Sci.,* vol. 97, pp. 16 - 24, 1980.

[41] J. G. Che, Z. Z. Zhu and C. T. Chan, "Change of ground state configuration induced by the stark shift of surface states in some bcc(001) surfaces," *Phys. Rev. Lett.,* vol. 82, pp. 3292 - 3295, 1999.

[42] H. -J. Ernst, E. Hulpke and J. P. Toennies, "Helium-atom-scattering study of the structure and phonon dynamics of the W(100) surface between 200 and 1900K," *Phys. Rev. B,* vol. 46, pp. 16081 - 16105, 1992.

[43] G. L. Kellogg, "The mobility and structure of nickel atoms on the (100) plane of tungsten," *Surf. Sci.,* vol. 192, pp. L879 - L886, 1987.

[44] R. A. Baker and P. J. Estrup, "Surface structures and phase diagram for the H/W(001) chemisorption system," *J. Chem. Phys,* vol. 74, pp. 1442 - 1452, 1981.

[45] N. W. Taylor and W. Rast, "The diffusion of helium and of hydrogen through pyrex chemically resistant," *J. Chem. Phys.,* vol. 6, pp. 612 - 619, 1938.

[46] D. A. Reed and G. Ehrlich, "In-channel clusters: Rhenium on W(211)," *Surf. Sci,* vol. 151, pp. 143 - 165, 1985.

[47] S. J. Koh, "Adatom diffusion and interactions: Pd on W(110)," Ph.D. dissertation, University of Illinois at Urbana-Champaign, Urbana, IL, 1998.

[48] G. Ehrlich and C. F. Kirk, "Binding and field desorption of individual tungsten atoms," *J. Chem. Phys.,* vol. 48, pp. 1465 - 1480, 1968.

[49] T. T. Tsong, *Atom-Probe Field Ion Microscopy*, New York: Cambridge University Press, 1990.

[50] T. T. Tsong and R. Casanova, "Elementary displacement steps in the migration of tungsten diatomic clusters on the tungsten (110) plane," *Phys. Rev. B,* vol. 21, pp. 4564 - 4570, 1980.

[51] K. Kyuno and G. Ehrlich, "Step-edge barriers: Truths and kinetic consequences," *Surf. Sci.,* vol. 394, pp. L179 - L187, 1997.

[52] G. Ehrlich, "Atomic displacement in one- and two-dimensional diffusion," *J. Chem. Phys.,* vol. 44, pp. 1050 - 1055, 1966.

[53] G. Kresse and J. Furthmiiller, "Efficiency of ab-initio total energy calculations for metals and semiconductors using a plane-wave basis set," *Comput. Mater. Sci.,* vol. 6, pp. 15 - 50, 1996.

[54] G. Kresse and J. Furthmuller, "Efficient iterative schemes for ab initio total-energy calculations using a plane-wave basis set," *Phys. Rev. B,* vol. 54, pp. 11169 - 11186, 1996.

[55] G. Kresse and J. Joubert, "From ultrasoft pseudopotentials to the projector augmented-wave method," *Phys. Rev. B,* vol. 59, pp. 1758 - 1775, 1999.

[56] G. Kresse and J. Hafner, "Ab. initio molecular dynamics for liquid metals," *Phys. Rev. B,* vol. 47, pp. 558 - 561, 1993.

[57] G. Henkelman, B. P. Uberuaga and H. Jónsson, "A climbing image nudged elastic band method for finding saddle points and minimum energy paths," *J. Chem. Phys.,* vol. 113, pp. 9901 - 9904, 2000.

[58] D. W. Bassett and M. J. Parsley, "Field ion microscope observatons of cluster formation in metal deposits on tungsten surfaces," *Nature,* vol. 221, p. 1046, 1969.

[59] D. W. Bassett and M. J. Parsley, "Field ion microscope studies of transition metal adatom diffusion on (110), (211) and (321) tungsten surfaces," *J. Phys. D Appl. Phys.,* vol. 3, pp. 707 - 715, 1970.

[60] T. Y. Fu, W. J. Weng and T. T. Tsong, "Dynamic study of W atoms and clusters on W (111) surfaces," *Appl. Surf. Sci.,* vol. 254, pp. 7831 - 7834, 2008.

[61] T. T. Tsong and R. Casanova, "Correlation between adatom-adatom pair interaction and adlayer superstructure formation: Si on W (110)," *Phys. Rev. Lett.,* vol. 47, pp. 113 - 116, 1981.

[62] F. Silly, M. Pivetta, M. Ternes, F. Patthey, J. P. Pelz and W. -D. Schneider, "Creation of an atomic superlattice by immersing metallic adatoms in a two-dimensional electron sea," *Phys. Rev. Lett.,* vol. 92, pp. 016101 1 - 4, 2004.

[63] F. Watanabe and G. Ehrlich, "Direct observations of pair interactions on a metal: Heteropairs on W(110)," *J. Chem. Phys.,* vol. 95, pp. 6075 - 6087, 1991.

[64] G. L. Kellogg, "Field ion microscope studies of single-atom surface diffusion and cluster nucleation on metal surfaces," *Surf. Sci.,* vol. 21, pp. 1 - 88, 1994.

[65] T. T. Tsong and R. Casanova, "Pair interaction of metal atoms on a metal surface," *Phys. Rev. B,* vol. 22, pp. 5590 - 5598, 1980.

[66] A. Bogicevic, S. Ovesson, P. Hyldgaard, B. I. Lundqvist, H. Brune and D. R. Jennison, "Nature, strength, and consequences of indirect adsorbate interactions on metals," *Phys. Rev. Lett.,* vol. 85, pp. 1910 - 1913, 2000.

[67] V. S. Stepanyuk, A. N. Baranov, D. V. Tsivlin, W. Hergert, P. Bruno, N. Knorr, M. A. Schneider and K. Kern, "Quantum interference and long-range adsorbate-adsorbate interactions," *Phys. Rev. B,* vol. 68, pp. 205410 1 - 5, 2003.

[68] H. W. Fink and G. Ehrlich, "Direct observation of three-body interactions in adsorbed layers: Re on W(110)," *Phys. Rev. Lett.,* vol. 52, pp. 1532 - 1534, 1984.

[69] J. Repp, F. Moresco, G. Meyer, K. -H. Reider, P. Hyldgard and M. Perrson, "Substrate mediated long-range oscillatory interaction between adatoms," *Phys. Rev. Lett.,* vol. 85, pp. 2981 - 2984, 2000.

[70] P. Hyldgaard and M. Persson, "Long-ranged adsorbate–adsorbate interactions mediated by a surface-state band," *J. Phys.: Condens. Matter,* vol. 12, pp. L13 - L19, 2000.

[71] J. C. Hamilton, M. R. Sørensen and A. F. Voter, "Compact surface-cluster diffusion by concerted rotation and translation," *Phys. Rev. B.,* vol. 61, pp. R5125 - R5128, 2000.

[72] T. Y. Fu and T. T. Tsong, "Structure and diffusion of small Ir and Rh clusters," *Surf. Sci.,* vol. 421, pp. 157 - 166, 1999.

[73] A. G. Naumovets and Z. Zhang, "Fidgety particles on surfaces: How do they jump, walk, group, and settle in virgin areas ?" *Surf. Sci.,* vol. 500, pp. 414 - 436, 2002.

[74] W. Xu and J. B. Adams, "W dimer diffusion on W(110) and (211) surfaces," *Surf. Sci.,* vol. 339, pp. 247 - 257, 1995.

[75] V. Chirita, E. P. Munger, J. E. Greene and J. -E. Sundgren, "Reptation: A mechanism for cluster migration on (111) face-centered-cubic metal surfaces," *Surf. Sci.,* vol. 436, pp. L641 - L647, 1999.

[76] Z. -P. Shi, Z. Zhang, A. K. Swan and J. F. Wendelken, "Dimer shearing as a novel mechanism for cluster diffusion and dissociation on metal (100) surfaces," *Phys. Rev. Lett.,* vol. 76, pp. 4927 - 4930, 1996.

[77] C. -L. Liu and J. B. Adams, "Structure and diffusion of clusters on Ni surfaces," *Surf. Sci.,* vol. 268, pp. 73 - 86, 1992.